Universidade do Algarve

Faculdade de Ciências e Tecnologia

Ocean Parameter Estimation with High-frequency Signals using a Vector Sensor Array

Mestre Paulo Jorge Maia dos Santos

Tese apresentada à Universidade do Algarve para a obtenção do grau de Doutor no ramo de Engenharia Electrónica e Telecomunicações, especialidade Processamento de Sinal.

2012

Universidade do Algarve

Faculdade de Ciências e Tecnologia

Ocean Parameter Estimation with High-frequency Signals using a Vector Sensor Array

Mestre Paulo Jorge Maia dos Santos

Orientadores: Doutor Sérgio Manuel Machado Jesus, Professor Catedrático da Faculdade de Ciências e Tecnologia, Universidade do Algarve

Doutor Paulo Alexandre da Silva Felisberto, Professor Adjunto do Instituto Superior de Engenharia, Universidade do Algarve

Tese apresentada à Universidade do Algarve para a obtenção do grau de Doutor no ramo de Engenharia Electrónica e Telecomunicações, especialidade de Processamento de Sinal.

2012

Ocean Parameter Estimation with High-frequency Signals using a Vector Sensor Array

Declaração de autoria do trabalho

Declaro ser o autor deste trabalho, que é original e inédito. Autores e trabalhos consultados estão devidamente citados no texto e constam da listagem de referências bibliográficas incluída.

À minha filhota Rita que deu os primeiros passos no início do meu trabalho de Doutoramento
e cresceu ao mesmo tempo que o trabalho desta Tese evoluía,
ao meu filho Francisco pela paciência que teve ao longo destes anos,
e à minha mulher Sandra pelo apoio incondicional e compreensão nos momentos mais difíceis.

Acknowledgements

I would like to thank my supervisors Prof. Sérgio M. Jesus and Prof. Paulo Felisberto for their permanent effort in providing the necessary conditions in the laboratory for accomplishing the objectives of this work, by organizing scientific projects and sea trials for collecting experimental data, their useful advises, and in particular, for their contributions through many suggestions and comments during the writing of this thesis.

I would like to thank also Prof. Orlando Rodríguez for the design of the TRACEO Gaussian beam model used in this work, which provides the particle velocity outputs, and for his help, advises, comments and suggestions during the writing of this thesis.

I thank my colleagues in Electrotecnic Engineering Department of the ISE, University of Algarve for giving me conditions to realize the work of this thesis. Thank also my colleagues in the Signal Processing Laboratory (SiPLAB) that daily contributed for an enjoyable social environment and their contributions to the work of this thesis.

I would like to thank Michael Porter, chief scientist for the Makai Experiment, Jerry Tarasek at Naval Surface Weapons Center for the loan of the vector sensor array used in this work. I also thank Bruce Abraham at Applied Physical Sciences for providing assistance with the data acquisition and the team at HLS Research, particularly Paul Hursky for their help with the data used in this work.

Finally, special thanks to my wife and my children, for their patience and support, specially during the writing of this thesis.

This work was partially funded by National Funds through FCT - Fundation for Science and Technology under project SENSOCEAN (PTDC/EEA-ELC/104561/2008).

Name: Paulo Jorge Maia dos Santos
College: Faculdade de Ciências e Tecnologia
University: Universidade do Algarve
Supervisors: Doutor Sérgio Manuel Machado Jesus, Full Professor of Faculdade de Ciências e Tecnologia, Universidade do Algarve and Doctor Paulo Alexandre da Silva Felisberto, Adjoint Professor of Instituto Superior de Engenharia, Universidade do Algarve
Thesis title: Ocean Parameter Estimation with High-frequency Signals using a Vector Sensor Array

Abstract

Vector sensors began to emerge in 1980s as potential competitors to omni directional pressure driven hydrophones, while their practical usage in underwater applications started in the last two decades. The crucial advantage of vector sensors relative to hydrophones is that they are able to record both the omni-directional pressure and the three vectorial components of the particle velocity. A claimed advantage of vector sensors over hydrophones is the quantity of information obtained from a single point spatial device, which potentially allows for high performance small aperture Vector Sensor Arrays (VSA). The capabilities of such small aperture VSA have captured the attention for their usage in high-frequency applications. The main contribution of this work is the understanding of the gain provided by vector sensors over hydrophones whenever ocean environmental parameter estimation is concerned. In a first step a particle velocity-pressure joint data model is proposed and an extended VSA-based Bartlett estimator is derived. This data model and estimator, initially developed for estimating direction of arrival, are generalized for ocean parameter estimation, assuming a particle velocity capable physical model - the TRACEO model. The highlighted capabilities of the VSA are first demonstrated for angle of arrival estimation, where a variety of spatial configurations of hydrophone arrays are compared to that of a vertical VSA. A vertical VSA array configuration is then used for estimating geoacoustic bottom properties from short range acoustic data, using two VSA-based techniques: the generalized Bartlett estimator and the reflection coefficient estimator proposed by Harrison *et al.*. The proposed techniques where tested on experimental VSA data recorded in shallow water area off the Island of Kauai (Hawaii) during the MakaiEx 2005 experiment. The obtained results are comparable between techniques and inline with the expected values for that region. These results suggest that it is indeed possible to obtain reliable seabed geoacoustic properties' estimates in a frequency band of 8-14 kHz using a small aperture VSA with only a few sensors.

Keywords: Vector sensor, Array processing, Matched-field processing, High-frequency tomography, Geoacoustic inversion, Underwater acoustics

Nome: Paulo Jorge Maia dos Santos
Faculdade: Faculdade de Ciências e Tecnologia
Universidade: Universidade do Algarve
Orientadores: Doutor Sérgio Manuel Machado Jesus, Professor Catedrático da Faculdade de Ciências e Tecnologia, Universidade do Algarve e Doutor Paulo Alexandre da Silva Felisberto, Professor Adjunto do Instituto Superior de Engenharia, Universidade do Algarve
Título da Tese: Ocean Parameter Estimation with High-frequency Signals using a Vector Sensor Array

Resumo

O oceano é um vasto e complexo mundo que cobre cerca de 75% do nosso planeta. O oceano é essencialmente opaco à luz e à radiação eletromagnética, mas transparente em relação aos sinais acústicos, sendo o som praticamente a única via para transmitir sinais a grandes distâncias. Assim, na exploração oceânica, a propagação do som na água é de grande importância, não só para a comunicação entre os animais marinhos, mas também para detetar objetos, medir a profundidade da água e correntes ou inclusive estimar parâmetros ambientais. O estudo da propagação do som na água insere-se na área de investigação conhecida como acústica submarina, onde um dos objetivos é prever a influência que as fronteiras do oceano (superfície e fundo) e os parâmetros ambientais (temperatura, salinidade, substâncias dissolvidas ou em suspensão, etc.) têm na propagação do som. A acústica submarina usa a informação da propagação do som na água para prever as suas características físicas e biológicas, para comunicar ou detetar objetos e intrusos.

Depois da segunda guerra mundial, e devido a conflitos regionais ao longa da costa dos diversos países, proteção de portos, exploração de gás e petróleo, influência das ondas, etc., o interesse da acústica submarina focou-se no estudo da propagação do som em águas pouco profundas (profundidades até 200 m). Nestas águas, a interação do som com a superfície da água e com o fundo marinho torna-se particularmente importante, pois os sinais são refletidos ou transmitidos ao longo dos sedimentos. As propriedades do fundo são geralmente desconhecidas ou conhecidas com uma elevada incerteza para largas áreas. As amostras do fundo só caracterizam uma determina área em particular, dificultando previsões da propagação do som a longas distâncias. Por conseguinte a estimação das propriedades do fundo com elevada exatidão e larga cobertura espacial é de extrema importância para as aplicações de acústica submarina em águas pouco profundas.

Na exploração oceânica, a localização de fontes acústicas em profundidade, distância e direção de chegada (DOA), e a estimação de outros parâmetros tais como as propriedades do fundo marinho ou da coluna de água, são normalmente obtidas utilizando sinais de baixa-frequência (abaixo de 2 kHz) e longas antenas de hidrófones, de modo a conseguir-se uma elevada resolução na estimação desses parâmetros. Os hidrófones medem a pressão acústica, uma grandeza escalar, e são tipicamente omnidirecionais, ou seja, são sensíveis à pressão igualmente em todas as direções. Contudo, as antenas longas têm problemas operacionais em termos da sua colocação na água e recuperação, não sendo possível utilizá-las em pequenas plataformas móveis ou veículos autónomos, onde o espaço é reduzido. Uma das formas de resolver este problema é a utilização de sinais de alta-frequência (tipicamente na

banda de 5-50 kHz). Recentemente, a utilização deste tipo de sinais tem tido um crescente interesse na comunidade científica quer no plano teórico quer na demonstração experimental da sua aplicabilidade, relacionado com aplicações nas comunicações submarinas, tomografia e bioacústica. O uso de sinais de alta-frequência, ou seja, utilização de sinais com menor comprimento de onda é potencialmente vantajoso em diversas aplicações submarinas entre as quais a caracterização dos parâmetros do fundo afim de se obter uma resolução mais fina destes. Outra vantagem da utilização de sinais de alta-frequência é permitir utilizar antenas de recetores mais curtas e fontes acústicas de menores dimensões. Uma vantagem adicional dos sistemas de alta-frequência é a multifuncionalidade, podendo um mesmo sistema ser utilizado em diversas aplicações tais como localização de fontes, monitorização de mamíferos marinhos, comunicações submarinas e ainda inversão geoacústica (técnica remota de estimação dos parâmetros do fundo marinho tais como velocidade compressional do sedimento, atenuação compressional, densidade, entre outros).

Com o desenvolvimento de novos materiais piezoelétricos chamados cristais de PMT-PT (*"Lead Magnesium Niobate / Lead Titanate"*), surge nos anos 80 uma nova geração de sensores acústicos, denominados de sensores vetoriais - *"Vector Sensors"*. Estes sensores, por serem direcionais, aparecem como uma solução alternativa aos sistemas de aquisição normalmente utilizados - hidrófones, principalmente na estimação da DOA. A maior vantagem dos sensores vetoriais relativamente aos hidrófones é que são capazes de medir para além da pressão acústica, as três componentes da velocidade das partículas, ou seja, são sensíveis à magnitude e à direção da onda acústica. Cada componente da velocidade das partículas pode ser determinada pelo gradiente da pressão, podendo para tal serem usados dois hidrófones (cuja distância é bem menor do que o comprimento de onda) medindo o diferencial de pressão ou através da utilização de acelerómetros (atualmente a solução mais utilizada). Neste trabalho foram utilizados sensores vetoriais em que cada elemento é constituído por um hidrófone e por três acelerómetros. Os acelerómetros são sensíveis à velocidade das partículas ao longo de um eixo específico x, y ou z. A quantidade de informação que pode ser obtida por um sensor vetorial num determinado ponto do espaço e a sua capacidade de filtragem espacial intrínseca, permite que uma antena de poucos sensores vetoriais (VSA - *"vector sensor array"*) tenha um elevado desempenho quando comparado com uma antena com o mesmo número de hidrófones.

A maior parte dos estudos científicos envolvendo o uso dos VSA estão relacionados com a estimação da DOA com dados simulados e sinais de baixa-frequência. Em ambos os casos foi verificado que um VSA com poucos elementos exibe um elevado desempenho na estimação da DOA face a uma antena de hidrófones. Um dos inconvenientes de se usar uma antena linear de hidrófones é o aparecimento da conhecida ambiguidade esquerda/direita na estimação da DOA, a qual é ultrapassada com o uso de um VSA linear. Destes estudos, algumas perguntas podem ser colocadas, nomeadamente: Quais as principais semelhanças e diferenças entre o campo acústico da velocidade das partículas e o campo de pressão acústica? Será que a elevada capacidade de filtragem espacial de um VSA pode ser usada para melhorar a estimação de outros parâmetros tais como a temperatura da coluna de água ou as propriedades do fundo marinho? Qual será a sensibilidade de cada componente da velocidade das partículas relativamente a um parâmetro ambiental específico? Poderá o VSA curto combinado com a utilização de sinais de alta-frequência ser usado com vantagem na localização tridimensional de fontes acústicas, ou mais especificamente na inversão geoacústica?

Tendo em conta o exposto, a principal ideia do trabalho proposto nesta tese é o de responder a estas questões específicas e outras relacionadas que surjam ao longo da inves-

tigação. O estudo da aplicabilidade do VSA para estimação de parâmetros genéricos no ambiente subaquático e a quantificação do ganho que advém da utilização deste sistema de aquisição, será a maior contribuição do trabalho proposto. Para este fim, técnicas de estimação normalmente usadas com sinais adquiridos pelos hidrófones (por ex.: *"Beamforming"* ou *"Matched-field Processing"*), serão adaptadas de modo a incluir a informação da velocidade das partículas. Destacam-se as principais contribuições deste trabalho:

- É proposto um modelo de dados que agrupa a pressão acústica com a velocidade das partículas, tendo em conta a relação entre a velocidade das partículas e a pressão dada pela equação de *"Euler"*. O modelo de dados é baseado no modelo físico de propagação de raios, usando para isso a aproximação de feixes Gaussianos;

- São desenvolvidos estimadores VSA baseados no estimador linear - *Bartlett*, o qual correlaciona diretamente os dados medidos experimentalmente com as respetivas réplicas fornecidas por um modelo físico. São derivados dois estimadores: um que considera o modelo de dados só com as componentes da velocidade das partículas e outro que para além destas inclui também a pressão acústica. A vantagem dos estimadores que incluem a velocidade das partículas relativamente ao estimador Bartlett tradicional, que considera somente a pressão, é deduzida analiticamente, demonstrando-se que os estimadores para VSA são proporcionais ao estimador só de pressão. Os fatores de proporcionalidade estão relacionados com a diretividade do VSA, constituindo a vantagem crucial da utilização da velocidade das partículas na estimação de parâmetros genéricos. Os fatores de diretividade proporcionam assim uma redução ou mesmo eliminação dos lobos laterais nas superfícies de ambiguidade dos parâmetros geométricos ou do fundo, e por conseguinte uma melhoria na sua resolução;

- Os estimadores VSA desenvolvidos são testados com dados simulados e dados experimentais, tanto para a estimação da DOA como na estimação dos parâmetros do fundo marinho. Os dados experimentais considerados neste trabalho foram adquiridos por um VSA vertical de quatro elementos durante a experiência de mar "Makai Experiment 2005" (MakaiEx'05). A experiência ocorreu na costa oeste da ilha de Kauai, Hawaii (Estados Unidos da América), entre 15 de setembro e 2 de outubro de 2005. A MakaiEx'05 foi organizada pela *HLS Research* e financiada pelo *Office of Naval Research* (ONR), tendo sido especificamente planeada para adquirir dados de suporte à investigação e validação de diferentes aplicações de acústica de alta-frequência. Esta experiência de mar integrou um considerável número de investigadores de várias instituições internacionais, entre eles uma equipa do SiPLAB da Universidade do Algarve, com interesses em diferentes aspetos da acústica de altas-frequências: comunicação acústica, tomografia acústica oceânica de alta resolução, modelação de propagação acústica na banda das altas-frequências, deteção de alvos, etc. A MakaiEx'05 foi a primeira experiência científica que incluiu um VSA no conjunto dos equipamentos usados para recolha de sinais acústicos, os quais se encontram na banda de frequência 8-14 kHz;

- Por fim, a mais importante contribuição deste trabalho é o estudo da aplicabilidade dos VSA à inversão geoacústica de alta-frequência, isto é, caracterização do fundo marinho baseado na informação da velocidade das partículas. Do que é conhecido do estado da arte, a aplicação de um VSA com poucos elementos e sinais de alta-frequência em

inversão geoacústica é uma contribuição original deste trabalho nesta área do conhecimento. O que se propõe é o uso de uma antena VSA de poucos elementos e sinais de alta-frequência para estimação dos parâmetros do fundo marinho, usando duas técnicas baseadas na velocidade das partículas. Na primeira técnica, o estimador do coeficiente de reflexão proposto por C. Harrison *et.al* usando o ruído ambiental, é adaptado de modo a incluir as medidas verticais do VSA. A elevada capacidade do VSA em discriminar os sinais na horizontal e a correspondente resolução em termos verticais permite olhar para o sinal de interesse e distinguir os raios que chegam ao sistema de aquisição vindos da superfície daqueles que vêm pelo fundo. A razão entre a energia das chegadas que vêm pela superfície e a energia das chegadas vindas do fundo é uma aproximação do coeficiente de reflexão. As perdas por reflexão no fundo estimadas através dos sinais adquiridos são comparadas com as perdas por reflexão modeladas pelo modelo SAFARI, para um conjunto de parâmetros do fundo, número de sedimentos e respetivas espessuras. A melhor aproximação entre as superfícies de ambiguidade das perdas por reflexão permite obter o conjunto de parâmetros que caracterizam o fundo em determinada área. Na segunda técnica, os estimadores VSA desenvolvidos no trabalho são aplicados à inversão dos parâmetros do fundo marinho usando *"Matched-field Processing"*, de modo a ilustrar-se a vantagem do uso da informação da velocidade das partículas nesta técnica de estimação remota. Verifica-se que o uso do VSA contribui para uma melhoria significativa da resolução de estimação destes parâmetros tais como a velocidade compressional, atenuação compressional e densidade do sedimento, face às tradicionais antenas de hidrófones. A densidade e atenuação compressional são parâmetros normalmente difíceis de serem estimados com elevada resolução usando as antenas de hidrófones, mesmo que tenham uma elevada abertura. Este trabalho mostra que uma antena curta de apenas quatro elementos de sensores vetoriais, consegue obter uma elevada resolução de estimação destes parâmetros bem como uma boa estabilidade dos resultados ao longo do tempo. De realçar que estes resultados podem ainda ser conseguidos usando só a componente vertical da velocidade das partículas.

Esta tese de doutoramento está organizada da seguinte forma: no Capítulo 1 é feita uma introdução à acústica submarina bem como é relatado o estado da arte. Faz-se referência às várias técnicas usadas normalmente nesta área do conhecimento, são descritos os vários trabalhos científicos quer teóricos quer com dados experimentais feitos com o uso do VSA e apresentam-se as motivações e contribuições relevantes e inovadores deste trabalho para a comunidade científica. No Capítulo 2 é feita uma abordagem à técnica de *Beamforming* com ondas planas, onde é realizado um estudo comparativo na estimação da direção de chegada usando antenas de hidrófones e de sensores vetoriais. Várias configurações de antenas de hidrófones são comparadas com a antena linear vertical de sensores vetoriais de modo a mostrar-se a vantagem do uso de um VSA na estimação da DOA. No Capítulo 3 é desenvolvido o modelo de dados que agrupa a pressão com as várias componentes da velocidade das partículas, bem como a teoria relacionada com o estimador de *Bartlett* baseado na informação da velocidade das partículas para a estimação de parâmetros genéricos. Os estimadores propostos são aplicados, com dados simulados, na estimação da DOA e ainda com grau de inovação na estimação de parâmetros do fundo marinho. É mostrado que o VSA exibe uma elevada resolução na estimação destes parâmetros quando comparado com uma antena equivalente de hidrófones. É realizado ainda um breve estudo das perdas por transmissão (*TL - Transmission Loss*) com sinais de alta-frequência em que se compara a

resposta de dois modelos físicos capazes do cálculo da velocidade das partículas, denominados *TRACEO Gaussian beam* e *MMPE - Monterey-Miami Parabolic Equation*. Ambos os modelos mostram resultados do TL na coluna de água semelhantes, tanto para a pressão como para as componentes horizontal e vertical da velocidade das partículas, ilustrando que a resposta impulsiva do canal na banda das altas-frequências tem ainda suficiente estrutura para suportar a estimação dos parâmetros do fundo marinho. O Capítulo 4 descreve a experiência MakaiEx'05 em termos geométricos, informação da batimetria da área assim como os sinais emitidos durante a experiência. É descrito ainda a antena de sensores vetoriais usada neste trabalho, bem como os resultados obtidos com ela em termos de direção de chegada das várias fontes (usando sinais de baixa e alta-frequência), para os três dias em que o VSA esteve na água. O Capítulo 5 apresenta os resultados experimentais da inversão dos parâmetros do fundo marinho com os sinais de alta-frequência adquiridos pelo VSA, tendo em conta duas técnicas de estimação: comparação das perdas por reflexão obtidas por um modelo e pelos dados experimentais e por *"Matched-field Processing"* baseado nos estimadores propostos com o VSA. Finalmente o Capítulo 6 revela as conclusões obtidas com este trabalho e aponta direções a seguir em termos de investigação com o uso dos sensores vetoriais.

Palavras-chave: Sensores vectoriais, Processamento de antenas, Processamento por ajuste de campo, Tomografia de alta frequência, Inversão geoacústica, Acústica submarina

Contents

List of Figures

List of Tables

Chapter 1

Introduction

Covering almost 75% of the planet, the ocean is a vast, complex, mostly dark world, largely unknown and unexplored by man. Understanding the ocean and its behavior is important to scientists in diverse areas such as oceanography, seismic exploration, weather and climate monitoring, etc., and has barely been touched by today's science and technology [1]. The ocean is essentially opaque to light and electromagnetic radiation but it is transparent to acoustic signals. Therefore, sound is the only practical way to propagate signals to great distances in the ocean. The propagation of sound in the ocean is of vital importance, not only for communication between marine animals but also for finding objects, measuring water depth, currents, or other environmental parameters.

Underwater acoustics is the study of the propagation of sound in water and its interaction with the ocean boundaries (surface and seafloor), consequently underwater acousticians use this knowledge to predict the characteristics of physical and biological parameters of the ocean through which it has traveled, to communicate or to find objects and intruders. As a mechanical wave of energy, sound changes the pressure of the medium. Changes in sound speed can be related to small changes in the average temperature of the ocean which in turn is strongly influenced by the environmental conditions. Sound speed is an empirical function

of temperature, salinity and depth [2] and these parameters are affected not only by seasonal and diurnal changes but also depend on the geophysical properties of the water column and seabed [3].

Ocean acoustic tomography (OAT) is a remote sensing technique used in underwater acoustics to study average temperatures over large regions of the ocean. It was proposed in 1979 by Munk and Wunsch [4, 5] for global ocean monitoring. Due to interest in large scale monitoring, OAT techniques measure the perturbation of sound travel time between a source and a receiver at known locations to estimate sound speed disturbances, and has been thoroughly investigated normally at low frequency (below 2 kHz), both theoretically and experimentally [5, 6, 7].

After the cold war, due to regional conflicts in costal countries, self protection and port entrance security, gas and oil exploration, ocean wave influence, etc., the interest in underwater acoustics shifted to shallow water - say for depths less than 200 m [8]. In shallow water, the interaction of sound with the sea surface and seabed, where it can be reflected and transmitted into the sediments, is particularly relevant. Seabed parameters are generally not known in sufficient detail and with enough accuracy to permit satisfactory long-range predictions [2]. Therefore, the estimation of such parameters with sufficient resolution is important to characterize the environment for underwater acoustic applications. A further complication being that shallow water is usually a noisy environment affected by ship traffic and other human activity along the costal zones.

In order to provide high estimation resolution of ocean parameters using low frequency signals led to large aperture hydrophone arrays with many elements used to cover most of the water column. Paradoxically, large aperture arrays create operational problems as well

as difficulties in deployment and long term operation, even in shallow water. Therefore, the use of high-frequency (HF) signals in OAT (defined here as in the 5-50 kHz band) has become the subject of investigation [9]. This frequency band, historically included torpedo interception, is the subject of renewed interest related to research in acoustic communication, target scattering, HF tomography and bioacoustics. OAT with HF signals (short wave length) can be potentially advantageous in fine resolution of ocean disturbances and seabed parameters characterization over a particular area. Furthermore, using HF signals has operational advantages since it allows for small aperture arrays, and a single system can be used in various acoustical applications such as source localization, underwater communications and geoacoustic inversion.

Recent developments in new piezoelectric materials (PMN-PT crystals) and new electromechanical design have led to a new generation of sensors - the vector sensors [10]. Each vector sensor is constituted by one omni-directional hydrophone and three uni-axial accelerometers. The omni-directional hydrophone is sensitive to the acoustic pressure, in the following termed as acoustic pressure-only; each accelerometer is sensitive to the acoustic particle velocity only along a specific axis while being very insensitive in the other two axes, in the following termed as particle velocity components. Therefore, a vector sensor is able to measure both the acoustic pressure and the three particle velocity components providing the directional capabilities of the sensor. A crucial advantage of vector sensors over hydrophones is the quantity of information obtained from a single point spatial device. The spatial filtering capabilities of vector sensors have become a subject of investigation, predominantely in direction of arrival (DOA) estimation [11, 12, 13, 14]. The potential gain verified in DOA estimation can be extended to other underwater acoustic applications, which potentially

allow for high performance small aperture Vector Sensor Arrays (hereafter VSA). Taking advantage of its directionality and its performance in DOA estimation, the proposal of this work is to estimate geoacoustic and geometric parameters with a VSA of a few elements, to provide better estimation resolution than equivalent arrays of hydrophones (with same number of elements). The ability of a vector sensor to measure signals in one direction while ignoring possible noise sources from other directions can be useful to improve the estimation of ocean parameters. Additionally, it is intended to use HF signals, consequently a VSA can be very compact and easy-to-deploy, providing a good alternative to be embarked on reduced dimension autonomous platforms or vehicles where space is very limited.

1.1 State of the Art

Acoustic sensor array signal processing is an active area of research, whose objective is to estimate relevant spatial parameters such as the number of emitting sources and their locations - range, depth and DOA, through the analysis of the data collected at several sensors. H. Krim and M. Viberg [15] discussed and summarized many of the parameter estimation methods in sensor array processing. First of all, a signal processing technique known as beamforming where the objective is to estimate the signal DOA. The signals from different sensors are delayed, weighted and summed in order to create a pattern whose maximum gives the true source DOA estimate. Beamforming techniques can be classified in two categories, depending on how the weights are chosen: data independent (or conventional beamformers) and statistically optimal [16]. Conventional beamformers use a fixed set of weights independent of the array data (only the information about the location of the sensors in space is used) and they are selected according to a specified response for all signal and interfer-

ence scenarios. In contrast, in statistically optimal beamformers the weights are selected based on the statistics of the array data; such selection automatically optimizes the array response according to given criteria. Multiple Sidelobe Canceller (MSC), Reference Signal, Maximization of Signal to Noise Ratio (Max SNR) and Linearly Constrained Minimum Variance (LCMV) are different approaches of implementing optimum beamformers. However, the statistics of the array data are usually unknown and may change with time, so adaptive algorithms such as Least Mean Squares (LMS) or Recursive Least Square (RLS) are used to determine weights that converge to the statistically optimal solution [16].

Beamforming was extended to the estimation of other parameters and a generalized beamformer was introduced by Hinich [17] and Bucker [18] as a source localization method - Matched-Field Processing (MFP). MFP consists of correlating the measured signal at the sensors with the modelled replica field, in order to obtain the parameter that gives the highest correlation, which in fact is the parameter estimate. Hinich was the first to examine source localization, using the spatial complexity of the underwater acoustic field to localize the source (in range and depth) with a vertical array, but Bucker was credited with the formulation of MFP, using realistic environmental models and introducing the concept of ambiguity surfaces. Since this technique is a simple correlator, the most widely used processor is the Bartlett processor, which directly correlates the measured data with the modelled replica data. The accuracy of range and depth estimation in conventional MFP depends on the accurate knowledge of the ocean environmental parameters. To overcome this stringent requirement several methods were introduced. Yang [19] proposed a method of range and depth estimation based on modal decomposition, where the reflection/scattering loss parameters needed to accurately model the acoustic field as a function of range and depth are not

required. The author estimated range and depth, either separately or simultaneously, by decomposing the array data and beamforming on the mode amplitudes. The normal mode amplitudes were used for source depth estimation while the phase differences between the normal modes were used to source range estimation. This method was successfully applied for data acquired during the 1982 FRAM IV experiment in the Arctic Ocean. Another source localization method, which eliminates the need of an accurate knowledge of the ocean environmental parameters by including these parameters in the search space, was introduced by M. Collins in 1991 [20], namely Focalization. Focalization is a method where both the source parameters and the environmental parameters are unknown or partially unknown. The environmental parameters are adjusted in an attempt to localize the acoustic sources, i.e., simultaneously focus and localizes. But if MFP is sensitive to the environmental information and if the source locations are known or partially known, this technique can also be used to invert the environmental parameters. This concept has demonstrated an increased interest in underwater acoustics relating to a wide range of inversion problems - generically called Matched-Field Inversion (MFI) [21]. However, a first work suggesting that MFP could be used to environmental parameters was presented in 1987 by A. Tolstoy in [22]. The author examined the estimation of *rms* surface roughness for a known source with simulated data. Then, applications of MFI were suggested for tomography, where the estimation of deep water sound speed profiles was first proposed in [23] and later extended in [24] for the estimation of geoacoustic profiles in shallow water environments.

Thus, the 90s saw the beginning of the use of the MFP concept for environmental inversion. In particular, geoacoustic inversion based on MFI techniques is a research area that has had an increasing interest during the last two decades. Geoacoustic inversion is a none

intrusive remote sensing technique of great importance, since the geoacoustic properties such as sediment layer thickness, sediment sound speed profiles, density and attenuation, can be rapidly and efficiently estimated; in contrast with direct measurements, which are difficult and almost impossible to survey any region extensively [21]. In fact, assessing seabed parameters with *in situ* measurements such as grabs and cores [25], is an expensive task and time consuming process and only a limited area, where the measurements are collected, is characterized. In [26] properties of the ocean bottom were estimated using the concepts of MFI. The inversion method was illustrated for seabed parameters (sound speed, density, attenuation and layer thickness) in a range independent environment and for bathymetry and bottom sound speed in a range dependent environment. However, the number of parameters to be estimated can be extremely large and an exhaustive search of the optimal solution could be very difficult. Thus, with the development of numerical models and the increase of computer power, the inversion of the geoacoustic parameters can be posed as an optimization problem using techniques, such as genetic algorithms [27, 28], simulated annealing [29, 30] or even based on a Bayesian formulation [31] to address a large number of parameters over a wide parameter search space.

In the implementation of those inversion methods is common to use vertical arrays of hydrophones to cover almost all the water column. In order to simplify the array systems and to create easier deployment and lower cost systems, research involving different array configurations suggested that it is possible to estimate seabed parameters from data acquired by horizontal hydrophone arrays, which could be towed [32, 33] or bottom moored [34]. Furthermore, in [35] it was proposed and tested with experimental results a geoacoustic inversion technique with a single hydrophone and broadband signals. The technique demon-

strated that a single transmission of a broadband (200-800 Hz) coded signal received at a single depth was sufficient to correctly estimate bottom properties. The results were compared with MFP of multitone data received on a vertical hydrophone array showing good agreement. Other experimental results of acoustic inversion methods with broadband signals and short aperture arrays were presented in [36].

At this point, it should be remarked that geoacoustic inversion is not only based on methods where the measured data is directly correlated with the modelled data to estimate the parameters of interest. The inversion of seabed parameters could also be obtained from measurements of the reflection coefficient as a function of the angle of incidence (or grazing angle). The technique takes advantage of the fact that the reflection loss at the water-sediment interface and, sound speed and attenuation profiles in the sediment influence the acoustic propagation. An inversion process based on the Biot's theory context is presented in [37], where the sensitivity of the reflection coefficient due to the geophysical properties (such as porosity, grain density, permeability, pore size, etc.) were discussed. Another method for estimating the elastic properties of the seafloor sediment, based on the reflection amplitude measurements from explosive charges, is described in [38]. This work noticed that the relationship between the signal amplitude and the angle of incidence can be described by the reflection coefficient, which was calculated for different values of density, compressional and shear-wave speeds. Another method of geoacoustic inversion based on the reflection loss estimation was proposed by C. Harrison *et al.* in [39]. The method consists on the extraction of the reflection loss from the vertical array measurements of ambient noise, such as surface generated noise in the 200-1500 Hz band. The method uses experimental data acquired on a 16 m vertical hydrophone array with 32 elements at half meter spacing. This work was

extended in [40] to 1-4 kHz using an array of 32 elements at 0.18 m spacing and length of 5.58 m. The ratio between downward and upward beam responses is an approximation of the bottom reflection coefficient, and the reflection loss versus angle is directly found by comparing the noise intensity arriving from equal down and up elevation angles. Then, comparisons between measurements and predictions provide the number of layers, their thickness and the respective bottom parameters. This technique will be described in more detail in Chapter 5.

The previously described techniques have been applied using acoustic pressure signals acquired by omni-directional hydrophones, which sense the acoustic pressure equally in every direction. Since the 1980s, the idea of measuring particle velocity beyond the acoustic pressure field appeared in underwater acoustics to improve the DOA estimation. The U.S. Navy has been using a DIFAR (DIrectional Frequency Analysis and Recording) sonobuoy to detect submarines, using two horizontal particle velocity components as well as the pressure. The horizontal particle velocity allows to determine the azimuth of low frequency sounds below 2 kHz. The DIFAR concept was only used for scientific purposes in the 90s [41], where a vertical line array of DIFAR sensors was designed and constructed by the Marine Physical Laboratory's. The main features of this DIFAR array were described in [42], where each element consisted of three orthogonally-oriented geophones to measure the corresponding particle velocity components and a hydrophone to measure the acoustic pressure. The array was constituted by 16 sensor elements, with 15 m spacing between elements, in the 10-270 Hz band; each element had a compass to measure the orientation of the two horizontal geophones with respect to magnetic North. The concept of acquiring the particle velocity in one direction could resolve ambiguities, normally present when only omni-directional

hydrophones are used. D'Spain *et al.* in [43] presented beamforming results with data collected from the first sea test of a DIFAR array. The DOA estimation results for a towed source, using conventional and adaptive beamforming methods, provided surprisingly good spatial resolution in azimuth estimation, in addition to the vertical resolution of the array's 225 m aperture.

The use of directional sensors becomes a subject of investigation, where several authors have been conducting research on theoretical aspects of vector sensor processing, initially for air [44, 45] and then extended for underwater acoustics [11, 12, 13]. Tabrikian *et al.* [44] proposed an efficient electromagnetic vector sensor configuration for source localization in air. The authors found that the minimum number of sensors, capable of estimating the DOA of an arbitrary polarized signal from any direction, is two electric and two magnetic sensors referred to as quadrature vector sensor. Nehorai and Paldi developed an analytical model, initially for electromagnetic sources [45], and then extended it to the underwater acoustic case [11], where an ideal vector sensor, consisting of one omni-directional pressure sensor and three particle velocity-meters that are sensitive in a specific direction (x, y or z), was considered. The performance of a VSA was compared to that of a hydrophone array for DOA estimation and it was suggested that this type of device has the ability to provide directional information, with a clear advantage in DOA estimation and gives rise to an improved accuracy. The authors also derived a compact expression for the Cramér-Rao Lower Bound (CRLB) on the estimation errors of the source DOA. Thus, the vector sensors emerged as a potential competitor to traditional omni-directional hydrophones. Cray and Nuttall [12] applied the plane-wave beamforming to particle velocity sensors and compared the results with that of hydrophone arrays. The authors show that the VSA has an increased

directivity gain not possible to achieve with an equivalent number of hydrophones. Wan *et al.* [13] performed a comparative simulation study of DOA estimation using classic methods such as MUltiple SIgnal Classification (MUSIC) and Minimum Variance Distortionless Response (MVDR) estimators, with vector sensors, gradient sensors and pressure sensors. The results show that VSAs outperform gradient hydrophone arrays, which consist of three pressure hydrophones symmetrically mounted in a circle.

Recently, theoretical work using quaternion based algorithms has been proposed for processing VSA data for DOA estimation [46, 47, 48]. Quaternions are a four dimensional hypercomplex number representation, where each quaternion is described by four components: one real and three imaginary numbers. In [46, 47, 48], the real part was attributed to the acoustic pressure and the imaginary part to the three particle velocity components. The authors proposed a quaternion based MUSIC algorithm (Q-MUSIC) for DOA and polarization parameter estimation. The results were compared to the classical MUSIC algorithm for scalar sensor array and to another MUSIC-like algorithm for VSA (V-MUSIC). It was shown that Q-MUSIC is clearly more accurate than classical MUSIC and presents equivalent results when compared to V-MUSIC; the Q-MUSIC reduces the computational memory requirements for covariance matrix estimation, which may be relevant for specific applications.

Since 2006, research involving experimental VSA data appeared in the scientific literature. Lindwall [49] showed the advantage of using vector data over scalar data for image structures in a 3-D volume. This was supported by a scale experiment with a vector sensor in a water tank. The author used the same type of vector sensor considered in this thesis, which was specially designed for use in water by the Naval Underwater Warfare Center in collaboration with Wilcoxon Research Inc. This type of sensor has long been desired by the U. S. Navy to

provide directional information on target noise sources. Shipps and Abraham [10] described the new vector sensor developed for the U.S. Navy, which can be particularly useful in underwater acoustic surveillance and port security. VSAs can improve the detection or localization of acoustic signals compared with hydrophone arrays and have the ability, for example, to detect acoustic signals from an intruder that are quieter than the surrounding noise sources, which can not be detected by a hydrophone array [10]. The VSA is able to estimate both elevation and azimuth angles, eliminates the well known left/right ambiguity of linear arrays and provides better resolution than hydrophone arrays. The crucial advantage of VSA verified in three dimensional DOA estimation can be potentially applied to the estimation of other geometric or environmental parameters. Therefore, applications of the VSA appear in underwater communications [50, 51] and geoacoustic inversion [52]. The results presented in [50, 51] suggest that a single vector sensor has better performance than a single pressure sensor or even pressure-only arrays. It was found that a single vector sensor improves significantly the signal-to-noise ratio (SNR) when compared with pressure-only arrays. The usefulness of particle velocity information in underwater communications was demonstrated and the vector sensor can offer an attractive acoustic communication solution for compact underwater platforms and underwater autonomous vehicles, where space is very limited. A geoacoustic inversion scheme based on experimental data measured by a VSA using low frequency signals (central frequency 400 Hz), was proposed by Peng and Li [52]. The authors showed that the vector sensor can reduce the uncertainty on the estimation of the sediment compressional speed.

High-frequency acoustics is another, albeit unexpected, emerging research topic [8]. HF signals in underwater acoustics can only be used for short distances because they suffer

of high attenuation in the ocean volume. Moreover, the propagation of short wave length (HF) signals is highly influenced by bottom and surface scattering, hence difficult to model. However, for surprise of many, the sound energy is not annihilated by contact with boundaries and it can reflect many times and still yield distinct echoes [53]. Some theoretical and experimental works proved that environmental properties can be characterized using HF signals [40, 54, 55]. A pioneer work in HF tomography was presented by Lewis *et al.* [9]. This work revealed that arrival times between source-receivers at short distances (3-5 km) at frequencies in the 8-11 kHz band were readily detectable and distinguishable. Furthermore, the use of HF signals provides [53, 55]:

1. The use of small aperture arrays due to short wave length;

2. The use of small sources to emit the signals;

3. A fine resolution of ocean variations in Ocean Acoustic Tomography and Matched-field Processing applications;

4. The characterization of bottom parameters in a particular area.

Additionally, the usage of HF signals in underwater acoustic communications is important, since a high bandwidth is required in order to transmit a higher data rate. In [51] a time reversal multichannel receiver was proposed to exploit the use of particle velocity information for underwater acoustic communications, using experimental data acquired during Makai experiment 2005. The authors compared the results of a single vector sensor with a pressure-only sensor array in HF band. Such results show that the vector sensor, besides a significant size reduction, outperforms the SNR at short communication ranges. Combining HF signals

with the VSA can be advantageous to increase the resolution of ocean parameters estimation and to reduce the array's aperture, providing more portable and compact systems to be used in underwater acoustics applications.

The present work addresses the above mentioned subjects aiming to contribute to the development of more efficient acoustic remote sampling systems. A particle velocity-pressure joint data model (VSA data model) and a VSA-based Bartlett estimator are proposed, in order to demonstrate the capabilities of using a VSA in ocean parameter estimation. The highlighted advantages of the VSA-based Bartlett estimator over pressure-only estimator will be tested for DOA estimation using low and HF signals, and most importantly for seabed parameter estimation using HF signals.

1.2 Work motivation and Contributions

Traditionally, source localization - range, depth and DOA - and the estimation of other parameters such as ocean bottom parameters, are found using low frequency signals and long hydrophone arrays, in order to get as higher estimation resolution as possible. In fact, long hydrophone arrays are not a practical solution to be embarked on reduced dimension autonomous moving platforms or vehicles where space is limited. During the last two decades, the use of directional sensors captured the attention of the scientific community; vector sensor arrays were designed in order to outperform traditional hydrophone arrays in DOA estimation. In fact, vector sensors have the ability to provide directional information because they measure the components of particle velocity along each spatial direction. The high directivity of a single vector sensor allows a VSA to emerge as a potential alternative to traditional hydrophone arrays, leading to the usage of short arrays.

Most of the research involving vector sensors is related to DOA estimation in a simulation context, or using low frequency signals; in both cases it was shown the feasibility of vector sensors for DOA estimation and it was also shown that vector sensors exhibit an improved performance over pressure-only sensors. From such studies the following questions arise:

- What are the common and differentiating features of the particle velocity field when compared to the pressure field?
- Why does the VSA performance increase when compared with equivalent hydrophone arrays?
- Can the high directivity of the VSA be used with advantage for the estimation of other ocean parameters such as water column temperature or seabed parameters?
- Can the potential gain of the VSA be extended to three-dimensional source localization and geoacoustic inversion using a small aperture VSA, acquiring HF signals?
- How is the sensitivity of each particle velocity component to a particular environmental parameter?

The main objective of the present work is to answer these questions (and additional others) along the discussion presented in the following sections. To such end, standard estimation techniques were extended in order to account for particle velocity, and extensive tests were performed based on simulations and on the processing of experimental data. On the basis of the obtained results the following contributions can be highlighted:

- A particle velocity-pressure joint data model - VSA data model - is derived, taking into account the relationship of the particle velocity with the acoustic pressure from

the linear acoustic equation (Euler's equation). The VSA data model is based on a ray physical description, using the Gaussian beam approximation of the ray pressure [56];

- An estimator based on an extension of the conventional pressure-only Bartlett estimator including particle velocity information is proposed. Two VSA-based Bartlett estimators are derived for generic ocean parameter estimation, bearing in mind the VSA data model with and without the acoustic pressure. The performance of the VSA-based Bartlett estimators relative to the pressure-only Bartlett estimator is analytically deduced, clearly showing the advantages of the VSA over pressure-only sensors. It will be seen that the VSA-based Bartlett estimators are proportional to the pressure-only Bartlett estimator, where the terms of proportionality are given by a directivity factor. Such directivity factor is the crucial advantage of using particle velocity information in underwater acoustic estimations, providing an improved sidelobe reduction or even supression and increasing the estimation resolution of the ocean parameters;

- The proposed VSA-based Bartlett estimators are tested, with simulated and experimental data, for DOA estimation and for geoacoustic inversion. The experimental data considered in this work was acquired by a four-element vertical VSA in the 100-14000 Hz band during Makai experiment 2005 (MakaiEx'05). The MakaiEx'05 was organized by HLS Research and was designed to bring together a number of researchers with interests in different aspects of HF acoustics (acoustic communications, target scattering, HF tomography, etc.). This experiment was conducted from 15 September to 2 October, 2005, off Kauai Island, Hawaii (USA) [55];

- The study of DOA estimation, which is a pre-processing requirement for the analysis

of the experimental data, will start with low frequency ship's noise signature (the VSA was tied to a vertical cable fairly close to the stern of Research Vessel Kilo Moana), where the orientation of the VSA axis in the horizontal plane, initially unknown, is estimated. Further, the horizontal orientation is validated with known sound sources DOA in the HF band.

- Finally, the most important contribution is the study of the application of the VSA for geoacoustic inversion. To the best of our knowledge, the application of a few elements VSA with HF signals in geoacoustic inversion is an original contribution in this research area. A small aperture VSA with HF signals, acquired during MakaiEx'05, is used for bottom properties estimation using two inversion VSA-based techniques. In the first one, the reflection coefficient estimator proposed by C. Harrison *et al.* [39, 40] is adapted for the vertical measurements of the VSA, taking into account the horizontal discrimination capability of the VSA and the corresponding beam extracted for vertical resolution analysis. The bottom reflection loss deduced by up/down beam response ratio and the modelled reflection loss using the SAFARI model [57] are compared for a candidate sets of seabed parameters, number of layers and their thickness. In the second one, the derived VSA-based Bartlett estimators are proposed for MFI in order to illustrate the advantage of including particle velocity information in this estimation problem. The use of the VSA contributes to a higher estimation resolution of parameters, such as sediment compressional speed, density and compressional attenuation, than hydrophone arrays. Density and compressional attenuation are parameters which are difficult to estimate using traditional hydrophone arrays, even with large aperture arrays. Moreover, it is shown that the highest estimation resolution of these parameters

can be achieved using only the vertical particle velocity component.

The geoacoustic inversion results obtained with VSA-based Bartlett estimators show good agreement with those obtained with the bottom reflection curves and with the historical data of the MakaiEx'05 area. It is important to remark that, the frequency band is well above that traditionally used in geoacoustic inversion. An interesting outcome of this work is that the channel impulse response has sufficient structure to support estimation of seabed parameters in the considered HF band.

1.3 Work dissemination

The determination of the DOA of low and high-frequency sound sources, using the beamforming technique with the experimental data considered in this work, was discussed in [58]. The results of bottom structure and respective geoacoustic parameters, applying the method proposed by C. Harrison *et al.*, were presented in [59]. Preliminary results of geoacoustic inversion based on VSA-based Bartlett estimator were presented in [60], where the particle velocity field replicas were generated using the Gaussian beam model - TRACEO [56], which is currently under development. To the best of our knowledge this work was the first that presented experimental results of geoacoustic inversion using a VSA and high-frequency signals. The methods described in [59, 60] were extended in [61], where the VSA data model and the related Bartlett estimator, based on particle velocity measurements for generic parameters estimation, were presented. The latter publication also presents the applicability of the VSA-based Bartlett estimator for DOA estimation and seabed geoacoustic inversion, using simulated and experimental data. Recently, in [62, 63, 64] a summary of the experimental results of VSA data processing to estimate geometric (range and depth) and geoacoustic

parameters was made.

1.4 Organization of this thesis

This thesis report is organized as follows: Chapter 2 presents a comparative study for DOA estimation using hydrophone and vector sensor arrays; several configurations of hydrophone arrays are compared with that of VSA to enhance the advantages of the usage of vector sensors. Chapter 3 develops the vector sensor data model and the theory related to the Bartlett estimator based on particle velocity for generic parameter estimation. The derived VSA-based Bartlett estimators are applied, with simulated data, for DOA estimation and, most importantly, for seabed parameter estimation. It is shown that the VSA is able to increase the estimation resolution of the seabed parameters when compared with an equivalent hydrophone array. A brief study of the transmission loss with HF signals is presented and the results of the TRACEO Gaussian beam model are compared with those of Monterey-Miami Parabolic Equation (MMPE) model. The two models are capable of particle velocity calculations and, regarding the water column only, both models show similar acoustic pressure, horizontal and vertical particle velocity fields at the receivers. Chapter 4 describes the VSA in the Makai Experiment 2005, providing a general description of the bathymetry, geometry information as well as the emitted signals. The chapter also reports the experimental results for DOA estimation, considering low and HF signals acquired during the MakaiEx'05 sea trial. Chapter 5 presents the inversion of the seabed parameters with the HF VSA data taking into account two VSA-based techniques: 1) by forward modelling of reflection loss and data comparison, and 2) by MFI based VSA Bartlett estimators. Finally, Chapter 6 draws the conclusions, the achievements of this thesis and higlights future directions of research.

Chapter 2

DOA estimation using hydrophones and a VSA

Underwater acoustic signal processing emerged as an active area of research centered on the ability to collect data from several sensors (an array) in order to estimate parameters of interest. One application of great importance is the estimation of the direction of arrival (DOA), in which the bearing of the acoustic sources is determined. The determination of the bearing (or arrival angle) is usually performed using a technique called beamforming, where the data from different sensors are weighted and summed, creating a pattern whose maximum gives the true bearing. Traditionally, the acoustic data is collected by hydrophones located at different points in space, which can be sensitive to the pressure and to the pressure gradient (which in fact represents particle velocity) [65].

Typically, in underwater acoustics, piezoelectric ceramic hydrophones are used to detect the acoustic pressure, a scalar quantity, and convert this pressure into a proportional output voltage, presenting no directional sensitivity; such acoustic pressure-only sensors are omni-directional hydrophones. Recent developments on new piezoelectric materials allowed sensors (known as vector sensors) to be sensitive to both the magnitude and the direction of the acoustic wave. Vector sensors have the ability to provide directional information due to their

response to particle motion [65]. Each particle velocity component can be determined either by pressure gradient using two omni-directional hydrophones (whose dimensions are small compared to the wavelength) connected as a dipole, or by using accelerometers (at present time the most common device for vector sensors) as the velocity measuring mechanism. In order to determine the particle velocity components with accelerometers the vector sensor requires three accelerometers, one for each space direction. The pressure gradient ∇p is directly related to the acceleration, $\mathbf{a}$, through the following equation:

$$\mathbf{a} = -\frac{1}{\rho}\nabla p, \tag{2.1}$$

where ρ represents the density of the medium. Taking into account that the acceleration corresponds to the temporal derivative of velocity $\mathbf{V}$, the previous expression can be written as [65]:

$$\rho\frac{\partial \mathbf{V}}{\partial t} = -\nabla p, \tag{2.2}$$

where t represents the time variable. For sinusoidal motion (2.2) can be written in the frequency domain as:

$$\mathbf{v} = \frac{i}{\omega\rho}\nabla P. \tag{2.3}$$

The directional characteristics of vector sensors and the advantage of using arrays of vector sensors in DOA estimation have been studied by several authors [11, 12, 13]; it is however convenient to review and discuss some features that influence DOA estimation and to understand the advantage of using vector sensors in this case. Thus, the objective of this chapter is to compare, through simulations, the performance of the VSA with different spatial configurations of hydrophone arrays, using plane-wave beamforming for DOA estimation.

2.1 Plane-wave beamforming

Beamforming is a spatial filtering approach where the data acquired by an array of sensors, located at a given spatial position, are weighted and delayed in order to coherently sum the signals from a given direction, while rejecting signals from other directions (interference signals). The beamformer improves the signal of interest and allows the cancellation of interference signals when compared with a single sensor [15, 16]. This way, the array response is steered in one direction at a time forming beams and the beam which has the highest energy indicates the true DOA estimate. The knowledge of the position of each sensor (receiver), the time delay (or spacing) between each sensor and the wave sound speed propagation are fundamental for DOA determination.

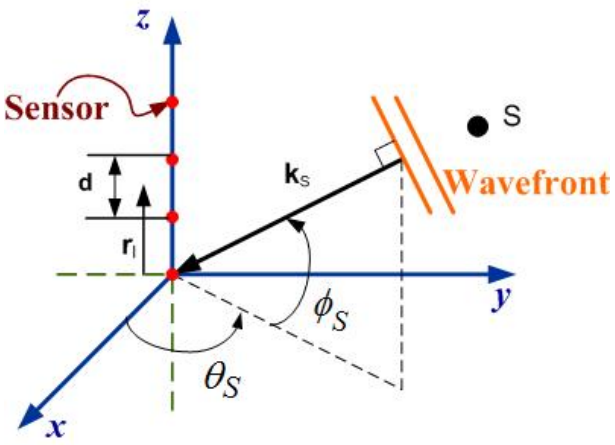

Figure 2.1: Array coordinates and geometry of acoustic plane-wave propagation emitted by source S, characterized by the wavenumber vector $\mathbf{k}_s$, with azimuth (θ_S) and elevation (ϕ_S) angles. The sensors are located along the z-axis with d spacing between sensors and the first element is at the origin of the Cartesian coordinate system, where $\mathbf{r}_l$ is the sensor vector position.

Assuming that the medium is homogeneous and the source-receiver range is much larger than the distance between each receiver (far field condition), the plane-wave approximation can be considered. Fig. 2.1 presents the array coordinates and the geometry of acoustic

plane-wave propagation for three-dimensional DOA estimation, considering a signal emitted by a single source (S), at a particular point in space; the plane-wave impinges onto an array of L sensors from a given direction (θ_s, ϕ_s), where $\theta_s \in [-\pi; \pi]$ is the azimuth angle and $\phi_s \in \left[-\frac{\pi}{2}; \frac{\pi}{2}\right]$ is the elevation angle. The signal emitted by the source at frequency ω_0 and direction (θ_s, ϕ_s) is characterized by a wavenumber vector $\mathbf{k}_s$:

$$\mathbf{k}_s = -\frac{\omega_0}{c}\left[\begin{array}{ccc} \cos(\theta_s)\cos(\phi_s) & \sin(\theta_s)\cos(\phi_s) & \sin(\phi_s) \end{array}\right], \tag{2.4}$$

where c is the sound speed.

Thus, in the frequency domain a narrowband signal at frequency ω_0 as observed on a L omni directional sensor array, considering a noise free case, is given by:

$$\mathbf{y}_p(\omega_0, \theta_s, \phi_s) = S_0(\omega_0)\left[1, \cdots, \exp(-i\mathbf{k}_s.\mathbf{r}_l), \cdots, \exp(-i\mathbf{k}_s.\mathbf{r}_L)\right]^T, \tag{2.5}$$

where $S_0(\omega_0)$ is the amplitude of the signal emitted by the source and $\mathbf{r}_l$ is the lth sensor vector position.

For a given direction (θ, ϕ) the beam power response is written by:

$$b_p(\omega_0, \theta, \phi) = |\mathbf{y}_p(\omega_0, \theta_s, \phi_s)\mathbf{e}_p^H(\omega_0, \theta, \phi)|^2, \tag{2.6}$$

where the vector $\mathbf{e}_p$ is the weighting vector for the acoustic pressure and is given by:

$$\mathbf{e}_p(\omega_0, \theta, \phi) = \left[1, \cdots, \exp(i\mathbf{k}.\mathbf{r}_l), \cdots, \exp(i\mathbf{k}.\mathbf{r}_L)\right]. \tag{2.7}$$

Therefore, a possible estimator $(\hat{\theta}_s, \hat{\phi}_s)$ of (θ_s, ϕ_s) is the direction (θ, ϕ) which maximize the beam power response of Eq. (2.6) as:

$$(\hat{\theta}_s, \hat{\phi}_s) = \arg\left\{\max_{(\theta,\phi)} b_p(\omega_0, \theta, \phi)\right\}. \tag{2.8}$$

When $(\theta, \phi) = (\theta_s, \phi_s)$ the output signals are coherently summed and the power result of (2.6) is maximum, indicating the true source DOA estimate.

2.2 Three-dimensional DOA estimation using hydrophone arrays

The acoustic receiving pattern or beam pattern is the relative sensitivity of a receiver as a function of a spatial angle for a given frequency. The distance between each sensor, the frequency of the emitted source, the configuration of the array and the number of sensors influence the resolution of the beam pattern, i.e., the ability to distinguish sources with close DOA. Depending on the array configuration, the left/right ambiguity of the source DOA may or may not be present.

Taking into account the equispaced array (assumed linear of spacing d and located along the z-axis, Fig. 2.1), the distance (d) between each sensor is related to the design frequency of the array, at which the spacing is equal to the half wavelength, and is provided by the Nyquist theorem:

$$d \leq \frac{\lambda}{2} = \frac{c}{2f_{max}}, \tag{2.9}$$

where λ is the wavelength, c is the sound speed and f_{max} is the maximum frequency present in the emitted signal.

For example, if d =1 m and c =1500 m/s the design frequency of the array is 750 Hz. So, for frequencies above 750 Hz spatial aliasing occurs due to an insufficient spatial sampling of the acoustic field. Fig. 2.2 illustrates the beam pattern for an azimuth angle of 40°, considering a linear horizontal array of 9 equispaced sensors at $d = 1$ m. On the one hand, for frequencies below the array design frequency (750 Hz), the beam pattern has a main lobe

which is wider as the frequency decreases. On the other hand, when the frequency is above the array design frequency (750 Hz), spatial aliasing appears and provides two lobes with equal amplitude, consequently two possible values for the azimuth angle are obtained.

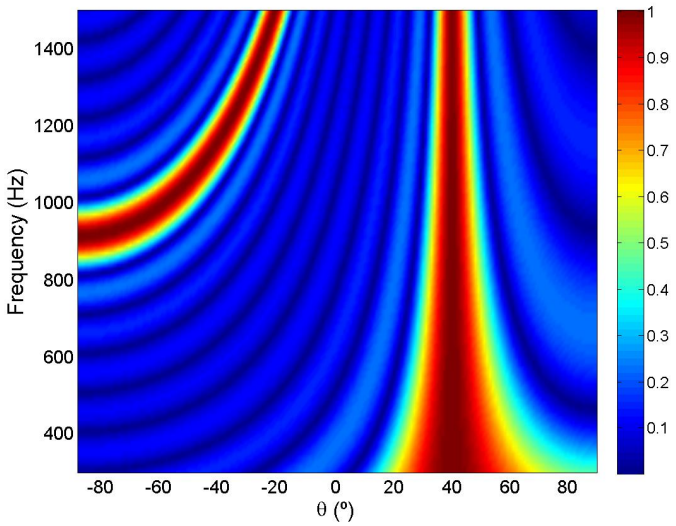

Figure 2.2: The normalized beam pattern of 9 equispaced sensors with 1 m spacing obtained for a source azimuth direction of $\theta_s = 40°$ in the 300-1500 Hz frequency band with $c = 1500$ m/s.

The array beam pattern does not only depend on the working frequency but also on the geometrical configuration of the array. Therefore, in next sections, the beam pattern characteristic of a variety of spatial hydrophone array configurations is addressed and compared to that obtained with a VSA. Ambiguity surfaces for different array configurations, such as the linear, the planar and the cubic configurations, are discussed for a source DOA of $(\theta_s, \phi_s) = (40°, 20°)$, with 8 equispaced hydrophones, for the latter configuration and 9, for the formers, at 1 m spacing and for a frequency of 500 Hz.

2.2.1 Linear array configuration

The general configuration of a vertical linear array is shown in Fig. 2.3 (a), with the hydrophones along the z-axis and the first hydrophone at the origin of the Cartesian coordinate

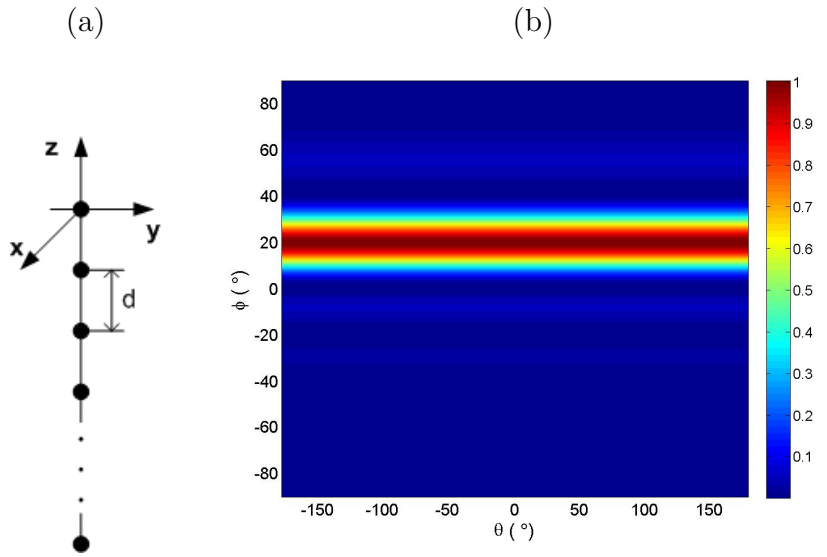

Figure 2.3: Vertical linear array of 9 equispaced sensors with 1 m spacing (a) and the normalized beam pattern obtained for $c = 1500\,\mathrm{m/s}$, at frequency 500 Hz and source DOA $(\theta_s, \phi_s) = (40°, 20°)$ (b).

system. The corresponding normalized ambiguity surface (or beam pattern) for such array, obtained with the plane-wave beamformer (2.6) is shown in Fig. 2.3 (b). This figure reveals that only the elevation angle (ϕ_s) is obtained due to the omni-directionality of the hydrophones in the horizontal plane; such horizontal omni-directionality is caused by the vertical linear configuration of the array. That is a consequence of the inner product between $\mathbf{k}$ and $\mathbf{r}_l$ in Eq. (2.7), which depends only on the elevation angle ϕ. The hydrophone is designed to be equally sensitive to every direction so, in this case, the azimuth angle can not be determined. As shown by the three-dimensional representation view of the beam pattern presented in Fig. 2.4, the vertical linear hydrophone array is "blind" in the azimuthal direction.

The number of sensors influences the estimation resolution of the beam pattern function because more terms are coherently summed in Eq. (2.6). The one-dimensional cross section at azimuth 40° of the beam pattern considering 9, 20 and 50 hydrophones, is shown in

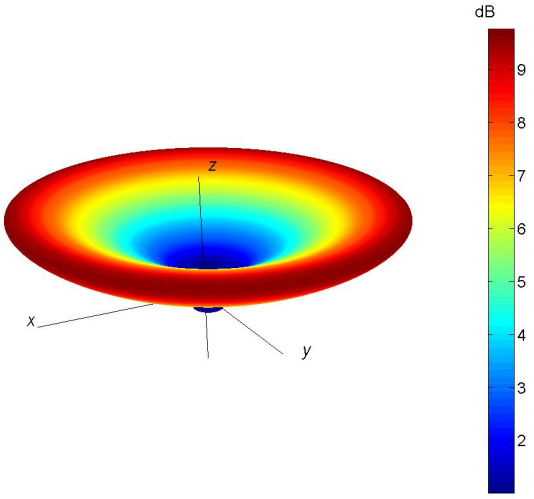

Figure 2.4: Three-dimensional representation view of the beam pattern considering 9 equispaced sensors with 1 m spacing in the vertical linear configuration, at frequency 500 Hz and source DOA $(\theta_s, \phi_s) = (40°, 20°)$.

Fig. 2.5. This figure reveals that as the number of hydrophones increases the resolution of the elevation angle improves. Thus a proper selection of the number of hydrophones allows to resolve the arrival angles of closely spaced sound sources.

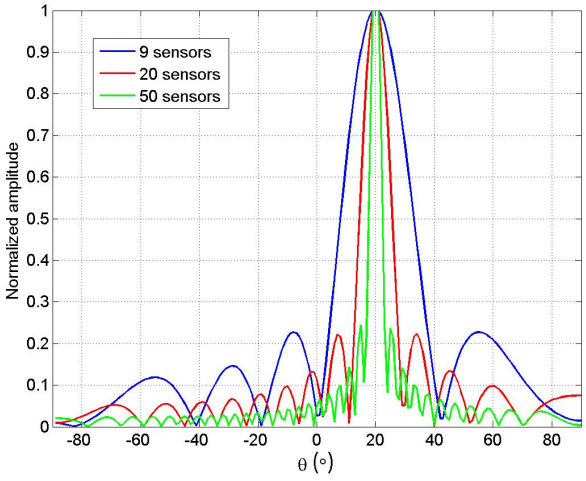

Figure 2.5: One-dimensional cross section of the normalized beam pattern obtained for 9, 20 and 50 equispaced hydrophones with 1 m spacing, for $c = 1500$ m/s, at frequency of 500 Hz and source DOA $(\theta_s, \phi_s) = (40°, 20°)$.

Another possible configuration of the linear array is the horizontal array. The configu-

ration of such array is shown in Fig. 2.6 (a), with the hydrophones along the y-axis. The corresponding normalized beam pattern is shown in Fig. 2.6 (b). For this case the vector $\mathbf{r}_l$ in (2.7) has a non zero y-component; thus the inner product $\mathbf{k}.\mathbf{r}_l$ depends only on $[\sin(\theta)\cos(\phi)]$, giving rise to a circular ambiguity surface due to the horizontal position of the sensors. This ambiguity surface is caused by the omni-directionality of the hydrophones (in this case in the vertical plane), which is illustrated in the three-dimensional view in the Fig. 2.7.

(a) (b)

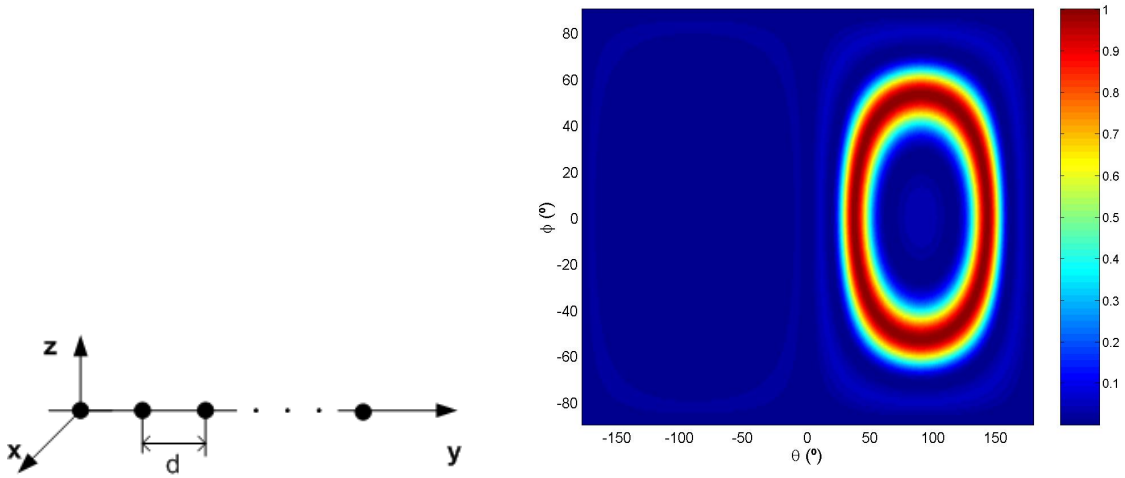

Figure 2.6: Horizontal linear array of 9 equispaced sensors with 1 m spacing (a) and the normalized beam pattern obtained for $c = 1500\,\mathrm{m/s}$, at frequency 500 Hz and source DOA $(\theta_s, \phi_s) = (40°, 20°)$ (b).

2.2.2 Planar array configuration

The planar horizontal configuration is shown in Fig. 2.8 (a) and the planar vertical configuration is shown in Fig. 2.8 (b); in both cases the arrays contain 9 equispaced sensors with 1 m spacing. The corresponding normalized beam pattern are shown in Fig. 2.8 (c) and (d), respectively. The beam pattern shown in Fig. 2.8 (c) reveals not the well known left/rigth ambiguity but an up/down ambiguity. Additionally, the elevation angle is obtained with

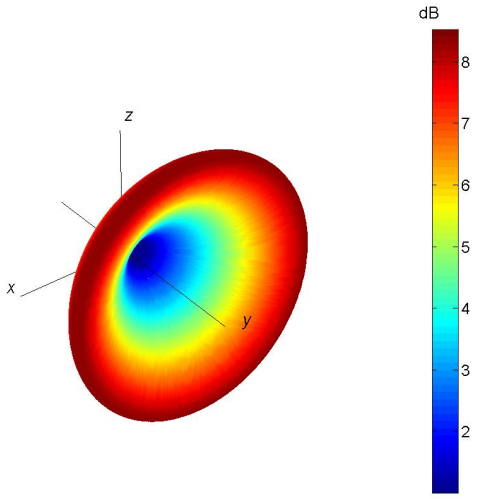

Figure 2.7: Three-dimensional representation view of the beam pattern considering 9 equispaced sensors with 1 m spacing in the horizontal linear configuration, at frequency 500 Hz and source DOA $(\theta_s, \phi_s) = (40°, 20°)$.

two maxima at the angles of (20°) and (-20°) for the true azimuth of (40°). Therefore, the horizontal planar configuration is not able to distinguish whether the plane-wave is coming from the upper side or the lower side of the planar array; this happens because the plane-wave impinges onto the array at equal time-delay from the two directions. When the vertical planar configuration of Fig. 2.8 (b) is considered, the ambiguity surface (shown in Fig. 2.8 (d)) exhibits two maxima: one for the DOA of $(\theta_s = 40°, \phi_s = 20°)$ and another for $(\theta_s = -40°, \phi_s = 20°)$. Although, the elevation angle is estimated correctly, the figure presents a left/right ambiguity for the azimuth angle. Therefore, the vertical planar array configuration is not able to discriminate whether the plane-wave comes from the left or right side of the planar array. The above results show that both planar configurations suffer from the left/right or up/down ambiguity; a configuration which overcomes such ambiguity is going to be discussed in the next section.

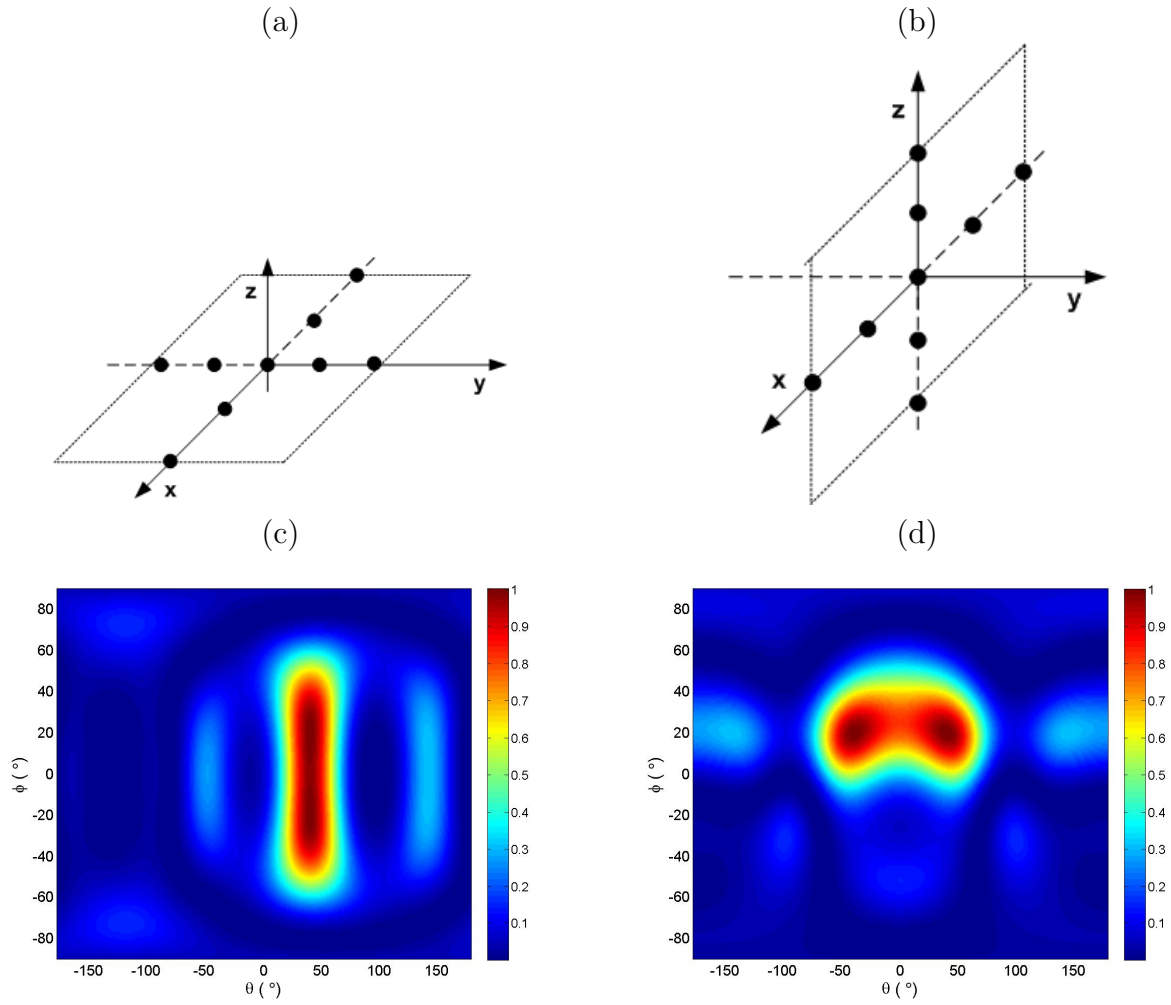

Figure 2.8: Planar array of 9 equispaced sensors with 1 m spacing, $c = 1500\,\mathrm{m/s}$, at frequency 500 Hz and source DOA $(\theta_s, \phi_s) = (40°, 20°)$, for: horizontal (a) and vertical configurations (b) and the normalized beam pattern obtained for the horizontal (c) and vertical configurations (d).

2.2.3 Cubic configuration

This section considers a cubic distribution of 8 equispaced sensors with 1 m spacing, as shown in Fig. 2.9 (a). The corresponding normalized beam pattern for a source DOA $(\theta_s, \phi_s) = (40°, 20°)$, calculated for $c = 1500\,\mathrm{m/s}$ and frequency 500 Hz is shown in Fig. 2.9 (b). The figure reveals that in contrast with the previous cases, the DOA is correctly obtained for both the azimuth and elevation angles, there is no left/right ambiguity; in other words, the cubic array configuration allows to achieve three-dimensional DOA estimation.

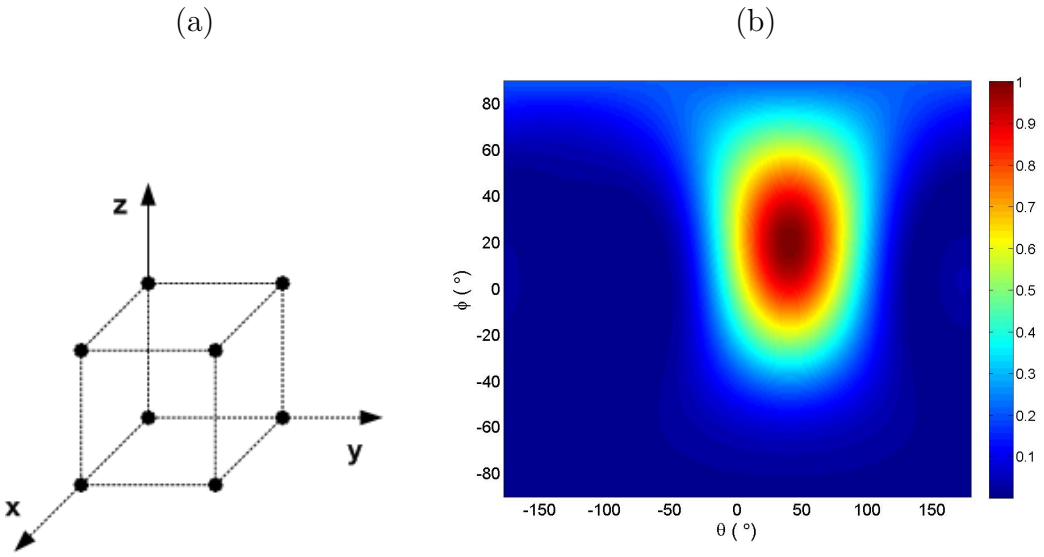

Figure 2.9: Cubic array configuration of 8 equispaced sensors with 1 m spacing, $c = 1500\,\mathrm{m/s}$, at frequency 500 Hz and source DOA $(\theta_S, \phi_S) = (40°, 20°)$ (a) and the corresponding normalized beam pattern (b).

All the cases discussed previously, in increasing order of configuration complexity, reveal how the determination of a three-dimensional DOA estimation can be improved. The cubic configuration is able to resolve the left/right ambiguity which affects the linear and planar configurations and to estimate both the azimuth and elevation angles. However, in practical applications and depending on the frequency of the emitted signal (which is related to the array dimensions), the cubic configuration is difficult or even impossible to implement because of the problems related to the distribution of the sensors in the cubic structure, and also because such array does not facilitate array deployment and its recovery. This is why linear configurations are often used despite the left/right ambiguity typical of such arrays. Such ambiguity can still be reduced by twin systems of linear arrays [66, 67].

It will be shown in the following section that the three-dimensional DOA estimation without ambiguities, provided by the cubic configuration, can be achieved by a linear array if directional sensors such as vector sensors are used. Such linear array of vector sensors

give rise to a more compact and easy-to-deploy system to be used in underwater acoustic applications.

2.3 VSA in DOA estimation

The main purpose of this section is to show that one can eliminate DOA left/right ambiguity and can resolve both vertical and azimuthal directions by using a linear VSA. A VSA has four output channels for each element, measuring both the acoustic pressure and the particle velocity in each independent axis. The measured particle velocity components provides the directional capabilities of such sensors. Therefore, for a hydrophone array to achieve the same performance on directionality as a VSA it will require a cubic configuration, which in some underwater acoustic applications are difficult or even impossible to implement.

In what follows the performances for DOA estimation of both the VSA and hydrophone array are compared by applying the plane-wave beamformer, where the individual sensor outputs are delayed, weighted and summed in a conventional manner.

Let us start by considering three-dimensional DOA estimation, where the vector sensor elements are located along the z-axis, as shown in Fig. 2.1. Assuming that:

$$\mathbf{y}_{pv} = \left[y_{p_1}, y_{v_{x1}}, y_{v_{y1}}, y_{v_{z1}}, \cdots, y_{p_L}, y_{v_{xL}}, y_{v_{yL}}, y_{v_{zL}}\right]^T, \tag{2.10}$$

is the signal received on a L vector sensor array, where y_{p_l} represents the acoustic pressure and $y_{v_{xl}}$, $y_{v_{yl}}$ and $y_{v_{zl}}$ represent the three particle velocity components of the signal received on the lth element of vector sensor. In the frequency domain a narrowband signal at frequency ω_0 as observed on such array can be written in a compact expression by:

$$\mathbf{y}_{pv}(\omega_0, \theta_s, \phi_s) = \begin{bmatrix} 1 \\ \mathbf{u}(\theta_s, \phi_s) \end{bmatrix} \otimes S_0(\omega_0) \left[1, \cdots, \exp(-i\mathbf{k}_s.\mathbf{r}_l), \cdots, \exp(-i\mathbf{k}_s.\mathbf{r}_L)\right]^T, \tag{2.11}$$

where $S_0(\omega_0)$ is the amplitude of the signal emitted by the source, $\mathbf{r}_l$ is the lth vector position of the VSA elements as shown in Fig. 2.1, $\mathbf{k}_s$ is the wavenumber vector defined by (2.4), $\otimes$ is the Kronecker product (which properties are presented in appendix A) and $\mathbf{u}(\theta_s, \phi_s)$ is the vector which define the direction cosines for particle velocity components as:

$$\mathbf{u}(\theta_s, \phi_s) = \left[\begin{array}{ccc} \cos(\theta_s)\cos(\phi_s) & \sin(\theta_s)\cos(\phi_s) & \sin(\phi_s) \end{array} \right]^T . \tag{2.12}$$

The search parameter is the direction (θ_s, ϕ_s) and the weighting vector is simply a combination of weights, which are direction cosines for the particle velocity components and unity for pressure. Thus, the weighting vector for the VSA is given by:

$$\mathbf{e}_{pv}(\theta, \phi) = \left[\begin{array}{c} 1 \\ \mathbf{u}(\theta, \phi) \end{array} \right] \otimes [1, \cdots, \exp(-i\mathbf{k}.\mathbf{r}_l), \cdots, \exp(-i\mathbf{k}.\mathbf{r}_L)]^T , \tag{2.13}$$

where $\mathbf{k}$ is the wavenumber vector corresponding to the chosen steering angle, or look direction (θ, ϕ) of the array, $\theta \in [-\pi; \pi]$ is the azimuth angle, $\phi \in \left[-\frac{\pi}{2}; \frac{\pi}{2}\right]$ is the elevation angle.

For a given direction (θ, ϕ), and following the same analysis presented in section 2.1, the beam power response for the VSA, which combines Eq. (2.11) with Eq. (2.13), is given by:

$$b_{pv}(\omega_0, \theta, \phi) = |\mathbf{y}_{pv}(\omega_0, \theta_s, \phi_s)\mathbf{e}_{pv}^H(\omega_0, \theta, \phi)|^2, \tag{2.14}$$

and the estimator $(\hat{\theta}_s, \hat{\phi}_s)$ of (θ_s, ϕ_s) is obtained by:

$$(\hat{\theta}_s, \hat{\phi}_s) = \arg\left\{ \max_{(\theta,\phi)} b_{pv}(\omega_0, \theta, \phi) \right\}, \tag{2.15}$$

where if $(\theta, \phi) = (\theta_s, \phi_s)$ the power result of (2.14) is maximum.

Comparing the acoustic pressure beam power response, Eq. (2.6), with the VSA beam power response, Eq. (2.14), the increased directionality provided by the VSA is deduced by

the inclusion of the vector $\mathbf{u}(\theta_s, \phi_s)$ in the beam response. Such effect will be demonstrated for a general parameter estimation in the next chapter.

The three-dimensional beam pattern obtained with a 9-element equispaced VSA at 1 m spacing along the z-axis, for a frequency of 500 Hz, is shown in Fig. 2.10. The figure illustrates the high directivity of the VSA in a linear array configuration; such directivity is in high contrast with the omni-directionality of the linear hydrophone array, which was described in section 2.2.1 (see Fig. 2.4). The VSA response has a narrow beam pattern that points to the source true DOA $(\theta_s, \phi_s) = (40°, 20°)$.

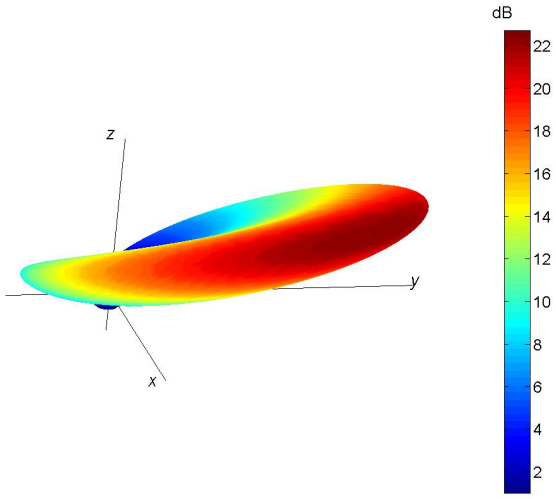

Figure 2.10: Three-dimensional representation of the beam pattern, calculated by the beamformer considering a VSA of 9 equispaced elements with 1 m spacing, at frequency 500 Hz and source DOA $(\theta_s, \phi_s) = (40°, 20°)$.

The normalized ambiguity surface for a VSA with 9 equispaced elements at frequency of 500 Hz and source direction $(\theta_s, \phi_s) = (40°, 20°)$ is shown in Fig. 2.11. The figure reveals that the VSA resolves both elevation and azimuth angles, and presents a narrow main lobe without ambiguities; as discussed in section 2.2.1 such result is not possible with a vertical linear hydrophone array configuration (see Fig. 2.3). The well known left/rigth ambiguity, typical

of hydrophone arrays, was eliminated and the combination of acoustic pressure with particle velocity provided a higher DOA resolution. The cubic hydrophone array configuration can achieve high directivity (see, for instance Fig. 2.9), but with a wider main lobe. Therefore, one can conclude that the VSA is able to resolve three-dimensional DOA with a linear array configuration of a few elements, which implies that a VSA can offer a significant reduction of the number of sensors with a better performance compared to hydrophone arrays.

Summary

In this chapter the conventional beamformer was used for DOA estimation and a preliminary comparative study was made between hydrophone and vector sensor arrays, for different spatial configurations. It was shown that the number of sensors influences the resolution of DOA estimation. The design frequency of the array has to be well selected in order to eliminate spatial aliasing, and to produce a valid DOA estimate. It was also shown that most of the hydrophone array configurations exhibit a left/right ambiguity. The only exception is the cubic configuration, which resolves both the elevation and the azimuth angles; however,

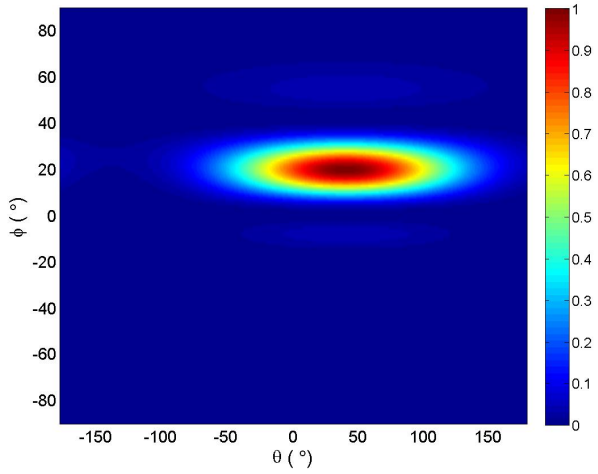

Figure 2.11: Two-dimensional normalized ambiguity surface considering a VSA of 9 equispaced elements with 1 m spacing, at frequency 500 Hz and source DOA $(\theta_s, \phi_s) = (40°, 20°)$.

depending on array dimensions, the deployment of a cubic configuration array introduces serious drawbacks in underwater applications. A viable alternative of a cubic configuration is a linear VSA which was discussed in the previous section. The VSA can resolve both elevation and azimuth angles and exhibits a narrower main lobe than an array with same number of hydrophones.

The higher directivity of the VSA was verified for DOA estimation with simulations. At this point the following question arises: can the spatial filtering capabilities and high directivity of the VSA be used with advantage for the estimation of other parameters? The answer to this question is going to be presented in the following chapters. The discussion will start in the next chapter, where it will be derived a VSA measurement model using Gaussian beams for generic parameter estimation, and the Bartlett estimator will be extended in order to include particle velocity. Additionally, the chapter will show that the VSA based Bartlett estimator can be used for DOA estimation and, most importantly, for the estimation of seabed parameters.

Chapter 3

Parameter estimation using a vector sensor array

In general sound propagates between a source and a receiver through multiple ray trajectories. The acoustic field impinges the receivers from different directions; depending on the characteristics and properties of the ocean environment, different classes of ray paths appear, namely direct, refracted, refracted and bottom or surface reflected, surface or bottom reflected, surface and bottom reflected, etc. Ray trajectories depend on the properties of the ocean environment; consequently, each class of ray path collects different environmental information. For example, direct and refracted paths provide information regarding the water column only, related directly to the temperature and the sound speed profile; rays, which are bottom reflected, are attenuated carrying information regarding the characteristics and properties of the seabed.

Underwater acoustic remote sensing techniques allow to characterize rapidly and efficiently large areas of the ocean. Acoustic estimation of ocean parameters can be casted as an inverse problem, which uses data and model predictions to infer the values of the parameters of interest. Matched-field processing (MFP), in particular, has been used in underwater acoustic signal processing to estimate parameters of interest such as the source position and

properties of the seabed. The idea of MFP is to correlate the data collected in the ocean with that modelled, given by an acoustic propagation model [21]. The candidate environmental parameters that show the highest correlation are considered to be the parameter estimates. A significant number of studies covering MFP relies on data collected by hydrophones, in either vertical or horizontal array configurations; additionally, when high estimation resolution is required, long hydrophone arrays must be used [68].

The information regarding the DOA, in both azimuth and elevation angles, can not be recovered from linear or even planar hydrophone arrays because hydrophones are omnidirectional and/or exhibit a left/right ambiguity. Therefore, the spatial filtering capabilities and high directivity of vector sensors, verified for DOA estimation in the previous chapter, could be advantageous in the estimation of the parameters of interest. The following question arises at this point: since, a vector sensor measures two horizontal and one vertical components of particle velocity, could different types of components be used for the estimation of different environmental parameters? Such issue is related to the fact that direct and perhaps refracted ray paths contribute mostly to the horizontal components of particle velocity; in contrast, the vertical component is mostly affected by surface and bottom reflected ray paths. On one hand, if the objective of estimation is related to the water column, the usage of the horizontal components may contribute to enhance the estimation of temperatures or sound speed profiles. On the other hand, if the objective of estimation is related to the ocean bottom characterization, the vertical component could be more reliable than the other components. Depending on the estimation problem, those aspects must be addressed when the particle velocity information and a VSA are used. Therefore, in order to understand how the vector sensor influences the parameter estimation, or if all components

are necessary, or if the acoustic pressure must be merged with particle velocity information, it is important to develop a model and to derive a processor, which accounts for particle velocity information.

In this chapter a VSA data model, which merges both acoustic pressure and particle velocity components, is proposed for generic parameter estimation. The signal component of the VSA data model is derived considering a Gaussian beam model, which accounts for particle velocity. The physical model used to generate the vector sensor field replicas was the TRACEO Gaussian beam model [56], which was designed to perform two dimensional acoustic ray tracing in ocean waveguides. The TRACEO model provides different sets of output information, which can be either geometric - ray coordinates, travel time, amplitude etc, or physical, like acoustic pressure, particle velocity or transmission loss. In the correlation process of the VSA data with the replica fields it will be used the well known Bartlett linear processor due to its robustness. In what follows it will be shown an extension of the Bartlett processor, which allows to include particle velocity outputs. In this context, and in order to understand the contribution that each particle velocity component has to the estimation problem, two VSA-based Bartlett estimators will be discussed. The first one includes only the particle velocity components and the second one merges the acoustic pressure with the particle velocity. After such discussion, both processors will be compared and tested for different underwater acoustic applications, namely DOA estimation and seabed parameter estimation.

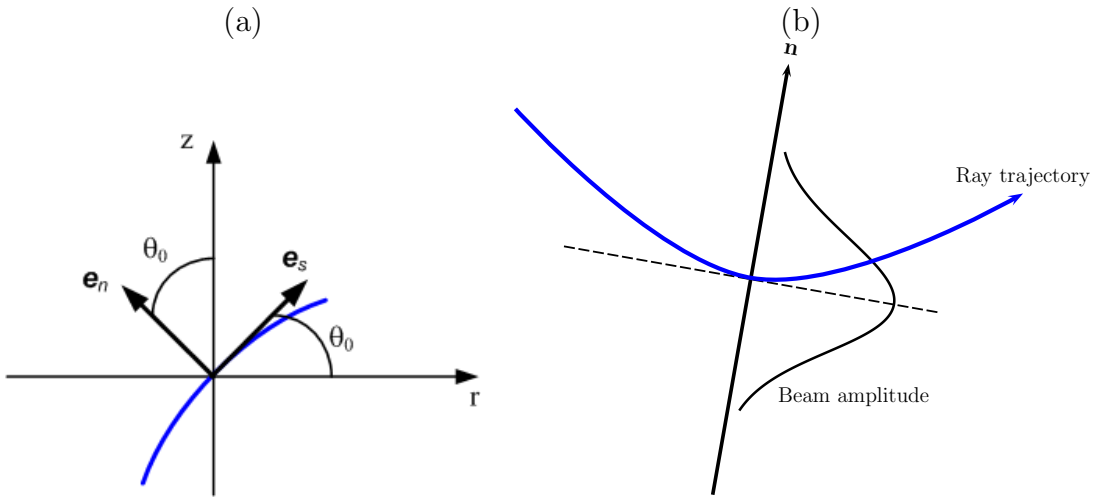

Figure 3.1: Ray tangent and normal vectors $\mathbf{e}_s$ and $\mathbf{e}_n$ (a); Beam amplitude along the ray normal direction (b).

3.1 Modeling particle velocity using Gaussian beams

A ray tracing model requires the solution of the Eikonal equations to determine the ray coordinates. Let us consider an arbitrary point on the ray trajectory and the corresponding tangent and normal unitary vectors, represented as $\mathbf{e}_s$ and $\mathbf{e}_n$, respectively, as shown in Fig. 3.1 (a). Within the Gaussian beam approach [2, 56] the ray trajectory represents the central axis of a beam, whose amplitude exhibits a Gaussian shape relative to the ray normal, as shown in Fig. 3.1 (b).

In general, particle velocity ($\mathbf{v}$) can be calculated from acoustic pressure in the frequency domain as:

$$\mathbf{v} = \frac{i}{\omega\rho}\nabla P, \tag{3.1}$$

where ρ represents the density of the water column assumed constant in space and ω is the working frequency of the propagating acoustic wave. Taking into account the tangent and

normal ray directions, the pressure gradient can be written as:

$$\nabla P = \left[\frac{\partial P}{\partial s}, \frac{\partial P}{\partial n}\right], \tag{3.2}$$

where s and n represent the ray arclength and ray normal directions, respectively. As indicated in Fig. 3.1 (a) the unitary vectors $\mathbf{e}_s$ and $\mathbf{e}_n$ can be projected onto the horizontal and vertical axes (r, z) as:

$$\mathbf{e}_s = [\cos\theta_0, \sin\theta_0] \quad \text{and} \quad \mathbf{e}_n = [-\sin\theta_0, \cos\theta_0], \tag{3.3}$$

where θ_0 represents the angle between $\mathbf{e}_s$ and the horizontal axis.

The normal and tangent derivatives given by Eq. (3.2) can be projected onto the range and depth axes (where $\mathbf{e}_r$ and $\mathbf{e}_z$ are the unitary vectors respectively) in order to determine the corresponding particle velocity components, providing the following expressions:

$$\begin{aligned} v_r &= \frac{i}{\omega\rho}\left(\frac{\partial P}{\partial s}\mathbf{e}_s + \frac{\partial P}{\partial n}\mathbf{e}_n\right)\cdot\mathbf{e}_r \\ &= \frac{i}{\omega\rho}\left(\frac{\partial P}{\partial s}\mathbf{e}_s\cdot\mathbf{e}_r + \frac{\partial P}{\partial n}\mathbf{e}_n\cdot\mathbf{e}_r\right) \\ &= \frac{i}{\omega\rho}\left(\frac{\partial P}{\partial s}\cos\theta_0 - \frac{\partial P}{\partial n}\sin\theta_0\right), \end{aligned} \tag{3.4}$$

and

$$\begin{aligned} v_z &= \frac{i}{\omega\rho}\left(\frac{\partial P}{\partial s}\mathbf{e}_s + \frac{\partial P}{\partial n}\mathbf{e}_n\right)\cdot\mathbf{e}_z \\ &= \frac{i}{\omega\rho}\left(\frac{\partial P}{\partial s}\mathbf{e}_s\cdot\mathbf{e}_z + \frac{\partial P}{\partial n}\mathbf{e}_n\cdot\mathbf{e}_z\right) \\ &= \frac{i}{\omega\rho}\left(\frac{\partial P}{\partial s}\sin\theta_0 + \frac{\partial P}{\partial n}\cos\theta_0\right). \end{aligned} \tag{3.5}$$

While the VSA has three particle velocity components (v_x, v_y and v_z), the TRACEO model generates only two components (v_r and v_z); therefore, the v_x and v_y components are

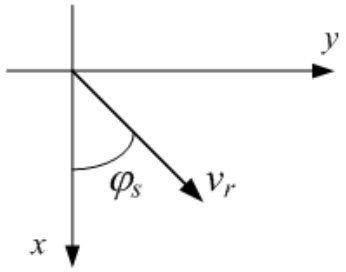

Figure 3.2: Projection of the horizontal particle velocity v_r on (x, y) axes with the azimuthal direction of the source, φ_s.

calculated, projecting the horizontal particle velocity v_r, Eq. (3.4), in the azimuthal direction of the source, φ_s, as shown in Fig. 3.2 which is supposed to be known, as:

$$v_x = v_r \cos\varphi_s \quad \text{and} \quad v_y = v_r \sin\varphi_s. \tag{3.6}$$

Under the Gaussian beam approach, the acoustic pressure can be written as:

$$P(s,n) = A\sqrt{\frac{c(s)}{rq(s)}} \exp\left\{-i\omega\left[\tau(s) + \frac{p(s)}{2q(s)}n^2\right]\right\}, \tag{3.7}$$

where A is an arbitrary constant, $c(s)$ is the sound speed along the ray, $\tau(s)$ is the time delay along the ray and $p(s)$ and $q(s)$ are parameters obtained from the solution of dynamic ray equations and are related to beamwidth and curvature [2].

The derivative of Eq. (3.7) along the normal direction is given by:

$$\frac{\partial P}{\partial n} = -i\omega\frac{p(s)}{q(s)}nP(s,n)\ . \tag{3.8}$$

The expression for the derivative along the arclength direction is cumbersome because of the dependence of the different arguments on s. Such expression can be greatly simplified by considering only the factors which affect mostly the beam phase, providing the expression:

$$\frac{\partial P}{\partial s} = -i\omega\chi(s)P(s,n)\ , \tag{3.9}$$

where

$$\chi(s) = \frac{d}{ds}\left(\tau(s) + n^2 \frac{p(s)}{2q(s)}\right) .$$

The previous discussion allows to rewrite the particle velocity components, Eq. (3.5) and Eq. (3.6), substituting the pressure derivatives, Eq. (3.8) and Eq. (3.9), as:

$$\mathbf{v}(\Theta_0) = \begin{bmatrix} v_x(\Theta_0) \\ v_y(\Theta_0) \\ v_z(\Theta_0) \end{bmatrix} = \begin{bmatrix} \frac{1}{\rho}\left(\chi(s)\cos\theta_0 - \frac{p(s)}{q(s)} n \sin\theta_0\right)\cos\varphi_s \\ \frac{1}{\rho}\left(\chi(s)\cos\theta_0 - \frac{p(s)}{q(s)} n \sin\theta_0\right)\sin\varphi_s \\ \frac{1}{\rho}\left(\chi(s)\sin\theta_0 + \frac{p(s)}{q(s)} n \cos\theta_0\right) \end{bmatrix} P(s,n), \tag{3.10}$$

where angle θ_0 depends on the characteristics of the acoustic channel and on the ray trajectory.

Assuming a small aperture array and a generic set of environmental parameters (Θ_0) that characterizes the channel, including ocean bottom parameters, from Eq. (3.10) the particle velocity can be written as:

$$\mathbf{v}(\Theta_0) = \mathbf{u}(\Theta_0) P(s,n), \tag{3.11}$$

where

$$\mathbf{u}(\Theta_0) = \begin{bmatrix} u_x(\Theta_0) \\ u_y(\Theta_0) \\ u_z(\Theta_0) \end{bmatrix} = \begin{bmatrix} \frac{1}{\rho}\left(\chi(s)\cos\theta_0 - \frac{p(s)}{q(s)} n \sin\theta_0\right)\cos\varphi_s \\ \frac{1}{\rho}\left(\chi(s)\cos\theta_0 - \frac{p(s)}{q(s)} n \sin\theta_0\right)\sin\varphi_s \\ \frac{1}{\rho}\left(\chi(s)\sin\theta_0 + \frac{p(s)}{q(s)} n \cos\theta_0\right) \end{bmatrix}, \tag{3.12}$$

is the vector defined for a ray trajectory (θ_0). In a real scenario, not only one ray but several rays impinge the array. In this case $\mathbf{u}(\Theta_0)$ in Eq. (3.11) is defined as to approximate the sum of the contributions of each ray.

3.2 Data model

Assuming that the propagation channel is a linear time-invariant system, p represents now the acoustic pressure and v_x, v_y and v_z are the three particle velocity components, then the

field measured at the vector sensor due to a source signal $s(t)$ is given by:

$$y_k(t, \Theta_0) = h_k(t, \Theta_0) * s(t) + n_k(t), \tag{3.13}$$

where $*$ is the convolution operator, Θ_0 is a parameter vector, $h_k(\Theta_0)$ is the channel impulse response and $n_k(t)$ is the additive noise for pressure and the three components of particle velocity for $k = p, v_x, v_y, v_z$, respectively.

Assuming a narrowband signal, the sensor output Eq. (3.13) at a frequency ω (omitting the frequency dependency in the following) for a particular set of channel parameters Θ_0 can be rewritten as:

$$y_k(\Theta_0) = h_k(\Theta_0)s + n_k, \tag{3.14}$$

where s is the source signal component at frequency ω, $h_k(\Theta_0)$ is the channel response and n_k is the additive noise.

Taking into account Eq. (3.11) and Eq. (3.12), the vector sensor model can be obtained as:

$$\begin{bmatrix} y_p(\Theta_0) \\ y_{v_x}(\Theta_0) \\ y_{v_y}(\Theta_0) \\ y_{v_z}(\Theta_0) \end{bmatrix} = \begin{bmatrix} h_p(\Theta_0) \\ u_x(\Theta_0)h_p(\Theta_0) \\ u_y(\Theta_0)h_p(\Theta_0) \\ u_z(\Theta_0)h_p(\Theta_0) \end{bmatrix} s + \begin{bmatrix} n_p \\ n_{v_x} \\ n_{v_y} \\ n_{v_z} \end{bmatrix}. \tag{3.15}$$

In the following formulation it is assumed that the additive noise is zero mean and white, both in time and space[1], with variance σ_n^2 and uncorrelated with the signal s, itself with zero mean and variance σ_s^2.

For an array of L vector sensors, the acoustic pressure for a given frequency ω is given by:

$$\mathbf{y}_p(\Theta_0) = \left[y_{p_1}(\Theta_0), \cdots, y_{p_L}(\Theta_0)\right]^T, \tag{3.16}$$

[1]Both between VSA elements and between sensors within each element.

where $y_{p_l}(\Theta_0)$ is the acoustic pressure at the lth vector sensor. The linear data model for the acoustic pressure is:

$$\mathbf{y}_p(\Theta_0) = \mathbf{h}_p(\Theta_0)s + \mathbf{n}_p, \tag{3.17}$$

where $\mathbf{h}_p(\Theta_0)$ is the channel frequency response at L pressure sensors and $\mathbf{n}_p$ is the additive acoustic pressure noise.

A similar definition has been adopted for the particle velocity, where the velocity part of the measurement is:

$$\mathbf{y}_v(\Theta_0) = \Big[y_{v_x1}(\Theta_0), \cdots, y_{v_xL}(\Theta_0), y_{v_y1}(\Theta_0), \cdots, y_{v_yL}(\Theta_0), y_{v_z1}(\Theta_0), \cdots, y_{v_zL}(\Theta_0)\Big]^T. \tag{3.18}$$

Considering short arrays, $\mathbf{u}(\Theta_0)$ is assumed to be approximately constant for all elements, and therefore the data model for the particle velocity components is given by:

$$\mathbf{y}_v(\Theta_0) = \mathbf{u}(\Theta_0) \otimes \mathbf{h}_p(\Theta_0)s + \mathbf{n}_v, \tag{3.19}$$

where $\mathbf{n}_v$ is the additive noise satisfying the above assumptions and $\otimes$ is the Kronecker product. For $\mathbf{h}_p(\Theta_0)$ with dimension $L \times 1$, $\mathbf{y}_v(\Theta_0)$ has dimension $3L \times 1$.

Combining Eq. (3.17) and Eq. (3.19) a complete VSA data model, formed by the acoustic pressure and the particle velocity, can be defined for a signal measured on L vector sensor elements as:

$$\mathbf{y}_{pv}(\Theta_0) = \begin{bmatrix} \mathbf{y}_p(\Theta_0) \\ \mathbf{y}_v(\Theta_0) \end{bmatrix} = \begin{bmatrix} 1 \\ \mathbf{u}(\Theta_0) \end{bmatrix} \otimes \mathbf{h}_p(\Theta_0)s + \begin{bmatrix} \mathbf{n}_p \\ \mathbf{n}_v \end{bmatrix}, \tag{3.20}$$

resulting in a $4L \times 1$ dimensional data model.

3.3 The VSA Bartlett estimator

The classical Bartlett estimator is a signal processing technique for parameter estimation and is usually expressed in terms of the acoustic pressure [21]. The Bartlett parameter estimate

$\hat{\Theta}_0$ is given as the argument of the maximum of the function:

$$P_B(\Theta) = E\left\{\hat{\mathbf{e}}^H(\Theta)\mathbf{y}(\Theta_0)\mathbf{y}^H(\Theta_0)\hat{\mathbf{e}}(\Theta)\right\}, \tag{3.21}$$

where $\mathbf{y}(\Theta_0)$ is the measured data and the replica vector estimator $\hat{\mathbf{e}}(\Theta)$ is defined as the vector $\mathbf{e}(\Theta)$ that maximizes the mean quadratic power:

$$\begin{aligned}\hat{\mathbf{e}}(\Theta) &= \arg\max_{\mathbf{e}(\Theta)} E\left\{\mathbf{e}^H(\Theta)\mathbf{y}(\Theta_0)\mathbf{y}^H(\Theta_0)\mathbf{e}(\Theta)\right\} \\ &= \arg\max_{\mathbf{e}(\Theta)} \mathbf{e}^H(\Theta)\mathbf{R}(\Theta_0)\mathbf{e}(\Theta),\end{aligned} \tag{3.22}$$

subject to $\mathbf{e}^H(\Theta)\mathbf{e}(\Theta) = 1$, where ^{H} represents the complex conjugate transpose operator, $E\{.\}$ denotes statistical expectation and $\mathbf{R}(\Theta_0) = E\left\{\mathbf{y}(\Theta_0)\mathbf{y}^H(\Theta_0)\right\}$ is the data correlation matrix.

In general the correlation matrix $\mathbf{R}(\Theta_0)$ is unknown; thus a correlation matrix estimator $\hat{\mathbf{R}}(\Theta_0)$ is obtained by:

$$\hat{\mathbf{R}}(\Theta_0) = \frac{1}{K}\sum_{k=1}^{K}\mathbf{y}_k(\Theta_0)\mathbf{y}_k^H(\Theta_0). \tag{3.23}$$

assuming that there are K snapshots of data available.

In the following sections the Bartlett estimator is developed considering the data and the replica vector as acoustic pressure only (subscript p), particle velocity components only (subscript v) and full vector sensor information (subscript pv).

3.3.1 Acoustic pressure only Bartlett estimator

Bearing in mind the acoustic pressure data model of Eq. (3.17) and the associated assumptions, the correlation matrix $\mathbf{R}_p(\Theta_0)$ can be written as:

$$\mathbf{R}_p(\Theta_0) = \mathbf{h}_p(\Theta_0)\mathbf{h}_p^H(\Theta_0)\sigma_s^2 + \sigma_n^2\mathbf{I}. \tag{3.24}$$

Therefore, a possible estimator $\hat{\mathbf{e}}_p(\Theta)$ of $\mathbf{e}_p(\Theta)$ is obtained as:

$$\hat{\mathbf{e}}_p(\Theta) = \arg\max_{\mathbf{e}_p(\Theta)} \left\{ \mathbf{e}_p^H(\Theta) \mathbf{R}_p(\Theta_0) \mathbf{e}_p(\Theta) \right\}, \tag{3.25}$$

subject to ${\mathbf{e}_p}^H(\Theta)\mathbf{e}_p(\Theta) = 1$. According to Eq. (3.24) it can be shown that the well-known nontrivial solution [15, 69] is:

$$\hat{\mathbf{e}}_p(\Theta) = \frac{\mathbf{h}_p(\Theta)}{\sqrt{\mathbf{h}_p^H(\Theta)\mathbf{h}_p(\Theta)}}, \tag{3.26}$$

where the denominator is a scalar normalization factor and $\mathbf{h}_p(\Theta)$ contains the replica of a unit signal structure as "seen" by the receiver.

Replacing Eq. (3.26) and Eq. (3.24) in the generic estimator Eq. (3.21) provides the Bartlett estimator for acoustic pressure (p-only) for search parameter Θ as:

$$\begin{aligned} P_{B,p}(\Theta) &= \frac{\mathbf{h}_p^H(\Theta)\mathbf{R}_p(\Theta_0)\mathbf{h}_p(\Theta)}{\mathbf{h}_p^H(\Theta)\mathbf{h}_p(\Theta)} \\ &= \frac{\mathbf{h}_p^H(\Theta)\mathbf{h}_p(\Theta_0)\mathbf{h}_p^H(\Theta_0)\mathbf{h}_p(\Theta)}{\mathbf{h}_p^H(\Theta)\mathbf{h}_p(\Theta)}\sigma_s^2 + \sigma_n^2 \\ &= B_p(\Theta)\sigma_s^2 + \sigma_n^2, \end{aligned} \tag{3.27}$$

where $B_p(\Theta)$ is the noise-free beam pattern for pressure only, while the parameter estimator is given by:

$$\hat{\Theta}_0 = \arg\max_{\Theta \epsilon \Omega} P_{B,p}(\Theta). \tag{3.28}$$

3.3.2 Particle velocity only Bartlett estimator

When only the particle velocity components of Eq. (3.19) are considered, the correlation matrix, $\mathbf{R}_v(\Theta_0)$, can be written as:

$$\mathbf{R}_v(\Theta_0) = \left[\mathbf{u}(\Theta_0) \otimes \mathbf{h}_p(\Theta_0)\right] \left[\mathbf{u}(\Theta_0) \otimes \mathbf{h}_p(\Theta_0)\right]^H \sigma_s^2 + \sigma_n^2 \mathbf{I}. \tag{3.29}$$

The replica vector for the particle velocity components can be defined as:

$$\hat{\mathbf{e}}_v(\Theta) = \arg\max_{\mathbf{e}_v(\Theta)} \left\{ \mathbf{e}_v^H(\Theta)\mathbf{R}_v(\Theta_0)\mathbf{e}_v(\Theta) \right\}, \tag{3.30}$$

subject to ${\mathbf{e}_v}^H(\Theta)\mathbf{e}_v(\Theta) = 1$. Carrying out the above maximization (see appendix A) gives:

$$\hat{\mathbf{e}}_v(\Theta) = \frac{\mathbf{u}(\Theta)}{\sqrt{\mathbf{u}^H(\Theta)\mathbf{u}(\Theta)}} \otimes \hat{\mathbf{e}}_p(\Theta), \tag{3.31}$$

where the vector $\hat{\mathbf{e}}_v(\Theta)$ is proportional to the replica vector for the acoustic pressure $\hat{\mathbf{e}}_p(\Theta)$.

Substituting Eqs. (3.29) and (3.31) in the generic expression Eq. (3.21), the Bartlett estimator for particle velocity outputs (v-only) can be written as:

$$P_{B,v}(\Theta) = \frac{\left[\mathbf{u}^H(\Theta)\mathbf{u}(\Theta_0)\right]^2}{\mathbf{u}^H(\Theta)\mathbf{u}(\Theta)} B_p(\Theta)\sigma_s^2 + \sigma_n^2 \tag{3.32}$$

where $B_p(\Theta)$ is the beam pattern for p-only as defined in Eq. (3.27).

The previous description assumed, for simplicity, that the additive noise is zero mean and white, both in time and space; it also assumed that the same noise power is considered for pressure and velocity sensors. This noise assumption is frequently used in vector sensor processing and in proposed methods of DOA estimation [11, 14, 70, 71]. Moreover, Hawkes and Nehorai in [72] proposed expressions for the auto- and cross-correlations between the pressure and particle velocity components for a wideband noise field. These expressions were obtained for three different spatial distribution of the noise field, first, for an azimuthal independence; second, for an azimuthal independence and elevational symmetry; and third, for a spherical isotropy. A number of interesting features were found, however the main conclusion was that the noise power at the pressure sensor's output is always larger than the corresponding noise power at each velocity sensor's output. Therefore, such discussion shows that the DOA estimation capabilities with the VSA are better for many source directions in

an ambient noise field than in spatially white noise (the worst case). The spatial filtering capabilities of vector sensors allow to attenuate signals from multiple directions, thus reducing the total noise power on each component in comparison with the noise power of pressure. Thus, the performance advantage that a vector sensor possesses over a pressure-only sensor is magnified.

Let us return to the discussion of the v-only estimator. Bearing in mind that the inner product between two vectors is proportional to the cosine of the angle between these two vectors, and considering only the signal part of Eq. (3.32), one can write the noise-free v-only Bartlett estimator as:

$$P_{B,v}(\Theta) \propto [\cos^2(\delta)] B_p(\Theta) \sigma_s^2, \tag{3.33}$$

where δ is the angle between the replica vector $\mathbf{u}(\Theta)$ and the data vector $\mathbf{u}(\Theta_0)$. Based on Eq. (3.33) one can conclude that the noise-free v-only Bartlett estimator response is proportional to the noise-free p-only Bartlett response, where the inner product $\mathbf{u}^H(\Theta)\mathbf{u}(\Theta_0)$ from Eq. (3.32) is the constant of proportionality, hereafter called *directivity factor*. The output power of Eq. (3.33) is maximum when (Θ) and (Θ_0) are collinear; δ is zero and the directivity factor is one. The directivity factor provides an improved sidelobe reduction (or sidelobe suppression) when compared to the p-only Bartlett response and thus allows to improve the resolution of the parameter estimation. Based on the discussion presented in [72] one can say that the capabilities of the v-only estimator will be less affected by the presence of noise than the p-only estimator.

3.3.3 VSA $(p+v)$ Bartlett estimator

In this section it will be introduced a Bartlett estimator, which merges the acoustic pressure with the particle velocity components.

The correlation matrix for the VSA data can be written similarly to Eq. (3.29), taking into account the data model Eq. (3.20), as:

$$\mathbf{R}_{pv}(\Theta_0) = \left\{ \begin{bmatrix} 1 \\ \mathbf{u}(\Theta_0) \end{bmatrix} \otimes \mathbf{h}_p(\Theta_0) \right\} \left\{ \begin{bmatrix} 1 \\ \mathbf{u}(\Theta_0) \end{bmatrix} \otimes \mathbf{h}_p(\Theta_0) \right\}^H \sigma_s^2 + \sigma_n^2 \mathbf{I}. \tag{3.34}$$

Based on the derivation of the v-only Bartlett estimator (see appendix A) it can be shown that the VSA replica vector is proportional to the replica for the acoustic pressure:

$$\hat{\mathbf{e}}_{pv}(\Theta) = \frac{\begin{bmatrix} 1 \\ \mathbf{u}(\Theta) \end{bmatrix}}{\sqrt{\begin{bmatrix} 1 \\ \mathbf{u}(\Theta) \end{bmatrix}^H \begin{bmatrix} 1 \\ \mathbf{u}(\Theta) \end{bmatrix}}} \otimes \hat{\mathbf{e}}_p(\Theta). \tag{3.35}$$

Thus, the VSA Bartlett estimator (VSA $(p+v)$), which includes both pressure and particle velocity components, is given by:

$$P_{B,pv}(\Theta) = \frac{\left(\begin{bmatrix} 1 \\ \mathbf{u}(\Theta) \end{bmatrix}^H \begin{bmatrix} 1 \\ \mathbf{u}(\Theta_0) \end{bmatrix} \right)^2}{\begin{bmatrix} 1 \\ \mathbf{u}(\Theta) \end{bmatrix}^H \begin{bmatrix} 1 \\ \mathbf{u}(\Theta) \end{bmatrix}} B_p(\Theta)\sigma_s^2 + \sigma_n^2. \tag{3.36}$$

Taking into account only the signal part and following the same analysis presented in section (3.3.2), one can show that the noise-free VSA $(p+v)$ Bartlett estimator is given by:

$$\begin{aligned} P_{B,pv}(\Theta) &\propto [1+\cos(\delta)]^2 B_p(\Theta)\sigma_s^2 \\ &\propto [4\cos^4(\frac{\delta}{2})] B_p(\Theta)\sigma_s^2. \end{aligned} \tag{3.37}$$

One can conclude that when the VSA $(p+v)$ Bartlett estimator is used, the noise-free output response is proportional to the noise-free p-only Bartlett response, where the constant of

proportionality is the directivity factor $[4\cos^4(\frac{\delta}{2})]$. By comparing Eq. (3.33) with Eq. (3.37) one can conclude that this directivity factor provides a wider main lobe, when compared to the v-only Bartlett estimator, due to the cosine of the half angle. However, the inclusion of pressure in the estimator eliminates also the ambiguities caused by the $[\cos^2(\delta)]$, even for frequencies higher than the array design frequency (at which array spacing equals a half wavelength) are used. Those conclusions are supported by the simulations, which are discussed in the next sections, for DOA estimation and most importantly, extended for seabed parameter estimation.

3.4 DOA estimation

Section 2.3 presented the VSA for DOA estimation using the conventional beamforming technique; in fact, this estimation problem can be stated as a particular case of the generic parameter estimation, discussed in the previous section. Thus, in the following, Eqs. (3.27), (3.33) and (3.37) will be used for DOA estimation. In order to determine the highest performance that could be reached with the VSA, the chosen high-frequency band, the four elements VSA, the geometrical and the environmental configuration used for this and next simulation studies are similar to that of the MakaiEx'05 sea trial. In such trial it was used a VSA with four equally spaced elements (10 cm spacing), located along the z-axis. The frequency considered is the array design frequency of 7500 Hz, for a true source DOA of (45°, 30°). The MakaiEx'05 sea trial is going to be described, in detail, in the next chapter.

The simulation of the DOA estimation, considering the VSA-based estimators, is presented in Fig. 3.3. The ambiguity surface obtained when the p-only estimator is used (see Eq. (3.27)) is shown in Fig. 3.3 (a) for reference. Since the array is placed along the ver-

tical axis and the hydrophones are omni-directional, only the elevation angle is resolved. The ambiguity surfaces for the directivity factors $[\cos^2(\delta)]$ and $[4\cos^4(\frac{\delta}{2})]$ (see Eq. (3.33) and Eq. (3.37)) are shown in Fig. 3.3 (b) and (c). These figures reveal the response of the directivity factors in the search space, where the maximum is obtained when $\delta = 0$, i.e., when the replica and the data vector are collinear - true source DOA, (see section 3.3). Comparing Fig. 3.3 (b) with Fig. 3.3 (c) one can see that $[4\cos^4(\frac{\delta}{2})]$ removes the ambiguity of $[\cos^2(\delta)]$, but with a wider main lobe. Such lobe is due to the cosine of the half angle. The ambiguity surfaces obtained with the v-only and the VSA $(p+v)$ estimators are shown in Fig. 3.3 (d) and (e), respectively. In both cases the estimators combine the directivity factors with the p-only estimator. These figures show that the v-only estimator presents the best resolution in both azimuth and elevation, but exhibits also an ambiguity, although of low amplitude. Such ambiguity is eliminated, at the cost of a wider main lobe, when the VSA $(p+v)$ estimator is used (see Fig. 3.3 (e)).

The results presented in Fig. 3.3 (d) and (e) were obtained from Eqs. (3.33) and (3.37), respectively. However, such results can also be obtained by visual superposition of Fig. 3.3 (b) and (c) with Fig. 3.3 (a), respectively. Therefore, one can conclude (as already discussed in chapter 2) that both directions are resolved, that the well known left/rigth ambiguity typical of hydrophone arrays was eliminated and that the conjugation of the acoustic pressure with the particle velocity provides a better sidelobe suppression; such performance in DOA estimation was achieved with an array of only a few vector sensor elements.

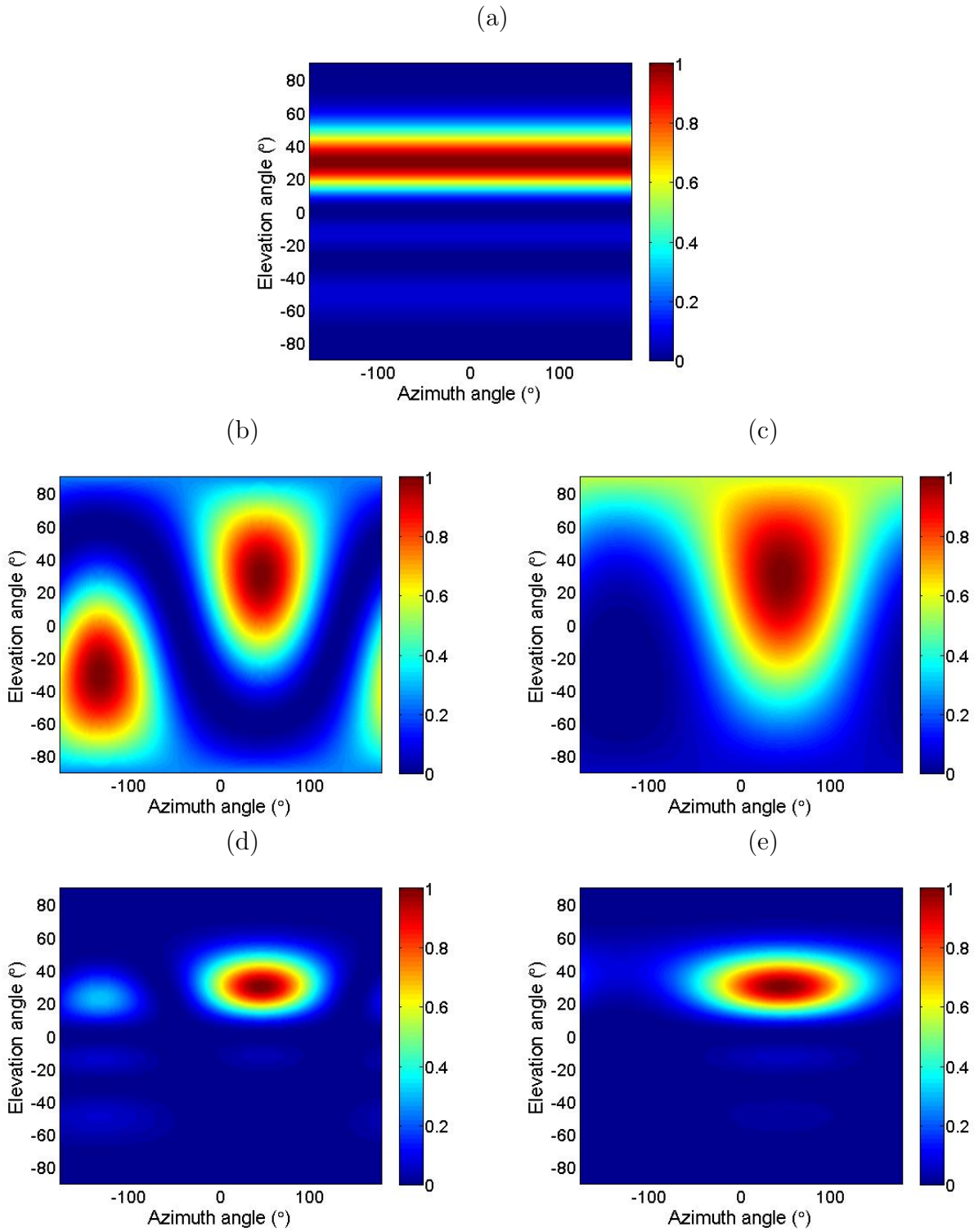

Figure 3.3: DOA estimation simulation results at frequency of 7500 Hz with azimuth $\theta_S = 45°$ and elevation $\phi_S = 30°$ angles considering: the p-only Bartlett estimator (a), the $[\cos^2(\delta)]$ of Eq. 3.33) (b), the $[4\cos^4(\frac{\delta}{2})]$ of Eq. (3.37) (c), the particle velocity only components (v-only) or Eq. (3.33) (d) and all sensors of the VSA ($p + v$) or Eq. (3.37) (e).

3.5 Seabed parameter estimation

The objective of this section is to include particle velocity information in geoacoustic inversion problems, and to compare the performance of the VSA with hydrophone arrays for seabed parameter estimation. As the discussion of the MakaiEx'05 sea trial (described in chapter 4) will show, the geometrical and water column parameters can be known to a degree of accuracy that allows one to consider only seabed parameters. Therefore, in the discussion that follows, it will be considered that the geometrical and water column parameters are known. Let us consider the following seabed parameters: sediment compressional speed (c_p), density (ρ) and compressional attenuation (α_p). Those parameters will be estimated taking into account the particle velocity outputs and based on the Bartlett estimators, previously discussed. The data and the field replicas will be generated using the TRACEO Gaussian beam model [56], which allows to consider only a seabed below the water column.

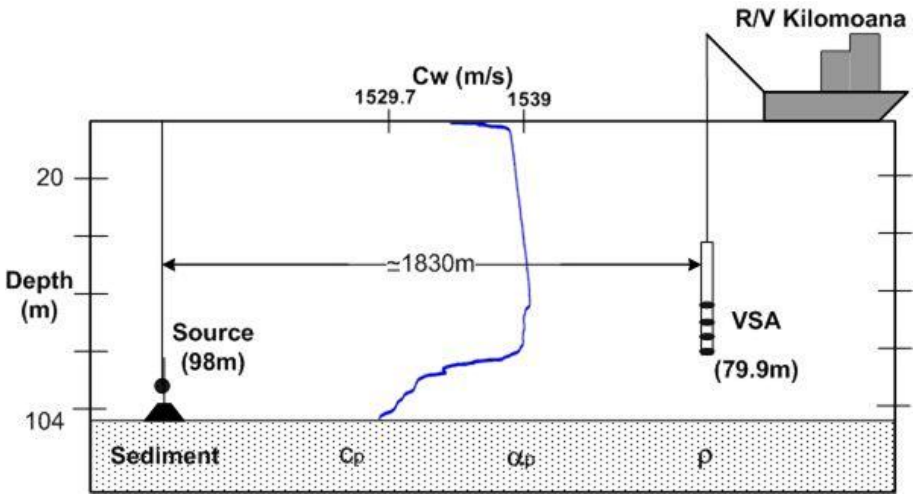

Figure 3.4: Simulation scenario based on a typical setup encountered during the MakaiEx'05 experiment with a deep mixed layer, characteristic of Hawaii. The source is bottom moored at 98 m depth and 1830 m range. The VSA is deployed with the deepest element positioned at 79.9 m.

The simulation scenario is shown in Fig. 3.4 and it is partially based on the MakaiEx'05

setup. The environment has a deep mixed layer, characteristic of Hawaii, and the bathymetry at the site is range independent with a water depth of 104 m. The source is bottom moored at 98 m depth and 1830 m range from the receiving VSA. Since the frequency band of the transmitted signals was well above that traditionally used in geoacoustic inversion, let us start the discussion with a preliminary study of transmission loss at the frequency of interest. The frequency that will be considered is 13000 Hz, which is the frequency that will be used for experimental geoacoustic inversion.

3.5.1 Transmission Loss

When the acoustic wave propagates outwards from the source, the intensity of the signal is reduced with increasing range, due to spreading and attenuation, which increases with frequency. In shallow water, the attenuation of the acoustic field due to boundary reflections (and in particular bottom reflections) is specially important. In underwater acoustics, the acoustic field medium interaction is traditionally expressed in terms of Transmission Loss (TL).

Fig. 3.5 presents the ray tracing output obtained with TRACEO, for the simulation scenario illustrated in Fig. 3.4. This figure reveals that due to the position of the acoustic source at 98 m and the thermocline positioned below 80 m, part of the rays are refracted and propagate between 60 m depth and the seabed, producing a wave guide. On the other hand, multiple rays paths are surface and bottom reflected. Therefore, a significant amount of energy impinge the receivers (positioned at 1830 m range, shown as a circle in Fig. 3.5) after bottom reflection.

The TRACEO model only calculates the TL in the water column. The influence of ray

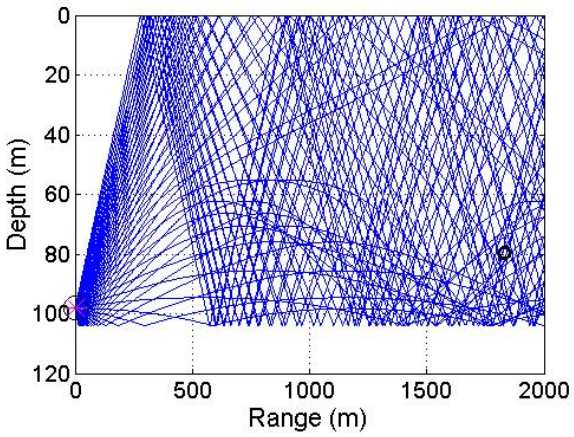

Figure 3.5: Ray tracing calculated with TRACEO for the simulation scenario presented in Fig. 3.4; source depth 98 m and receiver range 1830 m; the VSA is deployed with the deepest element positioned at 79.9 m. The symbol (x) indicates de position of the source and the symbol (o) indicates the position of the VSA.

propagation and reflection through the sediment layers is not well reproduced because the model is not designed to extend ray tracing calculations for both compressional and shear waves. The TL at 13000 Hz calculated by TRACEO in the water column is shown in Fig. 3.6. The TL for acoustic pressure is shown in Fig. 3.6 (a), while (b) and (c) show the TL for the horizontal and vertical components of the particle velocity, respectively [2]. On the one hand, Fig. 3.6 (a) and (b) reveal that both the p and the v_r fields at the receivers have a significant contribution from the refracted rays, sharing similar pattern, with part of the energy being reflected on the seabed. On the other hand, Fig. 3.6 (c) reveals that the v_z field has a higher contribution from the bottom and surface reflected rays. Therefore, in this HF band a sufficient amount of energy reaches the receiver after bottom reflections, which allows the propagated field to carry sufficient information to characterize the sediment regarding the most relevant parameters.

The discussion of Fig. 3.6 shows that the horizontal component is mostly affected by

[2]The TL for the particle velocity components was calculated relative to the reference 1 m/s.

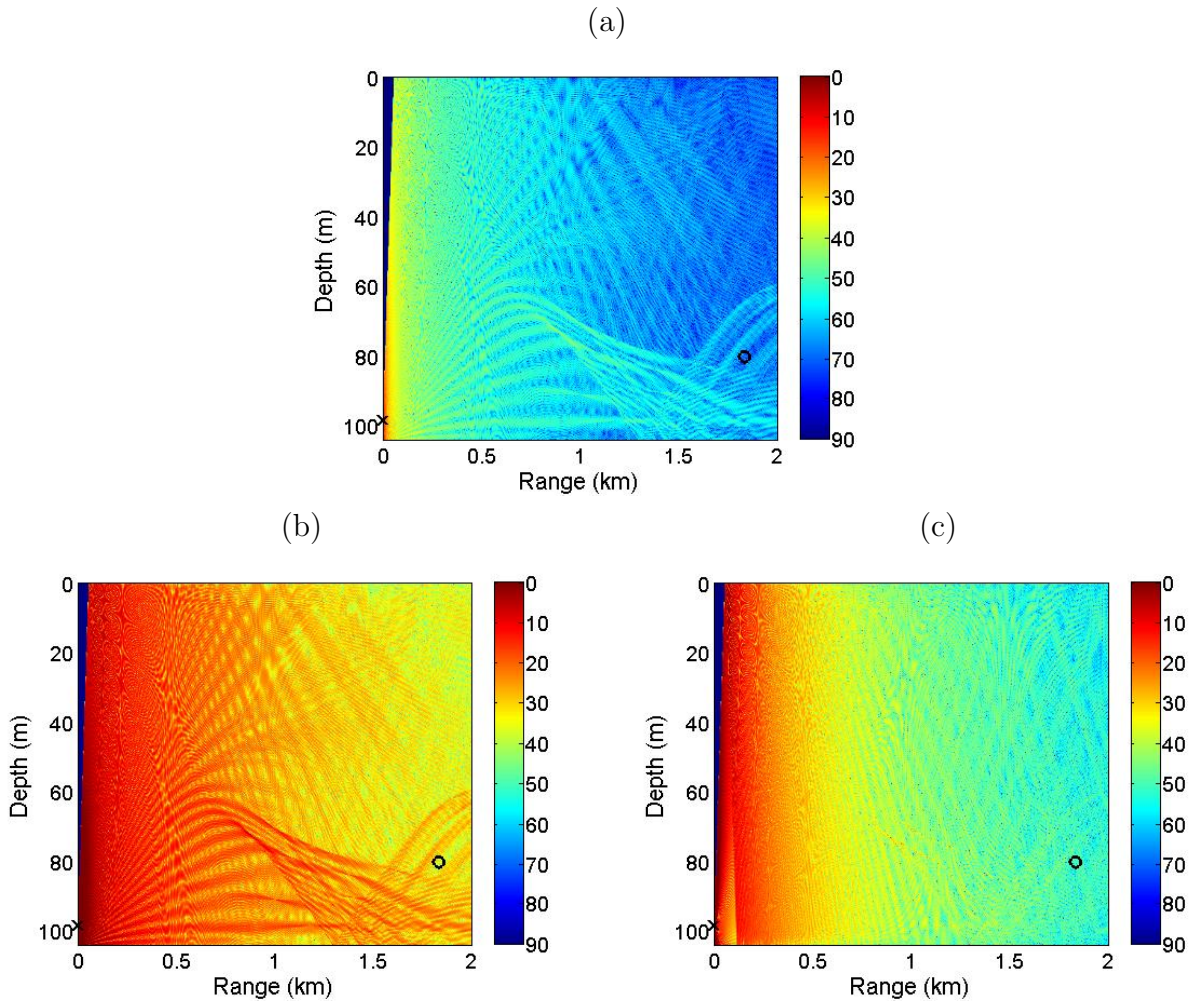

Figure 3.6: Transmission loss calculated with TRACEO Gaussian beam model, at 13000 Hz, for the acoustic pressure (a), horizontal particle velocity component (b) and vertical particle velocity component (c), considering the simulation scenario and the sound speed profile presented in Fig. 3.4. The symbol (x) indicates de position of the source and the symbol (o) indicates the position of the VSA.

refracted ray paths, while the vertical component is mostly affected by surface and bottom reflected ray paths. Moreover, the vertical component may be the most useful component to characterize the seabed. This could be an advantage when using vector sensors: depending on the ray paths, the propagation field has different contribution to different particle velocity components. The calculations of TL confirm that in this frequency band geoacoustic inversion is a viable option. They also confirm that different environmental information is provided by different particle velocity components.

In order to further support the previous set of results, the TL was calculated also with the Monterey-Miami Parabolic Equation (MMPE) model [73], which is capable of particle velocity calculations [3]. The MMPE model is capable to generate the TL in the water column, in the sediment layer and in the seabed.

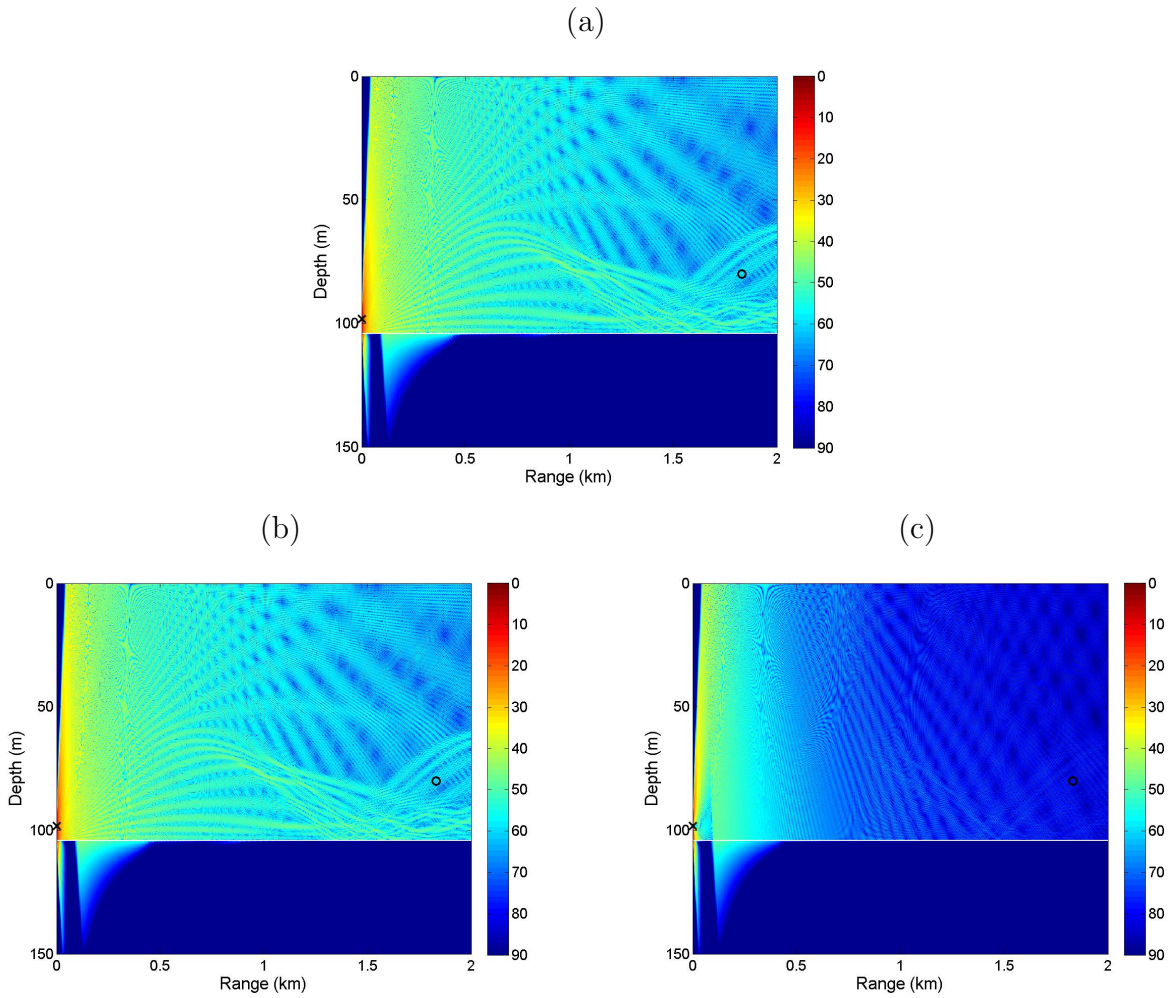

Figure 3.7: Transmission loss calculated with MMPE model, at 13000 Hz, for the acoustic pressure (a), horizontal particle velocity component (b) and vertical particle velocity component (c), considering the simulation scenario and the sound speed profile presented in Fig. 3.4. The symbol (x) indicates de position of the source and the symbol (o) indicates the position of the VSA.

The TL at 13000 Hz calculated with the MMPE model in the water column and the sediment layer is represented in Fig. 3.7. The TL for the acoustic pressure is shown in Fig. 3.7

[3]The reference level used by MMPE to calculate the TL of v_r and v_z is not indicated in the manual. Thus a direct comparison with the TL calculated by TRACEO is not possible.

(a), while (b) and (c) show the horizontal and the vertical particle velocity components, respectively. Regarding the water column only, Fig. 3.7 shows that similar p, v_r and v_z fields at the receivers are obtained to those of the TRACEO model (see Fig. 3.6). The ray paths present the same behaviour for both models and that is a common feature for all fields. Such results confirm the conclusions obtained from TRACEO TL calculations. Additionally, since MMPE is able to represent the acoustic field in the sediment layer, Fig. 3.7 reveals also that the acoustic field propagates through the sediment below 0.5 km for large grazing angles; for low grazing angles the energy is reflected back to the water column [4]. The similarities between the TL calculated with MMPE (capable of field calculations in the water column and the sediment) and TRACEO (capable of field calculations in the water column only) confirm that the features of the HF attenuated acoustic field, principally the vertical particle velocity component, were shown to have a potential for geoacoustic inversion.

3.5.2 Hydrophone array versus VSA

The discussion of the TL for the acoustic pressure, as well as for the horizontal and the vertical components of the particle velocity shown in the previous section, allowed to differentiate the types of field contributions, which can be obtained when a vector sensor is used. The VSA could have advantages in geoacoustic inversion, since it was confirmed that a sufficient amount of energy reaches the receivers after bottom reflections. Therefore, in this section, the inversion of seabed parameters based on the VSA Bartlett estimators, defined in section 3.3, will be discussed. To illustrate and to compare the estimation resolution of these estimators, the discussion will be divided in two steps: first, the performance of the VSA $(p + v)$ estimator will be compared with the performance of the p-only estimator; second,

[4] In underwater acoustics the grazing angle is generally considered relative to the horizontal direction.

the individual components estimators will be compared with the v-only and the full VSA $(p+v)$ estimators.

The estimation results are obtained taking into account the simulation scenario presented in Fig. 3.4, with a four-element (10 cm spacing) VSA deployed with the deepest element positioned at 79.9 m. The frequency of 13000 Hz was used in this simulation. The "true" values for the seabed parameters were taken as: sediment compressional speed $c_p = 1575\,\mathrm{m/s}$, density $\rho = 1.5\,\mathrm{g/cm^3}$ and compressional attenuation $\alpha_p = 0.6\,\mathrm{dB}/\lambda$. The Bartlett estimator power, $P_B(\alpha_p, \rho, c_p)$, is determined when each parameter varies in the following ranges: $\alpha_p \in [0.1, 0.9]\,\mathrm{dB}/\lambda$, $\rho \in [1, 2]\,\mathrm{g/cm^3}$ and $c_p \in [1500, 1800]\,\mathrm{m/s}$, considering the various estimators defined in section 3.3. Since the Bartlett estimator power, $P_B(\alpha_p, \rho, c_p)$, depends on three parameters, a three-dimensional matrix is obtained and the response of the estimators can be represented by a hypercube. The three-dimensional representation of the Bartlett estimator power output, with several slices for each parameter, is shown in Fig. 3.8. The p-only estimator power, considering 4 hydrophones, is presented in Fig. 3.8 (a), while the VSA $(p+v)$ estimator power is shown in (b). The p-only Bartlett estimator shows an amplitude power above 0.9, for sediment compressional speed values below 1600 m/s (see Fig. 3.8 (a)). The figure reveals a wider main lobe but when this is compared with the VSA $(p+v)$ estimator (see Fig. 3.8 (b)) the lobe is reduced, mainly for the sediment compressional speed.

In order to better understand the advantage of using the VSA $(p+v)$ estimator for geoacoustic inversion, the two-dimensional cross-sections ambiguity surfaces are presented in Fig. 3.9 for the following cases: sediment compressional speed versus density (for true compressional attenuation), sediment compressional speed versus compressional attenuation (for true density) and density versus compressional attenuation (for true sediment compres-

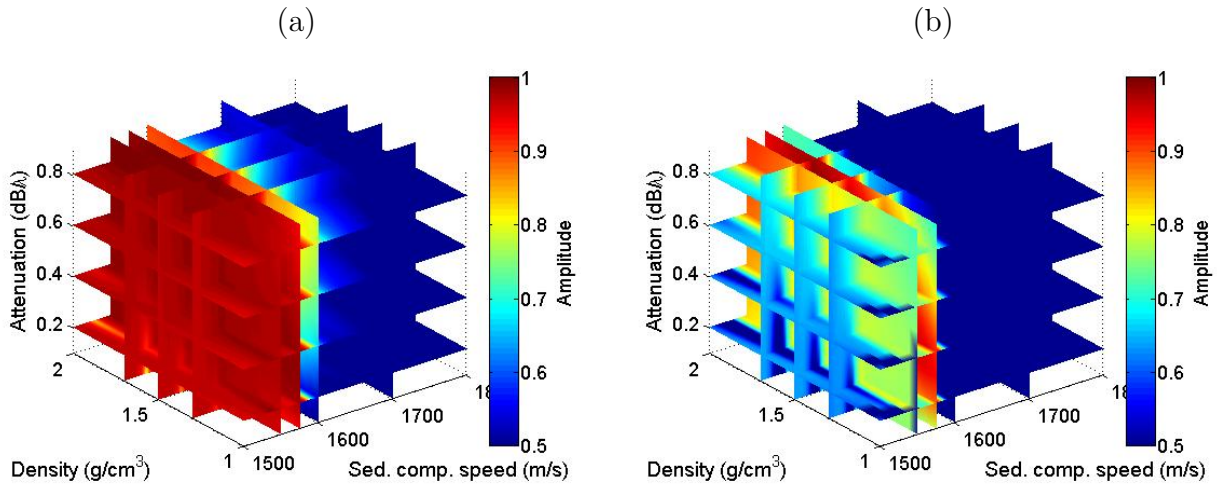

Figure 3.8: Three-dimensional representation of the Bartlett estimator power for three seabed parameters, at frequency 13000 Hz, considering the p-only estimator with 4 hydrophones (a) and the VSA $(p + v)$ estimator (b).

sional speed); the p-only estimator is shown on the left while the VSA $(p + v)$ estimators is shown on the right. On the one hand, the ambiguity surfaces obtained with the p-only estimator present a wider main lobe for all parameters (see left side of Fig. 3.9), showing that it is almost impossible to determine a reasonable estimate of these parameters. On the other hand, the VSA $(p + v)$ estimator (see right side of Fig. 3.9) presents a narrow main lobe, mainly for sediment compressional speed (see Fig. 3.9 (d) and (e)). These results reveal that the sediment compressional speed is a parameter, which may be obtained with higher estimation resolution than the other two parameters; they also show that the VSA $(p + v)$ estimator outperforms the p-only estimator for the estimation of density and compressional attenuation (compare Fig. 3.9 (c) with Fig. 3.9 (f)). The above discussed results confirm the advantage of the VSA over a hydrophone array for the seabed parameter estimation; in what follows this issue will be further illustrated considering one-dimensional cross sections for each parameter.

The performance obtained with the p-only estimator, Eq. (3.27), for 4 and 16 hydrophones

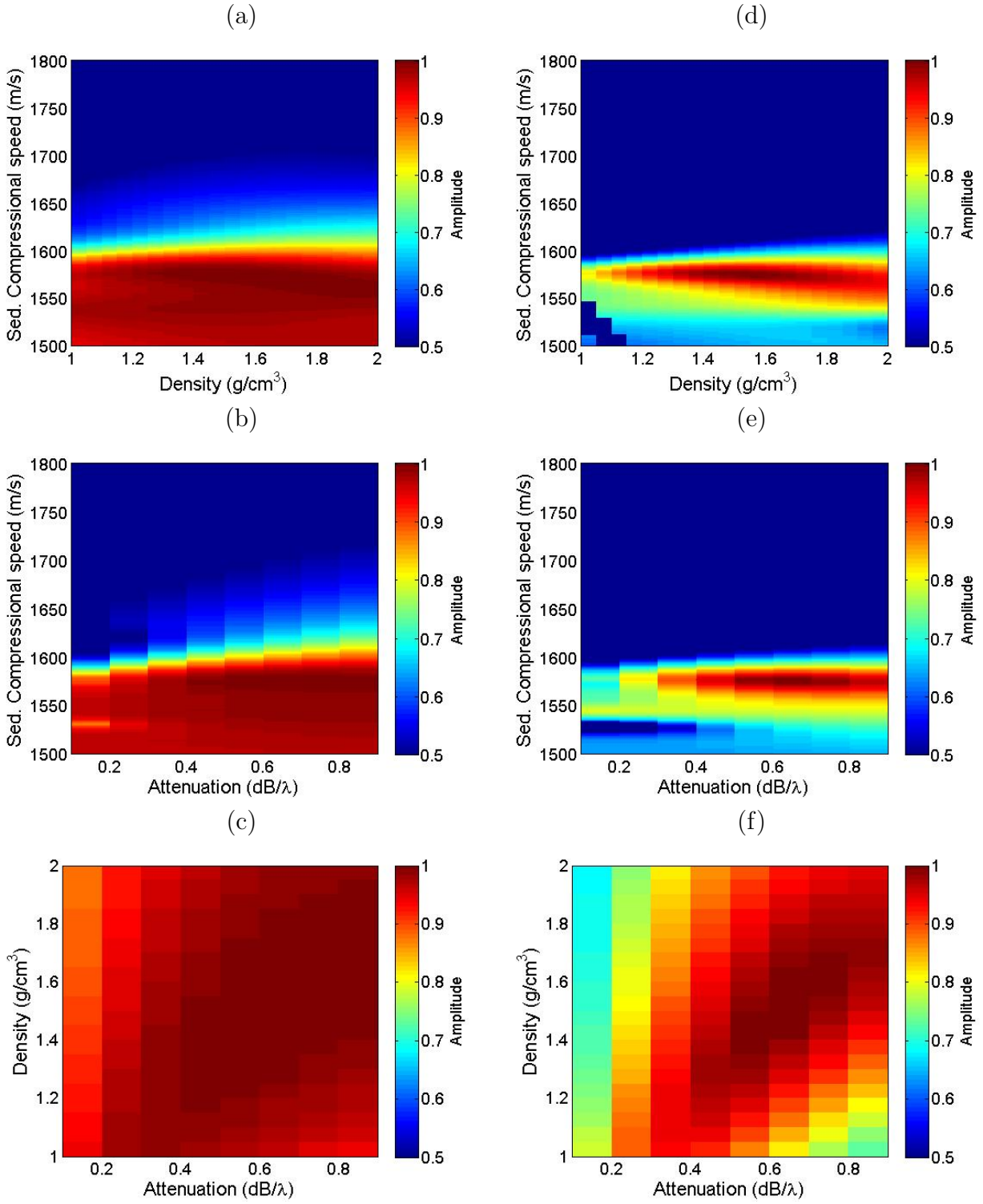

Figure 3.9: Two-dimensional cross-sections of ambiguity surfaces estimation simulation results, obtained with the Bartlett estimator at frequency 13000 Hz, for $c_p = 1575\,m/s$, $\rho = 1.5\,g/cm^3$ and $\alpha = 0.6\,dB/\lambda$ considering: the p-only estimator (4 hydrophones) for fixed compressional attenuation (a), fixed density (b) and fixed sediment compressional speed (c) and the VSA $(p+v)$ estimator (3.36) for fixed compressional attenuation (d), fixed density (e) and fixed sediment compressional speed (f).

is compared with the performance obtained with the VSA $(p + v)$ estimator, Eq. (3.36), in Fig. 3.10 for sediment compressional speed, density and compressional attenuation. The goal of comparing the 4-element VSA (16 output channels) with a 4 and 16 hydrophone array is two-fold: first, to compare arrays with the same aperture, and second, to compare arrays with the same amount of information. The estimators (see Fig. 3.10) show that, as expected, sediment compressional speed can be obtained with higher estimation resolution than density and compressional attenuation; the estimators also illustrate that the VSA improves the estimation resolution of the three seabed parameters, when compared with 4 and 16 hydrophone arrays. The results suggest that the VSA may offer a significant array size reduction with a better performance than hydrophone arrays.

3.5.3 Using individual particle velocity components

In the previous section, it was shown that the VSA improves the performance of seabed parameters estimation when compared with that of hydrophone arrays. The potential gain of using the VSA in inverse problems can be highlighted when the individual components of the particle velocity are used. Therefore, in the following, it will be considered the v-only estimator, Eq. (3.32), with individual particle velocity components; the results are compared with the VSA-based Bartlett estimator, with and without pressure.

The one-dimensional cross-sections ambiguity surfaces obtained for sediment compressional speed, density and compressional attenuation, are shown in Fig. 3.11 (a), (b) and (c), respectively. The ambiguity surfaces were obtained considering the individual particle velocity components, the v-only and the VSA $(p + v)$ based Bartlett estimators. From the analysis of the one-dimensional cross-sections the following conclusions can be drawn:

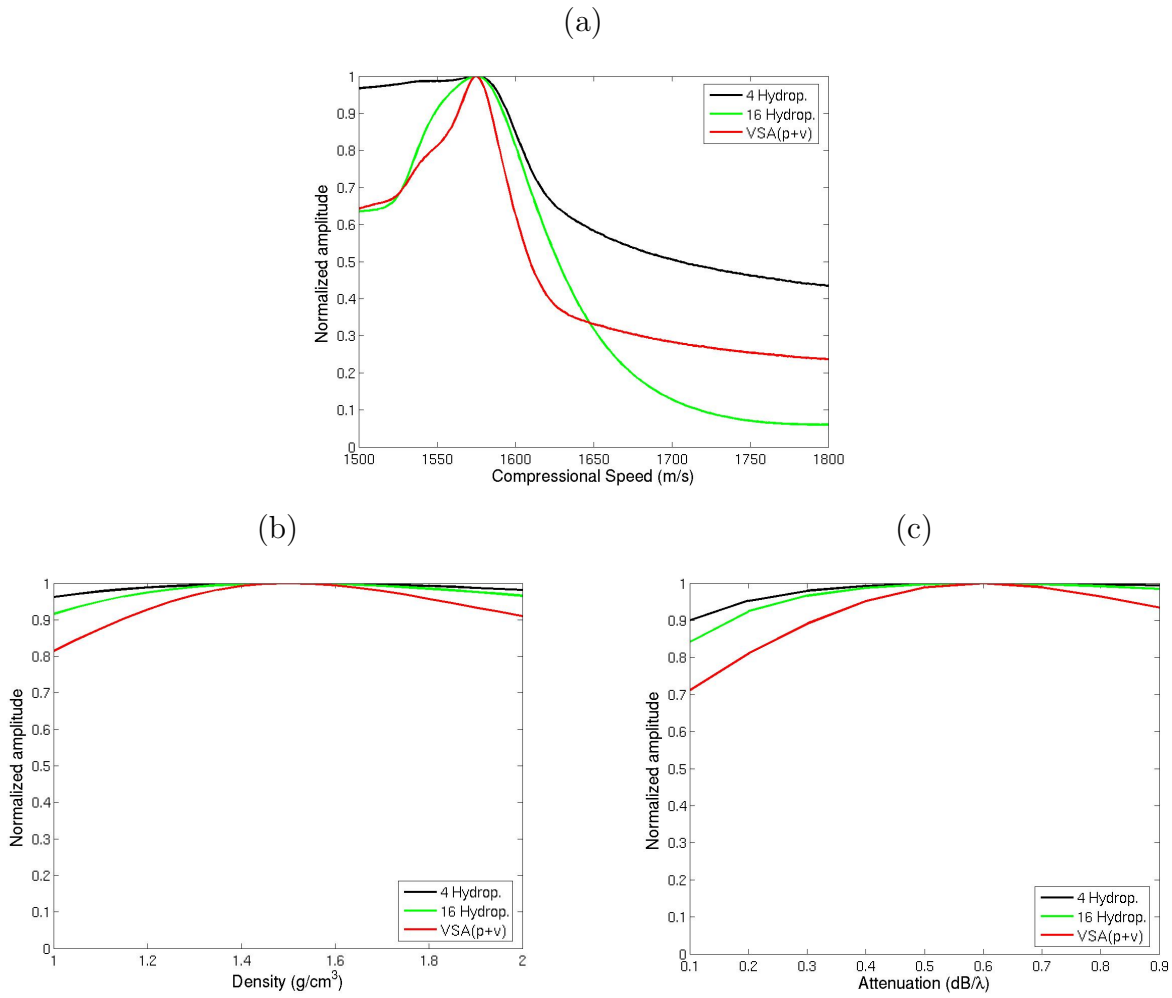

Figure 3.10: One-dimensional cross section ambiguity surfaces obtained with normalized Bartlett estimator at frequency 13000 Hz, for $c_p = 1575\,m/s$, $\rho = 1.5\,g/cm^3$ and $\alpha = 0.6\,dB/\lambda$ considering the p-only estimator with 4 and 16 hydrophones and the VSA $(p+v)$ estimator for: sediment compressional speed (a), density (b) and compressional attenuation (c).

1. The v-only Bartlett estimator (green) has a narrower main lobe than the VSA $(p+v)$ Bartlett estimator (red) due to the directivity factors obtained in Eqs. (3.33) and (3.37). The directivity factor $[4\cos^4(\frac{\delta}{2})]$ provides a wider main lobe than $[\cos^2(\delta)]$ eliminating possible ambiguities (similarly as for DOA estimation discussed in section 3.4);

2. The results obtained for horizontal particle velocity components, v_x (dashed) and v_y (circles), are coincident with an amplitude power above 0.9 and exhibit a very large main lobe, which is similar as those obtained for the p-only response with 4 hy-

drophones. Such results are due to the fact that horizontal components mostly depend on low-order modes [52], thus they depend on rays which have little or no interaction with the seabed. Moreover, those results confirm the conclusions regarding the analysis of the TL presented in section 3.5.1;

3. The most important conclusion is that the vertical component v_z (blue) has the highest sensitivity to ocean bottom parameters among all the other components, including the v-only and the VSA $(p + v)$ estimators. In fact, such sensitivity is influenced by the high-order modes with a large contribution to the vertical component due to their grazing angles. The vertical component depends on rays which suffer multiple surface and seabed reflections, as previously shown by the TL calculations presented in Figs. 3.6 (c) and 3.7 (c). Additionally, Fig. 3.11 shows that the v_z-only Bartlett estimator potentially provides the highest estimation resolution for all three seabed parameters.

Since the vertical particle velocity component has the best estimation resolution regarding the seabed parameters, the following discussion will consider the estimator Eq. (3.32) with the vertical only component of the particle velocity (v_z-only Bartlett estimator). The ambiguity surfaces for sediment compressional speed versus density, sediment compressional speed versus compressional attenuation and density versus compressional attenuation, are shown in Fig. 3.12 (a), (b) and (c), respectively. The figure reveals that the vertical component shows a narrow main lobe present in all ambiguity surfaces and all seabed parameters. Such results confirm the improvements of the estimation results obtained with the VSA $(p + v)$ estimator (see Fig. 3.9 (d), (e) and (f)) but with narrower main lobes.

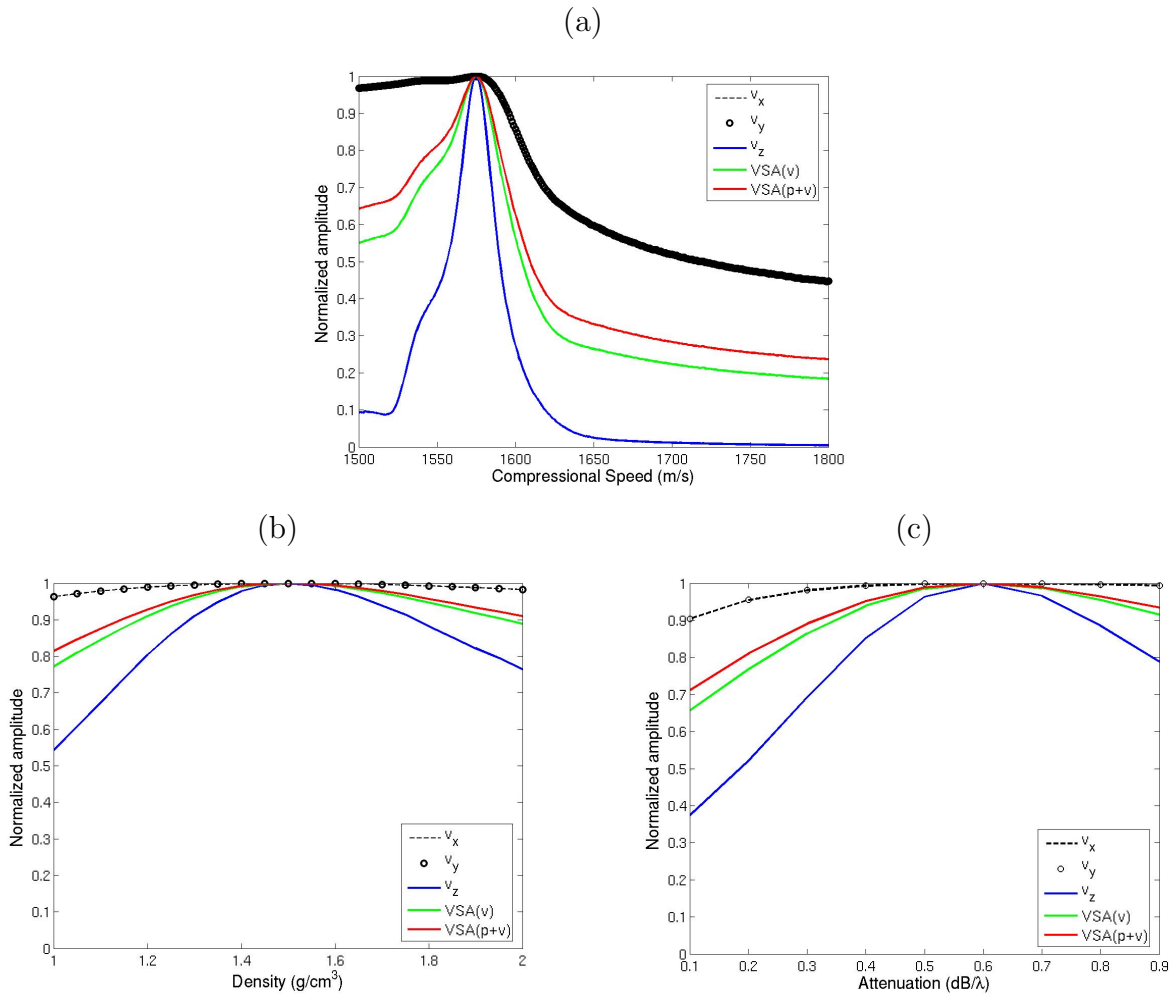

Figure 3.11: One-dimensional cross sections ambiguity surfaces obtained with normalized Bartlett estimator, at frequency 13000 Hz, for $c_p = 1575\,m/s$, $\rho = 1.5\,g/cm^3$ and $\alpha = 0.6\,dB/\lambda$ considering the individual data components (v_x, v_y and v_z), v-only estimator and the VSA ($p+v$) estimator for: sediment compressional speed (a), density (b) and compressional attenuation (c).

The analysis of the three-dimensional representation of the v_z-only Bartlett estimator, is shown in Fig. 3.13, which has several slices for each parameter. The figure confirms the highest estimation resolution of the vertical particle velocity component, even for density and compressional attenuation, which are difficult to estimate with the p-only estimator. Fig. 3.13 (a) shows six slices for various compressional attenuation values; it illustrates that the maximum appears at the true compressional attenuation value of 0.6 dB/λ, but a side lobe exists for values below 0.4 dB/λ, which peak-to-side lobe ratio does not exceed 0.6. This

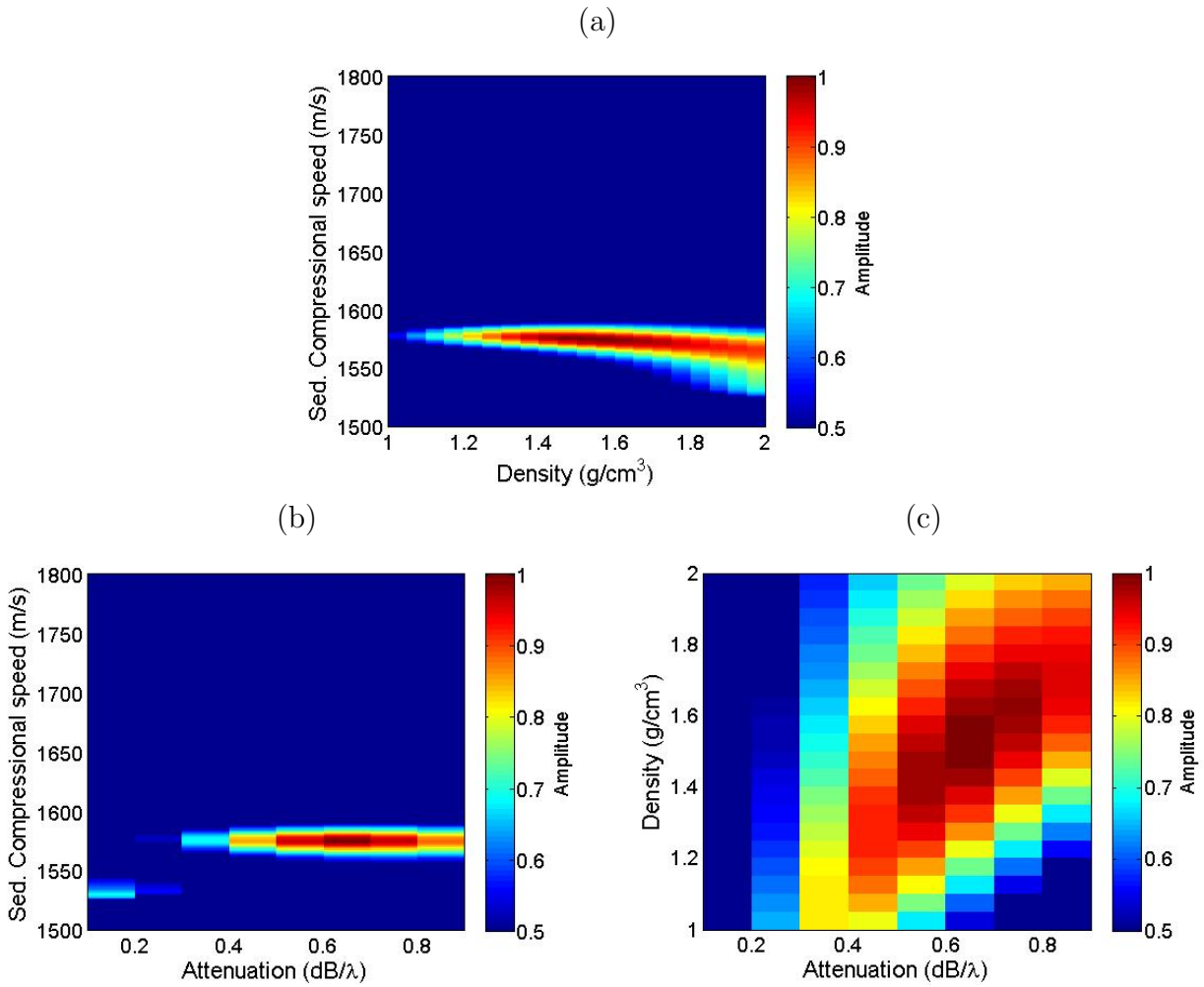

Figure 3.12: Two-dimensional cross-sections ambiguity surfaces simulation results obtained with Bartlett estimator, at frequency 13000 Hz, for $c_p = 1575\,m/s$, $\rho = 1.5\,g/cm^3$ and $\alpha = 0.6\,dB/\lambda$ considering the vertical particle velocity only component in Eq. (3.32) for fixed compressional attenuation (a), fixed density (b) and fixed sediment compressional speed (c).

ratio is confirmed for values of density above 1.5 g/cm^3, shown in Fig. 3.13 (b), and also for values of sediment compressional speed around 1550 m/s, shown in Fig. 3.13 (c).

The VSA-based Bartlett estimator, in particular, the v_z-only Bartlett estimator confirms that MF inversion is less sensitive to density and compressional attenuation than to sediment compressional speed; however, the best estimation resolution of such parameters is obtained with the v_z-only Bartlett estimator. One can conclude that a VSA with few elements is able to increase significantly the resolution of all seabed parameters, and the higher resolution

can be achieved using only the vertical particle velocity component.

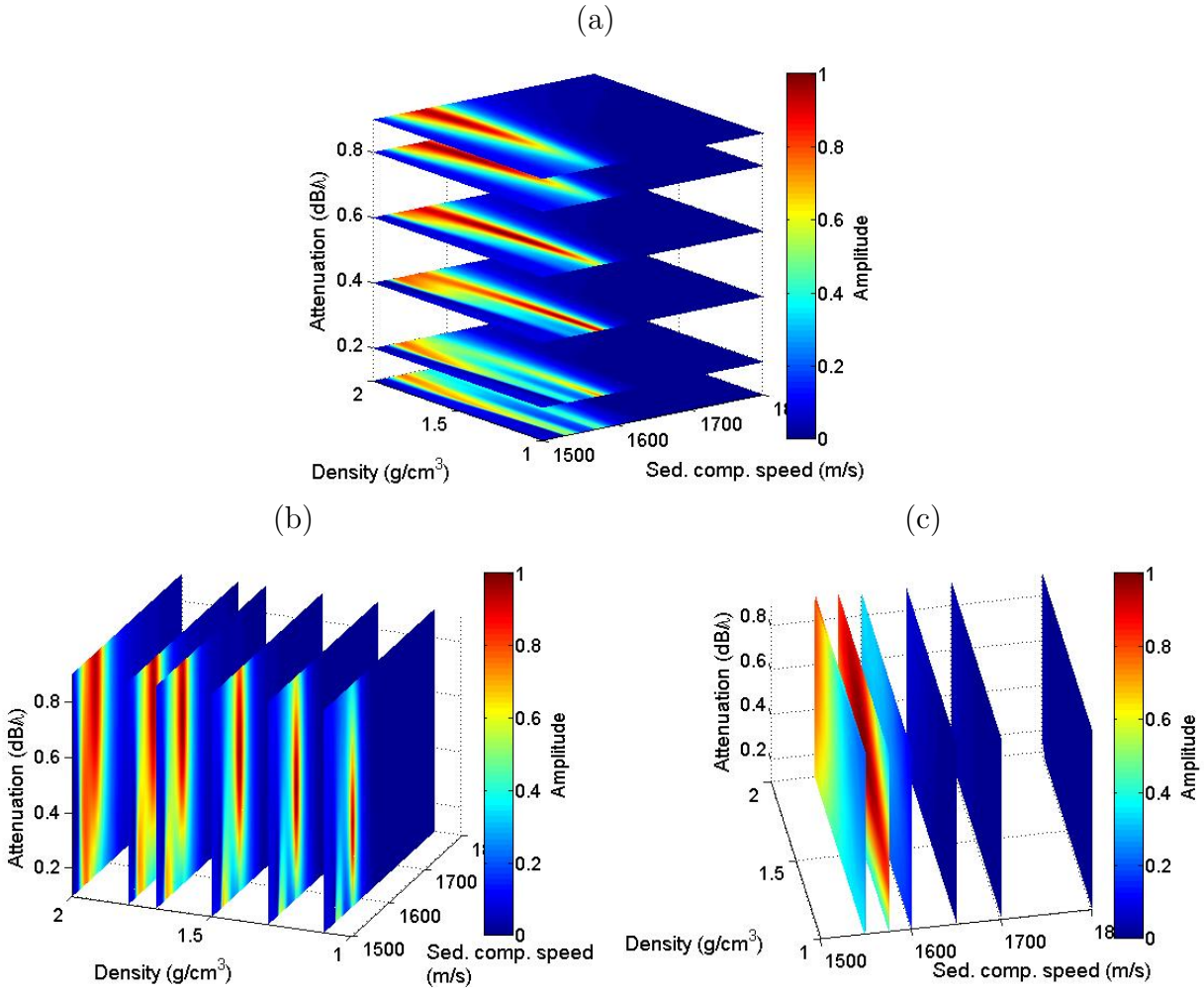

Figure 3.13: Three-dimensional representation of the v_z-only Bartlett estimator power, for the three seabed parameters, at frequency 13000 Hz, considering several slices for: compressional attenuation (a), density (b) and sediment compressional speed (c).

Summary

In this chapter a data model for generic parameter estimation was derived that accounts for particle velocity components. The conventional Bartlett processor was extended to include particle velocity outputs and two VSA-based estimators were proposed. It was shown that the v-only and VSA $(p+v)$ Bartlett estimators are proportional to the p-only Bartlett estimator, where the inner product between the replica vector and the data vector is the constant

of proportionality, called directivity factor. The two directivity factors presented, provide an improved sidelobe reduction (for v-only) or sidelobe suppression (for VSA (p+v)), when compared with the p-only Bartlett response; thus, both factors contribute to an improvement of the estimation resolution of the ocean parameters. The VSA-based Bartlett estimators were tested in DOA estimation and, most importantly, in the estimation of the seabed parameters. It was shown that a VSA, with only a few elements, is able to substantially increase the estimation resolution of seabed parameters, such as sediment compressional speed, density and compressional attenuation, when compared with an array with the same number of hydrophones. Furthermore, it was also shown that such results can be attained considering only the vertical particle velocity component, where the best resolution of seabed parameters estimation was obtained. A brief study of the transmission loss with HF signals for acoustic pressure, horizontal and vertical particle velocity components, was presented; the study showed that the propagation channel, at the considered HF band, reaches the receivers after bottom reflections with a sufficient amount of energy for geoacoustic inversion. The contribution of the field to the vertical component is important for bottom characterization and this issue was confirmed by MFI simulation results. The vertical component is the most useful component in the seabed characterization, providing the best seabed parameter estimates. At this point and regarding the conclusions of the simulations, the following question arises: can such conclusions hold in a real scenario? Such question will be discussed in the following chapters where experimental data will be considered for DOA estimation in Chapter 4 and for seabed parameter estimation in Chapter 5.

The next chapter will describe the MakaiEx'05 sea trial, during which vector sensor array was used. The VSA experimental results for DOA estimation of towed and fixed acoustic

sources, using high frequency signals acquired during the MakaiEx'05, will also be presented. The discussion will start with the horizontal plane orientation of vector sensor elements required for VSA data processing; the orientation of those elements will be determined using the ship's noise signature in the low frequency band.

Chapter 4

Experimental results on DOA estimation

The advantages of the VSA in parameter estimation and, in particular, its ability to acquire the particle velocity information, were discussed in chapters 2 and 3. A VSA measures the acoustic pressure and the three particle velocity components and it has the ability to provide substantially high directivity and gain not achievable with the same number of pressure-only sensors. The vertical VSA is able to estimate both elevation and azimuth angles and eliminates the left/right ambiguity which affects the linear and planar hydrophone array configurations, consequently improving DOA estimation. Such advantages of the VSA for DOA estimation were also confirmed for geoacoustic inversion, using simulated data. The various spatial components were found to be sensitive to different environmental information enlightening the improved performance of the VSA. In particular, the vertical particle velocity component revealed the highest sensitivity to bottom structure because it had a strong contribution of the acoustic field after bottom reflections.

In order to validate the advantages of the VSA in inversion problems, the VSA data model and VSA Bartlett estimators described in chapter 3 will be tested with experimental data acquired during the MakaiEx'05 sea trial. Therefore, this chapter describes the geometry and

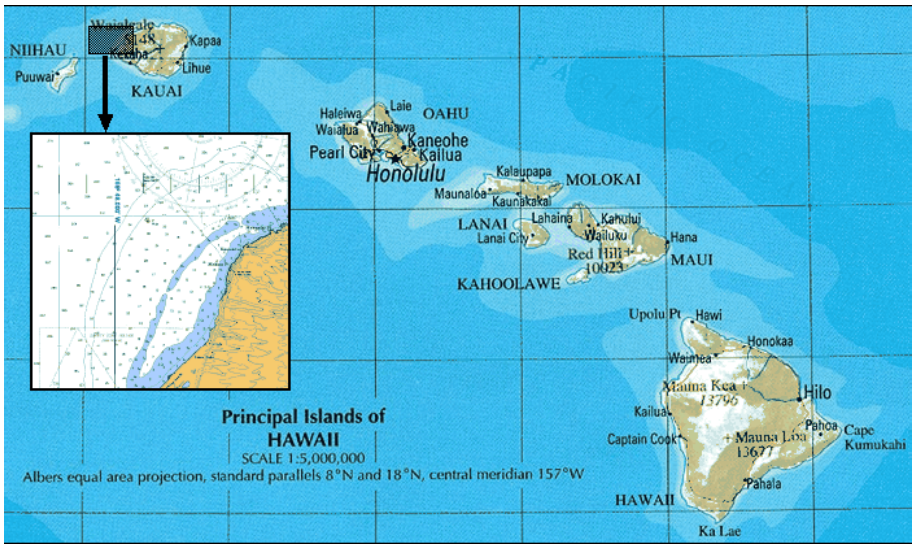

Figure 4.1: MakaiEx'05 site off the north west coast of Kauai Island, Hawaii, USA.

environmental data of the sea trial, the emitted signals and the VSA used in the MakaiEx'05 experiment. Moreover, this chapter presents the VSA experimental results for DOA estimation of acoustic sources using low and high frequency signals, for the three day deployments of the VSA. It should be remarked that the experimental results on DOA estimation are a pre-processing requirement for the analysis of the experimental results related to seabed parameter estimation. The DOA results are important for determining the horizontal plane orientation of the v_x and the v_y VSA components, initially unknown, and for determining the azimuth angle essentially for the v_x and the v_y components (in Eq. (3.6)). Preliminary results on DOA estimation using experimental results was discussed in [58], which describes how the orientation of the horizontal plane of the VSA axes was determined.

4.1 The Makai experiment 2005

The MakaiEx'05 sea trial took place off the coast of Kauai Island, Hawai, from 15 September to 2 October 2005. This was the third experiment specifically planned to acquire data to

support the High-Frequency initiative (HFi) [55], and was the first experiment that included a VSA to acquire HF signals. The HFi involved a wide spectrum of objectives that reflected specific interests such as: high-resolution tomography, acoustic propagation modelling in the high frequency band, understanding of the acoustic-environment interaction at high frequencies and its influence on underwater communications. The experiment, which was organized by HLS Research and financed by ONR, involved several teams from both government and international laboratories, universities and private companies, such as HLS Research, University of Algarve, University of Delaware, SPAWAR, Naval Research Laboratory, NATO Undersea Research Center, Woods Hole Oceanographic Institute, and others. The selected area for the MakaiEx'05 is shown in Fig. 4.1 and it is described in detail in [55, 74].

4.1.1 Environmental data

The bathymetry map of the MakaiEx'05 area is shown in Fig. 4.2, which shows an almost smooth and uniform area of depth around 80-100 m accompanying the island bathymetric contour, surrounded by the continental relatively steep slope to the deeper ocean to the West. Extensive data measurements were carried out in this area during previous experiments and have shown that most of the ocean bottom of the area is covered with coral sands over a basalt hard bottom. The sound velocity in coral sands is approximately 1700 m/s, while the sediment thickness in this area is unknown, but expected to be a fraction of a meter in most places according to previous sidescan surveys. It is expected that coral sands cover most of the plateau around the Kauai Island.

During MakaiEx'05 different environmental recording equipments were deployed, in an attempt to collect as much environmental data as possible. In particular the deployment

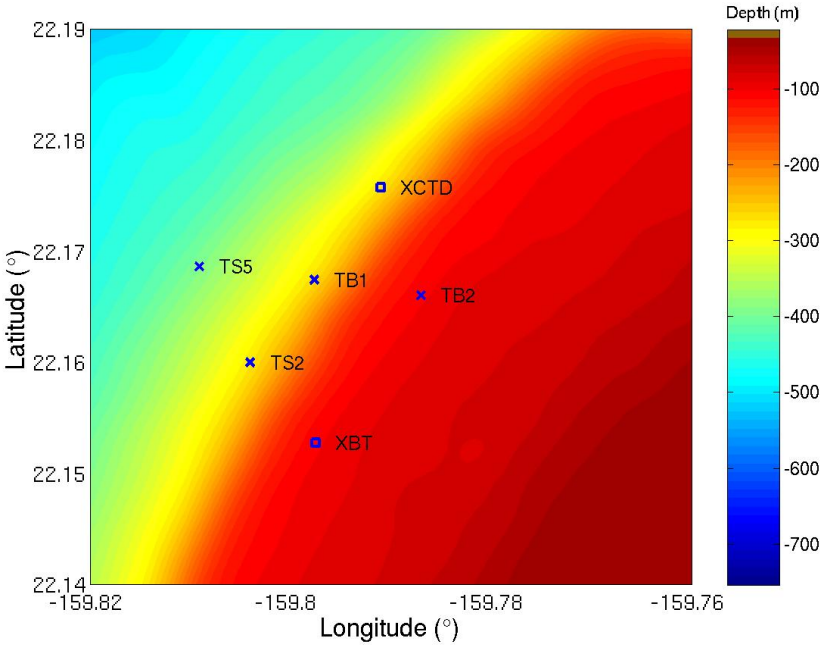

Figure 4.2: Bathymetry map of the Makai experiment area and the location of the testbed acoustic sources TB1 and TB2, thermistor strings TS2 and TS5, XBT and XCTD.

was aimed at determining water column variability. To such end two thermistor strings (TS2 and TS5), XBTs and XCTDs recordings were used. Fig 4.2 shows the localization of that equipment as well as the testbed acoustic sources TB1 and TB2.

The recorded temperatures for the thermistor strings: TS2 and TS5, between September 17th (Julian day 260) and September 29th (Julian day 273) are shown in Fig. 4.3 (a) and (b), respectively. The variability of the sound speed profile during September 20th (Julian day 264) is shown in Fig. 4.4, where the thick line represents the mean sound speed profile for TS2 which is used for data processing, due to the proximity of TS2 to the acoustic sources TB1 and TB2.

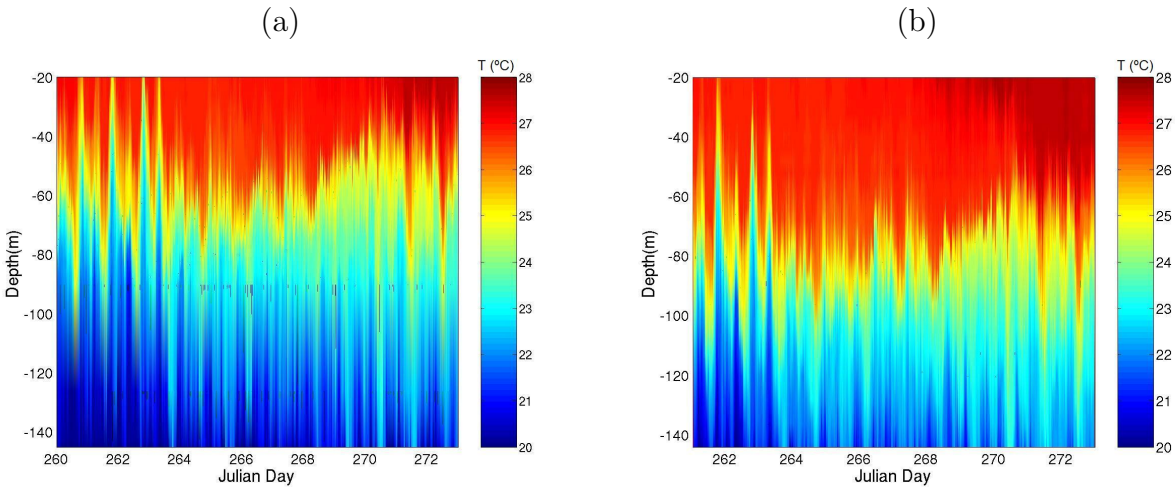

Figure 4.3: Thermistor strings temperature data in °C: TS2 (a) and TS5 (b) during MakaiEx'05 sea trial, between September 17th (Julian day 260) and September 29th (Julian day 273).

4.1.2 Vector Sensor Array in MakaiEx'05

The VSA used during MakaiEx'05 consisted of TV-001 type sensors, constructed by Wilcoxin Research Inc., with one omni-directional hydrophone (pressure-only sensor) and three uni-axial accelerometers arranged in a tri-axial configuration, measuring the particle velocity in a specific direction - x, y and z direction [10]. The hydrophone is constructed with conventional piezoelectric ceramic materials such as Lead Zirconate Titanate (PZT), while the accelerometers are constructed with a new piezoelectric material called Lead Magnesium Niobate / Lead Titanate, known as PMT-PT crystals. This new material increases the piezoelectric properties over the conventional piezoelectric ceramics, allowing to reduce the weight and the size of the sensors. The vector sensor was mounted in a neutrally buoyant package approximately 3.81 cm in diameter and 6.35 cm long, as shown in Fig. 4.5 [75].

A five-element vertical VSA, represented in Fig. 4.6, with 10 cm spacing between each element, was used during the MakaiEx'05 to collect data from towed and fixed acoustic sources. The VSA was deployed during three time periods corresponding to three data sets:

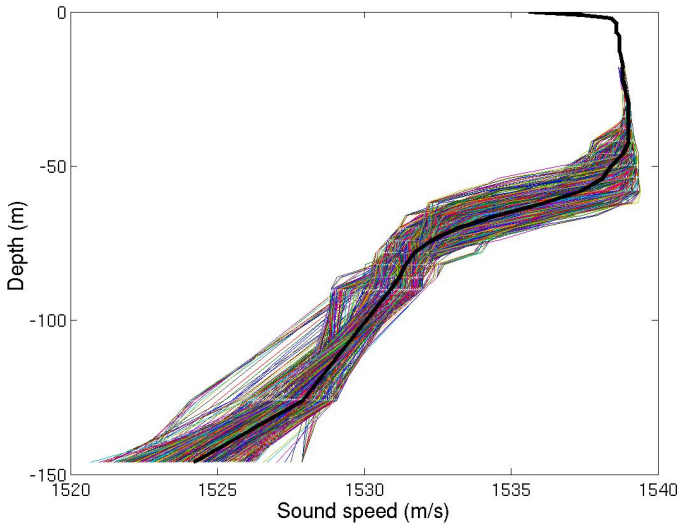

Figure 4.4: Sound speed profiles during September 20th (Julian day 264) and the mean sound speed profile - black thick line.

Figure 4.5: Constitution of a single vector sensor and x, y and z-axis orientation.

one on September 20th - Julian day 264 (deployment 1), where acoustic signals were emitted by two fixed testbed sources TB1 and TB2; another on September 23rd - Julian day 267 (deployment 2), where signals were emitted only by the testbed TB2; and a third and last recording on September 25th - Julian day 268 (deployment 3), where signals were emitted by the Lubell 916C source towed by a Rigid-Hull Inflatable Boat (RHIB). The time schedule of the VSA deployments during MakaiEx'05 is presented in Table 4.1. The VSA was fairly close to the stern of Research Vessel (R/V) Kilo Moana tied to a vertical cable, with a 100-150 kg weight at the bottom (only on deployments 2 and 3), to ensure that the array stayed

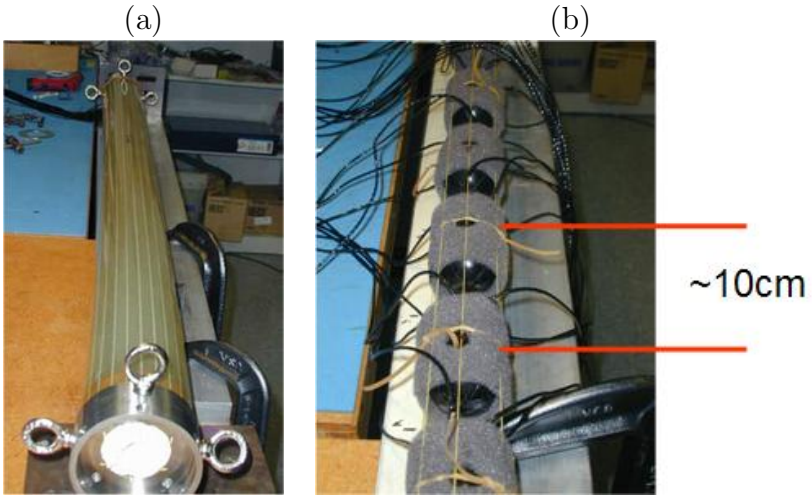

Figure 4.6: A five-element vertical VSA: hose (a) and 10 cm element spacing view (b).

VSA	*Start time*		*End time*	
	Local time	*Julian day*	*Local time*	*Julian day*
Deployment 1	20/09/05; 19:20	264.22	21/09/05; 05:30	264.5
Deployment 2	23/09/05; 19:00	267.21	23/09/05; 22:10	267.34
Deployment 3	25/09/05; 08:30	268.77	25/09/05; 10:22	268.85

Table 4.1: Time schedule of VSA deployments during MakaiEx'05.

as close to the vertical as possible. Each element of the VSA produces four streams of data, one for the pressure-only output and three for the particle velocity outputs. Therefore, 5 elements produce 20 data channels time series. Unfortunately, the 5th element did not work and therefore only 16 channels were acquired.

The VSA was deployed with the z-axis vertically oriented with respect to the bottom but the orientation of x and y-axis were unknown and could change over time due to R/V Kilo Moana displacements and cable rotation. As a first attempt to overcome this lack of information, the horizontal orientation of the VSA was determined by beamforming the acoustic noise signature generated by the R/V Kilo Moana which, combined with the R/V Kilo Moana heading and GPS positioning, allows for placing the VSA x and y-axis in an

absolute referential. Next, the experimental VSA data will be used for DOA estimation of the emitting acoustic sources in order to validate the initial estimation of the x-y VSA axes orientation.

4.2 Beamforming of ship's noise

During the processing of the data collected by the VSA in the low frequency band it was noticed that the spectral characteristics of the signal are fairly stable for all days during which the VSA was deployed. The noise spectrogram generated by the R/V Kilo Moana is shown in Fig. 4.7, which was obtained on the VSA pressure-only sensor at 79.6 m depth on September 20th and it is representative of the noise generated in other deployments. Two dominant frequencies, 180 Hz and 300 Hz, were found in all output signals of the VSA (pressure-only and particle velocity components), as shown in Fig. 4.8. These frequencies were assumed to be part of ship's noise signature and were used to estimate the orientation of the VSA on the horizontal plane, initially unknown.

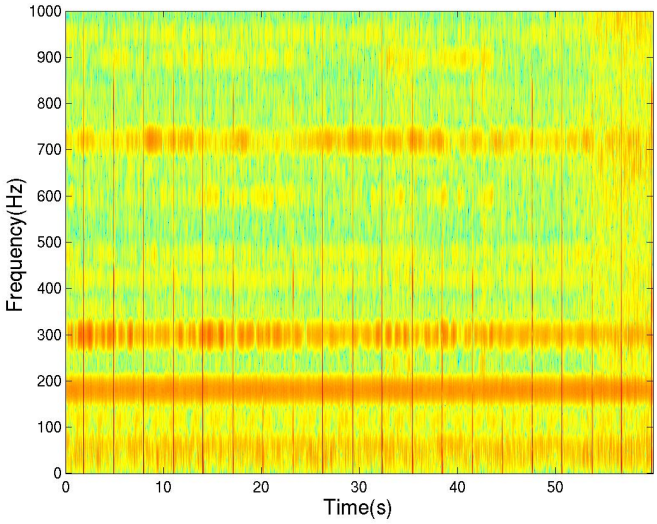

Figure 4.7: Spectogram of noise generated by R/V Kilo Moana on VSA pressure-only sensor at 79.6 m depth, on September 20th (Julian day 264).

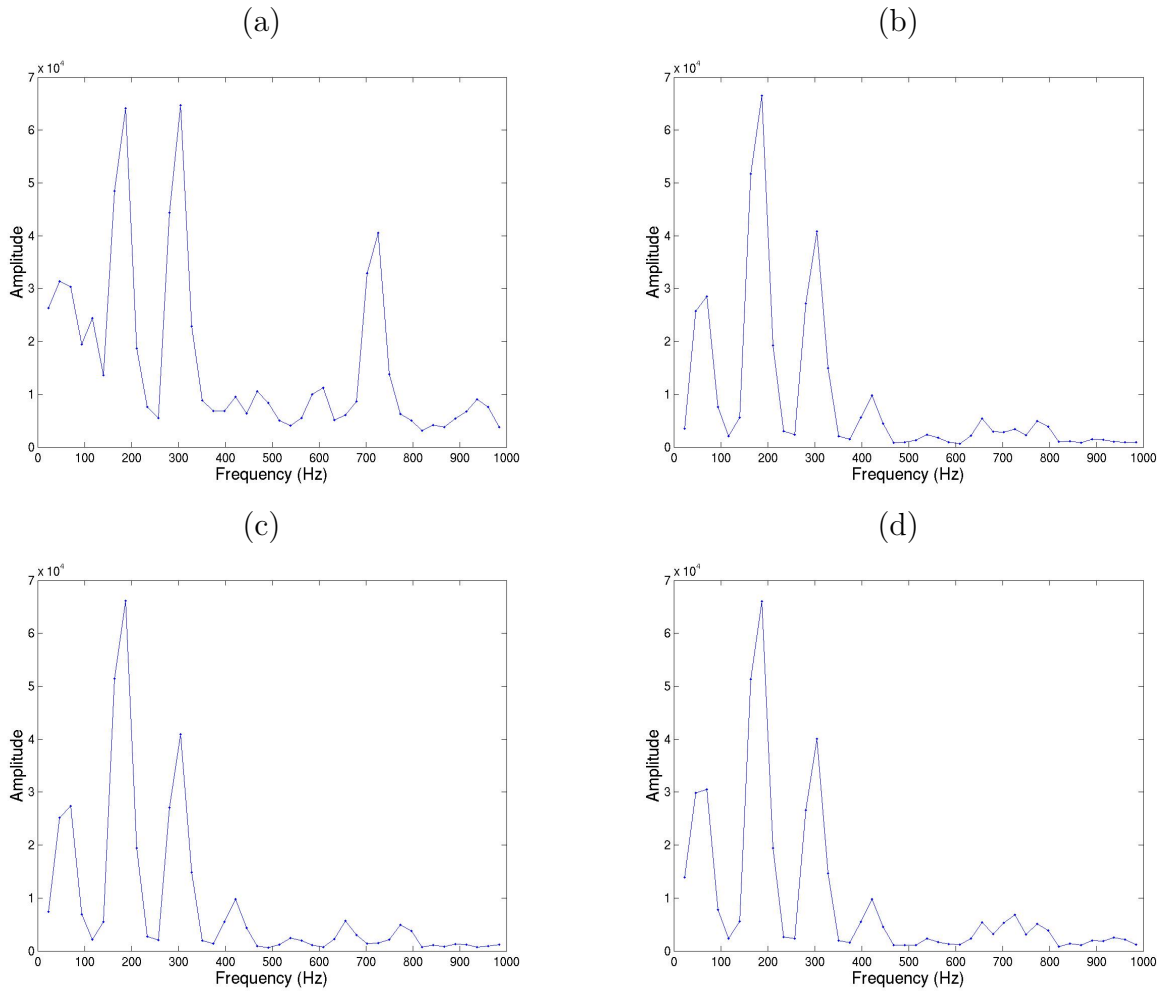

Figure 4.8: Power spectrum estimates (periodogram with 1 s averaging time) of noise generated by R/V Kilo Moana on September 20th, on vector sensor at 79.6 m depth for: pressure-only sensor (a), v_x component (b), v_y component (c) and v_z component (d) of particle velocity sensors.

The normalized ambiguity surfaces obtained when the plane-wave beamformer is applied to the measured VSA data, at frequency 300 Hz, are shown in Fig. 4.9. The results obtained with the v-only Bartlett estimator Eq. (3.32) and with the VSA $(p + v)$ Bartlett estimator Eq. (3.36), are presented in Fig. 4.9 (a) and (b) respectively. In this case, the replica vectors are given by:

$$\mathbf{e}_v(\theta_S, \phi_S) = [\mathbf{u}(\theta_S, \phi_S)]^T \otimes \exp(i\mathbf{k}.\mathbf{r_l}), \tag{4.1}$$

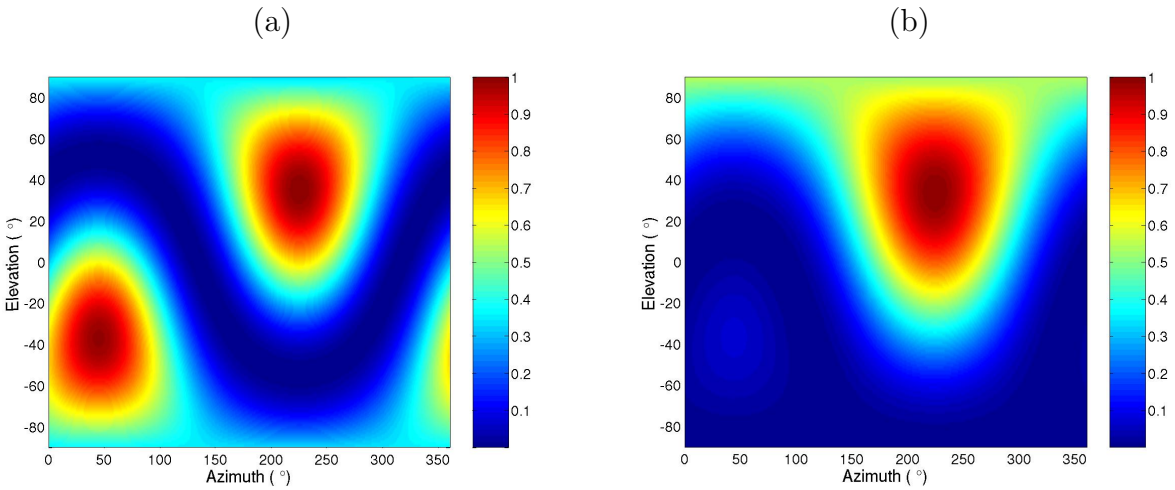

Figure 4.9: The normalized ambiguity surfaces for DOA estimation, obtained with measured VSA data on September 20th at frequency 300 Hz, using the Bartlett beamformer considering: v-only (a) and VSA $(p+v)$ (b).

for the v-only Bartlett estimator and:

$$\mathbf{e}_{pv}(\theta,\phi) = \left[\begin{array}{cc} 1 & \mathbf{u}(\theta,\phi) \end{array}\right]^T \otimes \exp(i\mathbf{k}.\mathbf{r}_l), \tag{4.2}$$

for the VSA $(p+v)$ Bartlett estimator, where the weigthing vector $\mathbf{u}(\theta_S,\phi_S)$ is the direction cosines given by:

$$\mathbf{u}(\theta_S,\phi_S) = \left[\begin{array}{ccc} \cos(\theta_S)\sin(\phi_S) & \sin(\theta_S)\sin(\phi_S) & \cos(\phi_S) \end{array}\right]^T. \tag{4.3}$$

As already discussed in the simulations, the measured data DOA estimation with v-only presents an ambiguity, shown in Fig. 4.9 (a), due to the directivity factor $[\cos^2(\delta)]$, which is eliminated when the acoustic pressure is included (see Fig. 4.9 (b)). The ambiguity surface is remarkably consistent for all days, with the main lobe at an azimuth angle of 226° and an elevation angle of 34°.

Bearing in mind the objective of the horizontal orientation of the VSA x and y axes, the determination of the azimuth angle is necessary. The estimation results of the azimuth angle, for all VSA deployments and during the data acquisition period at the frequency

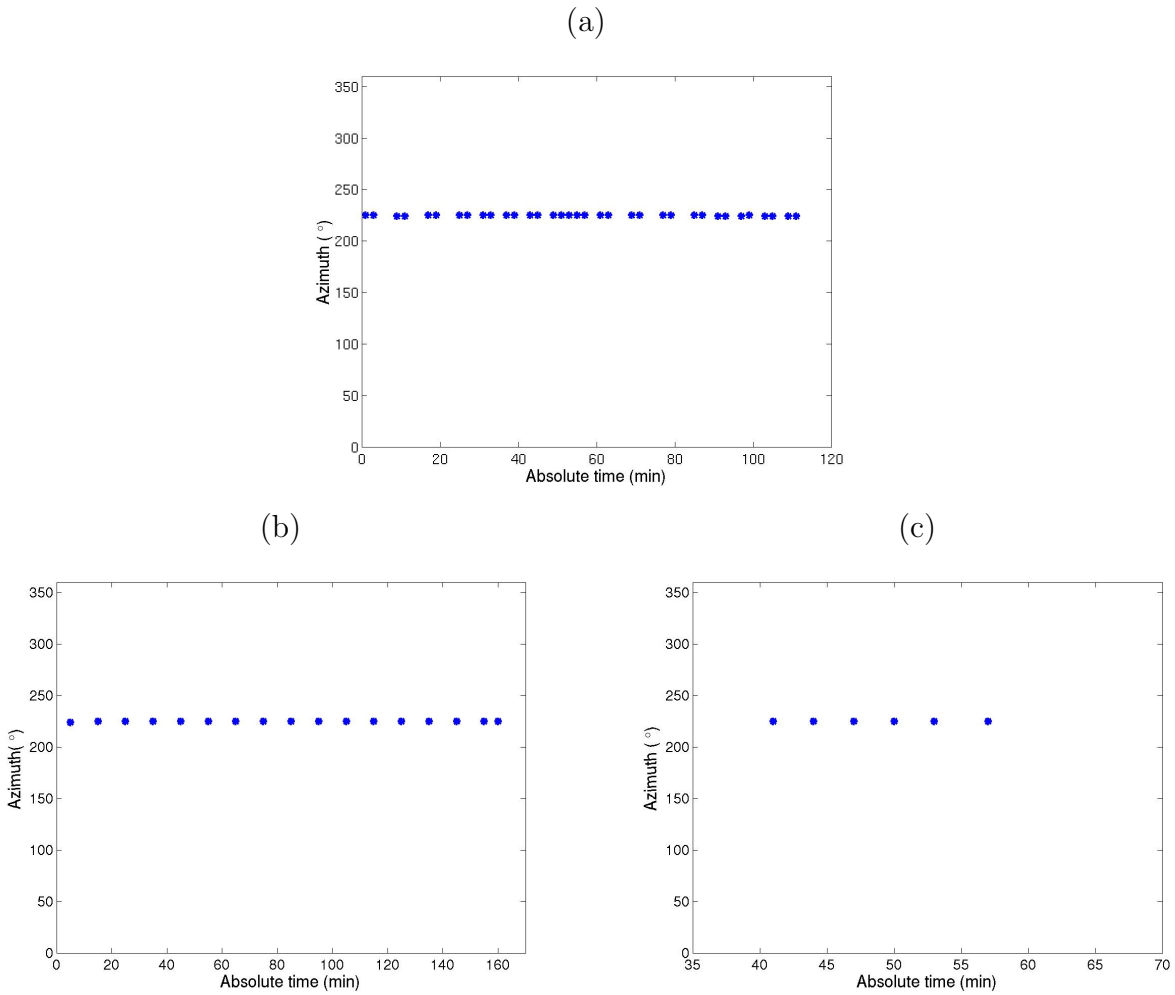

Figure 4.10: Azimuth estimation results during the VSA data acquisition period at the frequency 300 Hz on: September 20th (a), September 23rd (b) and September 25th (c).

of 300 Hz, are shown in Fig. 4.10. The azimuth estimates on September 20th is shown in Fig. 4.10 (a), while (b) and (c) present the results for September 23rd and September 25th, respectively. Although the ship's noise signal is continuous in time, the results presented in Fig. 4.10 were only determined when the acoustic sources were emitting; consequently, the estimation is represented as successive points in the figure. The figure reveals that the estimated azimuths do not vary over the processing interval; moreover, one can conclude that the VSA was deployed with the same orientation relatively to the R/V Kilo Moana for all days, which can be used to determine the horizontal plane orientation of the VSA.

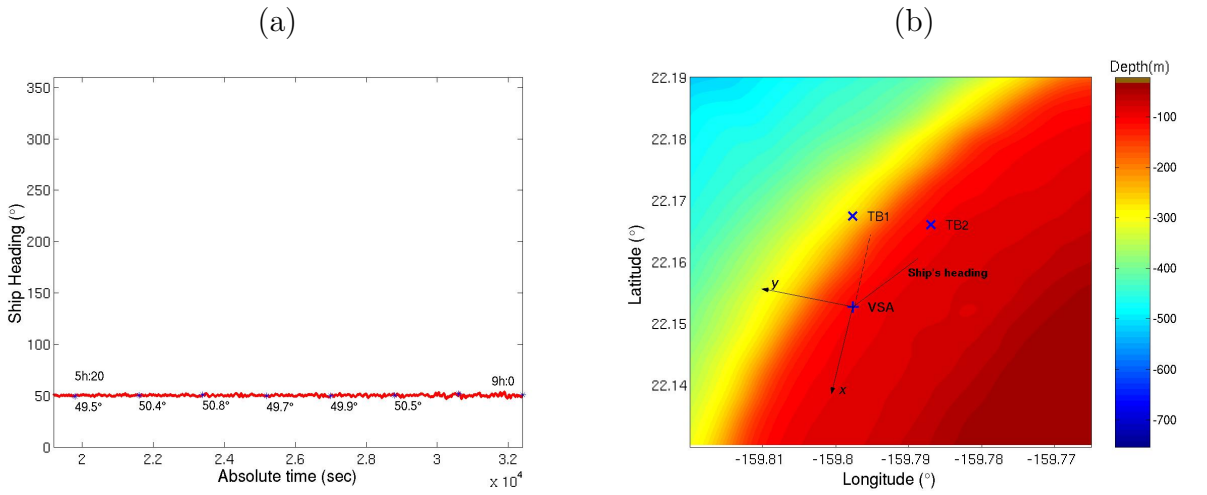

Figure 4.11: The heading data from ship's instruments (a) and the x and y-axis orientation of VSA relatively to Kilo Moana's heading, bearing in mind the ship's noise azimuth angle estimation on September 20th.

In order to determine the horizontal orientation of the VSA, the ship's heading information must be combined with the azimuth angles previously estimated. The heading data as given by the ship's instruments, on September 20th, is shown in Fig. 4.11 (a). This figure indicates that the R/V Kilo Moana was heading approximately 50° with respect to North and did not change its position during the data acquisition period. Comparing the heading data with the azimuth estimation results obtained with ship's noise, one can conclude that the x-axis component of the VSA was oriented approximately to the South and the y-axis component oriented to the West. From this, it follows the horizontal plane orientation of the x-y axis presented in Fig. 4.11 (b), which includes the bathymetry map with the location of the bottom moored acoustic sources TB1 and TB2.

On September 23rd, the R/V Kilo Moana with the VSA at the stern was drifting from TB2 location to the North, as shown in Fig. 4.12 (a). The figure exhibits the ship's heading variability, from 45° with respect to North (at the beginning of the data acquisition) to approximately 100° (at the end of the data acquisition). The figure also shows that the R/V

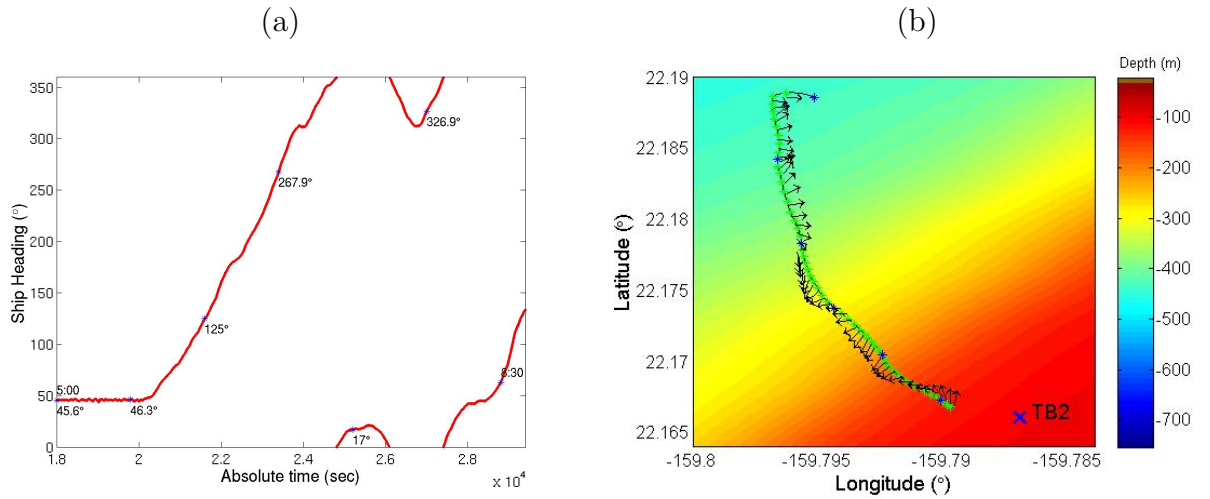

Figure 4.12: The heading data from ship's instruments (a), the trajectory of the R/V Kilo Moana (green line) and the orientation of x particle velocity component of the VSA obtained from ship's noise and ship's heading during the drift, on September 23rd (b).

Kilo Moana's orientation passed twice through heading zero (North), confirming the great variability of the ship's heading. The orientation of the x-axis (which changes during the drift), the ship's trajectory and the location of the acoustic source TB2, are depicted in Fig. 4.12 (b). The x-axis orientation was obtained adding the estimated azimuth of the ship's noise, 226°, with the ship's heading during the period of data acquisition (approximately two hours). The figure shows that the x-axis changes considerably on September 23rd, resulting on changes of the horizontal plane orientation of the VSA.

The last VSA deployment occurred on September 25th. For this deployment the heading data, obtained from R/V Kilo Moana's instruments and shown in Fig. 4.13 (a), indicates a constant heading at approximately 40° with respect to North. The Lubell 916C source trajectory, the VSA location and the estimated horizontal orientation of the VSA elements, combined with the ship's heading on September 25th, are depicted in Fig. 4.13 (b). The figure shows that the Lubell 916C source approachs the VSA almost from the same azimuth angle.

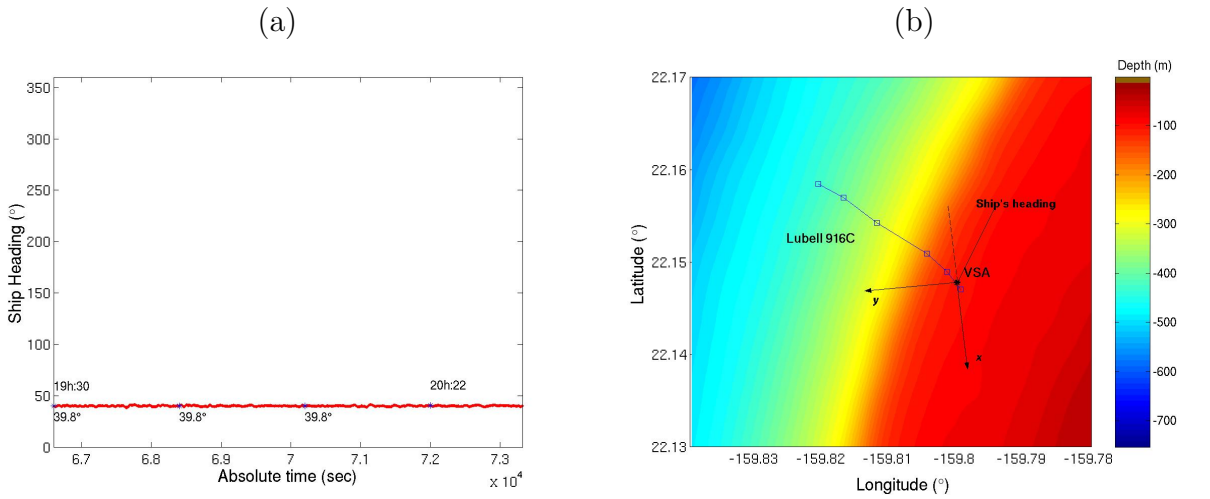

Figure 4.13: The heading data from ship's instruments (a), the orientation of x and y-axis of the VSA obtained from ship's noise and ship's heading, and the trajectory of the acoustic source Lubell 916C, on September 25th.

In the following section the fixed and towed acoustic sources DOA estimation will be presented for the three VSA deployments, in order to validate the previous horizontal plane orientation of the VSA elements.

4.3 Acoustic sources DOA estimation

The ship's noise signature discussed in the previous section was used to define the orientation of the x and y-axis of the VSA components. The knowledge of the horizontal orientation of the VSA can be used for DOA estimation of the acoustic sources during the MakaiEx'05 experiment for the three VSA deployments. The results of DOA estimation will be compared with expected bearings in order to validate the initial estimates of the horizontal orientation. The expected bearings of the acoustic sources were found from GPS data.

	Latitude (°)	Longitude (°)	WD (m)	SD (m)	Distance to VSA (km)
TB1	22.1675 N	-159.7977 W	215.2	201.5	1.650
TB2	22.1661 N	-159.7870 W	104	98	1.830

Table 4.2: Geographic localization and geometric characteristics of acoustic sources, TB1 and TB2; last two columns show the estimated source depth (SD) and the estimated source range between the acoustic sources and the VSA, obtained from GPS and R/V Kilo Moana ship's instruments.

4.3.1 Deployment 1 - September 20th

On September 20th, corresponding to the first deployment, the VSA was fixed with the deepest element positioned at 79.9 m depth, in a water depth of approximately 104 m. The acoustic sources TB1 and TB2 were bottom moored at 201.5 and 98 m depth and 1650 and 1830 m range from the VSA, respectively. The geographic localization and the geometric characteristics of the acoustic sources are reported in Table 4.2. The bathymetry map of the MakaiEx'05 area and the position of the equipment on September 20th is depicted in Fig. 4.14. The bathymetric contours between the VSA and the sources TB1 and TB2 are represented in Fig. 4.15 (a) and (b), respectively. The figure reveals that the bathymetry between VSA and TB1 was range dependent, with a water depth varying from 104 to 265 m, while between VSA and TB2 was nearly range independent, with a water depth of approximately 104 m.

The acoustic signals acquired by the VSA were emitted from the two fixed testbeds TB1 and TB2 in the 8-14 kHz band. The two testbeds transmitted alternatively every 2 minutes, a sequence of LFM's, multitones, an M-sequence and a communication signal sequence [74]. Fig. 4.16 shows the spectogram of a 10 s block of the received signals on the VSA emitted by TB1 (a) and by TB2 (b) on September 20th. The multitone signal with 8 tones in

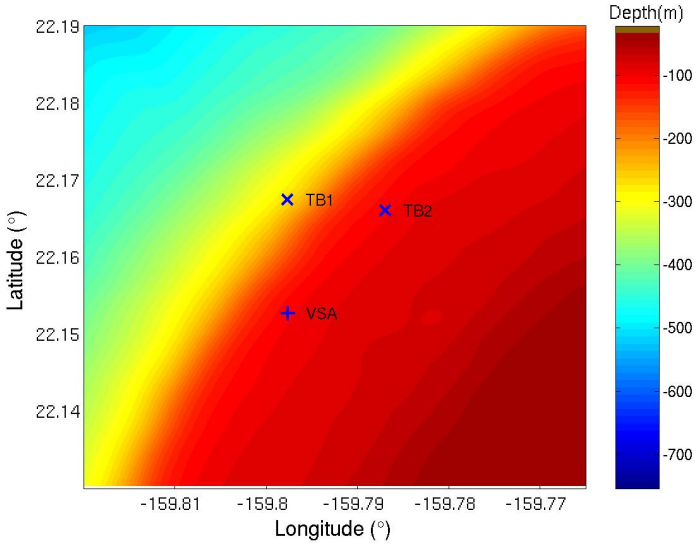

Figure 4.14: The bathymetry map of the MakaiEx'05 area and the position of the acoustic sources TB1, TB2 and the VSA on September 20th - deployment 1.

the 8-14 kHz band was used for the processing. Each acoustic source has a specific set of frequencies: 8250, 8906, 8976, 11367, 11789, 12774, 13055 and 13992 Hz for TB1 and 8250, 9820, 9914, 11367, 11789, 11882, 13078 and 13500 Hz for TB2, which are used to differentiate the two testbeds.

The frequency 8250 Hz was used to perform the beamforming for source DOA estimation because this frequency is common to both testbeds and close to the design frequency of the VSA. The normalized ambiguity surfaces for DOA estimation for TB1 at minute 1 and TB2 at minute 3 are shown in Fig. 4.17 (a) and (b), respectively. The figure reveals a narrow main lobe obtained with the VSA and shows that, the main lobe for source TB1 appears at $(127°, 81°)$ and for source TB2 at $(160°, 95°)$. Moreover, the DOA estimation was applied for the data acquisition period (which corresponds to almost two hours), and the estimated azimuth results are presented in Fig. 4.18. In this figure the estimated azimuth angles are shown, with blue asterisks for TB1 and red triangles for TB2, as well as the expected

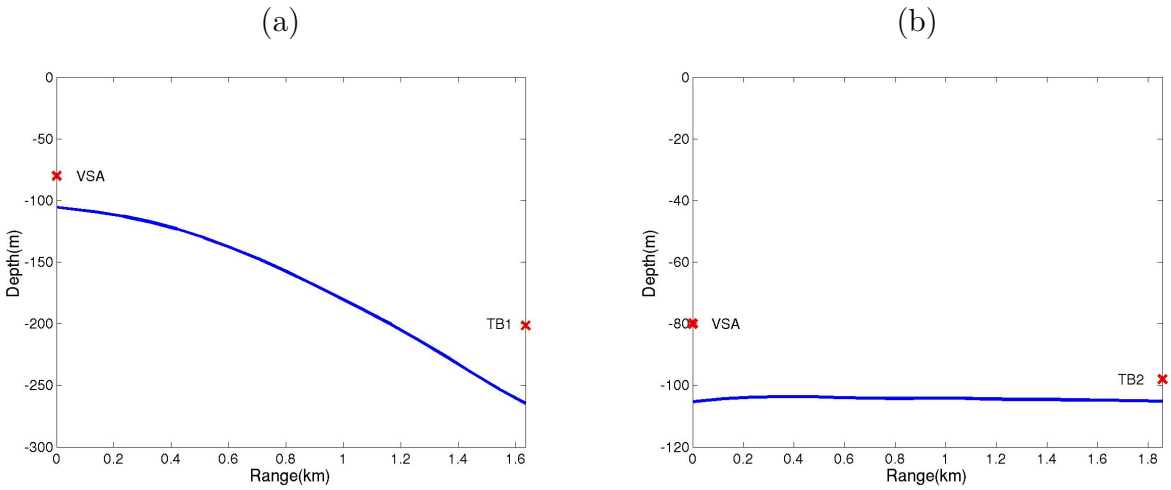

Figure 4.15: The bathymetric profile between the VSA and TB1 (a) and TB2 (b) on September 20th - deployment 1.

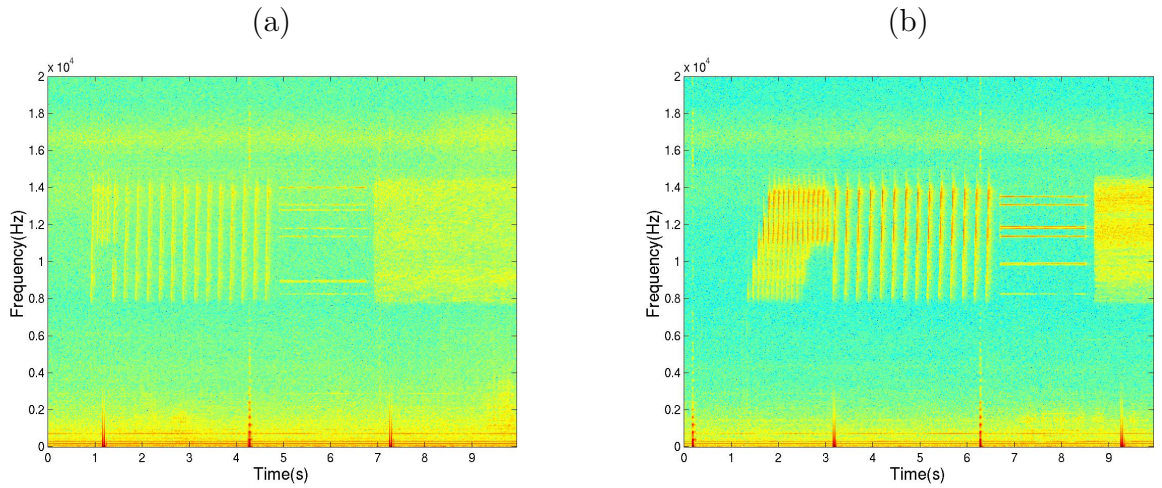

Figure 4.16: The 10 s received probe signals on VSA and transmitted by the acoustic sources: TB1 (a) and TB2 (b) on September 20th, constituted by LFM's, multitones, an M-sequence and a communication signal sequence.

bearings, with black asterisks for TB1 and black triangles for TB2. The expected bearings were obtained taking into account the GPS position, the ship's heading and the estimated horizontal orientation of the VSA discussed in section 4.2 (see Fig. 4.11). The expected bearings are constant during the period of data acquisition, since the R/V Kilo Moana on this day was in dynamic positioning and both sources were fixed. The estimated azimuth

results during this data acquisition period are not constant, but they are consistent around the expected bearing and the difference between the estimated source angles is stable, which validate the horizontal orientation of the VSA as discussed in section 4.2. The observed variability may be due to the slighty variability of the R/V Kilo Moana that was in dynamic positioning. In fact, during this first deployment the VSA was tied to the vertical cable without the weight at the bottom.

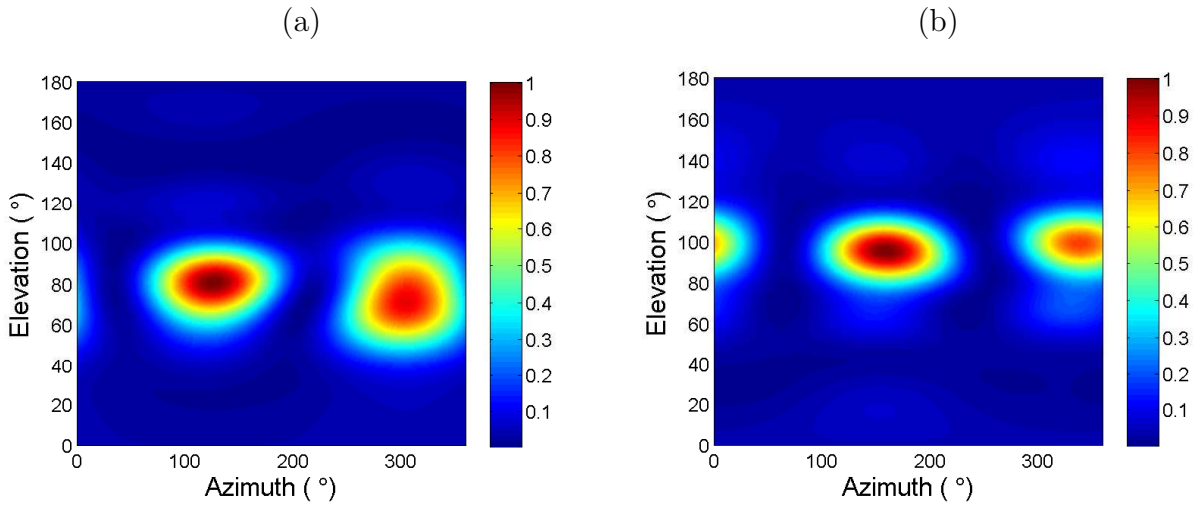

Figure 4.17: Source DOA estimation results obtained for frequency 8250 Hz, for: TB1 at minute 1 where the maximum is at $(127°, 81°)$ (a) and TB2 at minute 3 where the maximum is at $(160°, 95°)$ (b).

4.3.2 Deployment 2 - September 23rd

On September 23rd (second VSA deployment) the R/V Kilo Moana, with the VSA at the stern and the deepest element positioned at 39.9 m depth, drifted from the TB2 location to the position 22.1889 N and -159.7968 W. The drift of the VSA and the localization of TB2 are represented in Fig. 4.12 (b). The bathymetric profile during the drift and source-receiver range are shown in Fig. 4.19 (a) and (b), respectively; the figure shows that the VSA moved away from the source testbed TB2 to a distance of 2300 m in a range dependent bathymetry.

During September 23rd the signals were emitted only by the acoustic source testbed TB2, in the 8-14 kHz band, at a fixed position 22.1660 N, -159.7870 W and depth 89.5 m in 104 m water depth. The estimated azimuths (blue asterisks) and the expected bearings (red asterisks) for the source TB2, during the VSA drift, are shown in Fig. 4.20. The expected bearings were obtained from GPS position related to ship's heading and the horizontal orientation of the VSA discussed in section 4.2 (see Fig. 4.12). Fig. 4.20 reveals that the source azimuth estimation follows the expected bearing during almost two hours of data acquisition period, with some outliers observed, mainly, at the initial period up to minute 30. Therefore, one can conclude that during the data acquisition period, in drift conditions, the azimuth results and the expected bearings are in good agreement, validating the VSA horizontal orientation discussed in section 4.2.

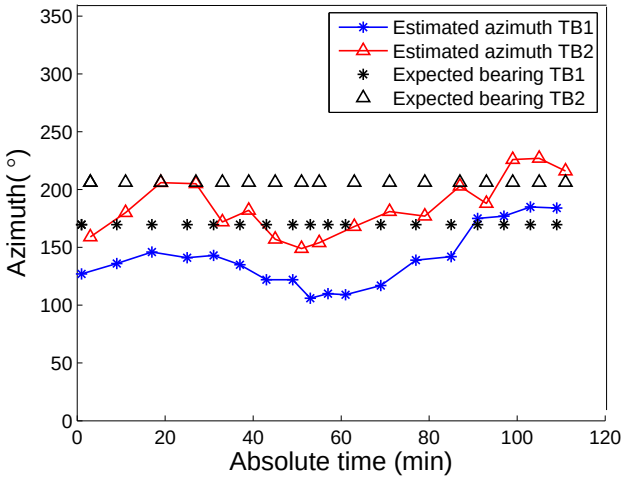

Figure 4.18: The estimated azimuth results obtained for frequency 8250 Hz during the data acquisition period, for: TB1 (blue asterisk) and TB2 (red triangle); and the expected bearing obtained from the GPS data, ship's heading and the estimated VSA horizontal plane orientation discussed in section 4.2, black asterisk for TB1 and black triangle for TB2.

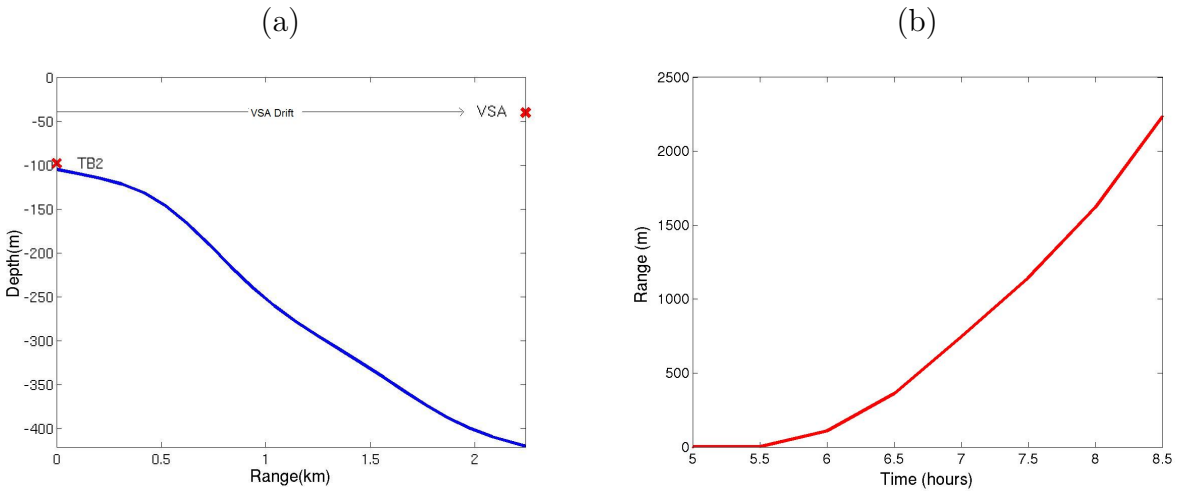

Figure 4.19: Bathymetric profile during the drift (a) and source - receiver range (b) on September 23rd - deployment 2.

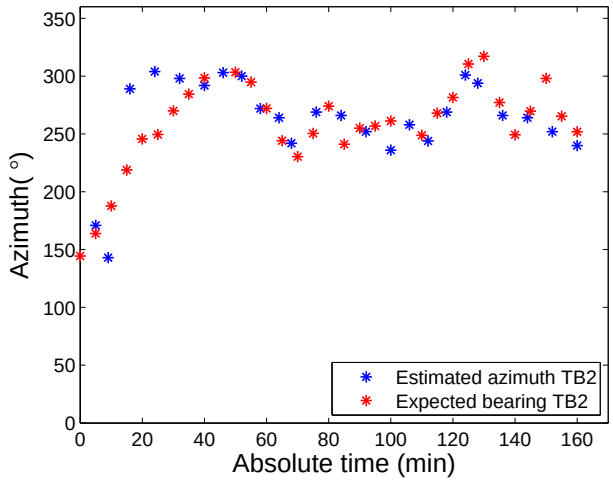

Figure 4.20: The estimated azimuth results obtained for frequency 8250 Hz during the period of data acquistion for TB2 (blue asterisk) and the expected bearing obtained from GPS data, ship's heading and the estimated VSA horizontal plane orientation discussed in section 4.2 (red asterisk), on September 23rd - deployment 2.

4.3.3 Deployment 3 - September 25th

The third and last VSA deployment occurred on September 25th. During this day, the acoustic source Lubell 916C was used. The source was towed by a RHIB at 10 m depth and approached the VSA from 2300 m, whose trajectory is depicted in Fig. 4.21. The VSA

was deployed with the deepest element at 39.9 m depth and fixed at location 22.15 N and -159.80 W. The bathymetric cut along track and source-receiver range, between the Lubell 916C and the VSA, are shown in Fig. 4.22 (a) and (b), respectively.

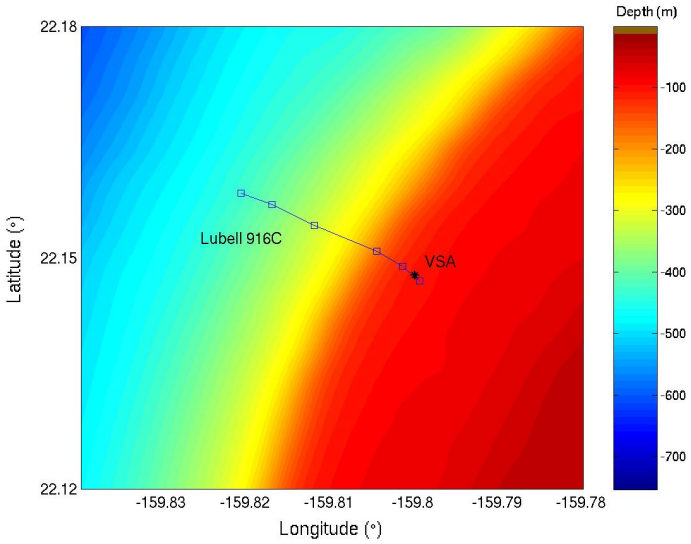

Figure 4.21: The location of VSA and the RHIB track during part of September 25th - deployment 3.

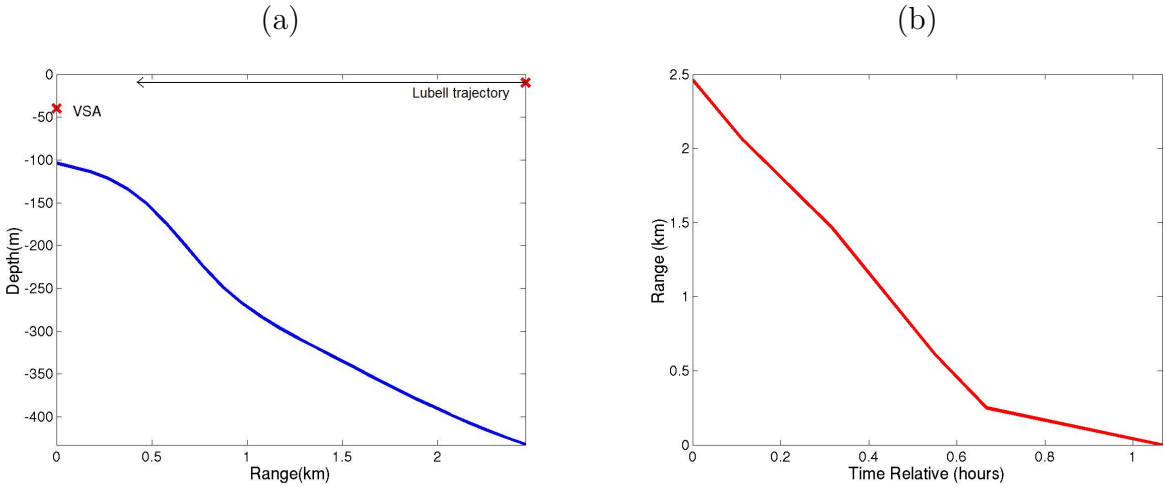

Figure 4.22: The bathymetric profile (a) and source-receiver range (b) between VSA and Lubell source, on September 25th - deployment 3.

During September 25th, a much wider frequency band was explored thanks to the transmission's characteristics provided by the Lubell 916C source. Fig. 4.23 shows the emitted

signal received on the VSA, which was a sequence of LFM's, M-sequences and multitones in the 500-14000 Hz band. Such sequence of different signals had a 2 minutes duration, but only the 10 s of multitones, at frequencies 6550 and 9030 Hz, were used to process the VSA data because they are close to the design frequency of the array.

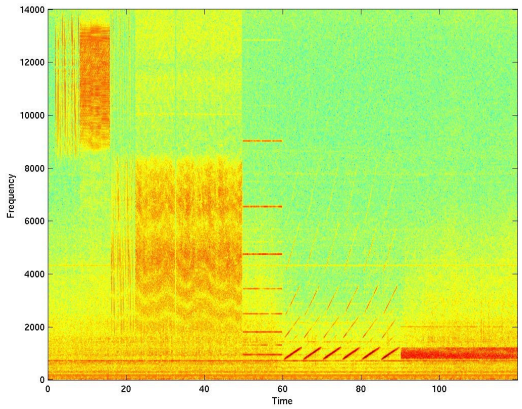

Figure 4.23: The 2 minutes received signal on the VSA, transmitted by the Lubell 916C source on September 25th, constituted by LFM's, M-sequences and multitones in the 500-14000 Hz band.

The estimated azimuth results and the expected bearings for source Lubell 916C, during the drift and near the VSA location, are represented in Fig. 4.24 by blue and black asterisks, respectively. These results were determined using two tones: one below the array design frequency 6550 Hz and the other above 9032 Hz, shown in Fig. 4.24 (a) and (b), respectively. Additionally, the figure shows another result represented with red asterisks, namely, the estimated azimuth with offset. Such result was added because it was verified during the data processing, that a constant offset of -90° appeared between the DOA estimation and the expected bearing. The value of 90°, constant for all data acquisition period, was substracted from the estimated azimuth of the source Lubell 916C. The reason for such offset is unknown; it may be due to an electronic bias or perhaps because the x and y output channels were interchanged in the acquisition system. Consequently, the estimated azimuth with offset

(red asterisks in Fig. 4.24) are in line with the expected bearing (black asterisks in the same figure) and with the horizontal orientation obtained in previous section (see Fig. 4.13 (b)).

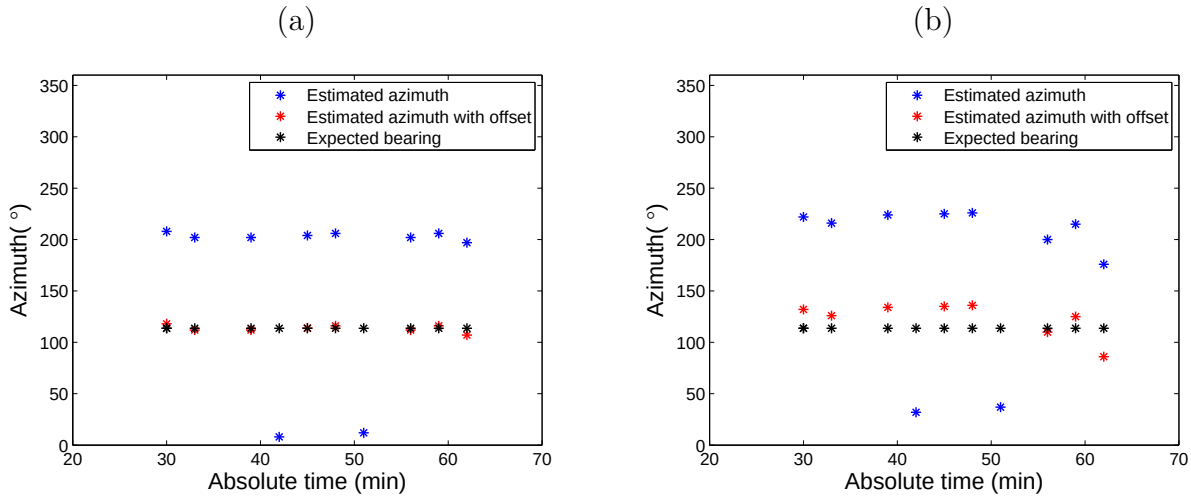

Figure 4.24: The estimated azimuth results for the source Lubell 916C (blue asterink) with a 90° offset deducted (red asterisk), obtained on September 25th for frequency: 6550 Hz (a) and 9032 Hz (b) and the expected bearing from GPS data (black asterisk).

Summary

In this chapter a brief description of the MakaiEx'05 sea trial was presented as well as the description of the VSA used during this experiment. The VSA was deployed three times and it acquired signals in the 500-14000 Hz band, from fixed and towed sources. The VSA was deployed with the z-axis vertically oriented to the bottom and with an unknown horizontal orientation. In order to determine such orientation the ship's noise signature at low frequency was beamformed; beamforming results were combined with GPS and heading data information. Furthermore, the DOA estimation of the sources was determined, and the results exhibited a variability related to the expected bearing along the three days of deployment. The expected bearings were obtained from the GPS data. On September 20th, the azimuth estimation was around the expected bearing; the remaining variability was

perhaps induced by displacements of the VSA. On September 23rd, the R/V Kilo Moana with the VSA at the stern drifted from TB2 position and the drift caused some outliers, mainly at the beginning of the data acquisition period; for the rest of the drift the results were in good agreement. On September 25th, the azimuth estimation results exhibited a -90° offset; accounting for the offset the results were in agreement with the expected bearing and with the horizontal plane orientation of VSA. From the previous discussion the following conclusions can be drawn: first, that the estimated and expected azimuth angles were, generally, in good agreement; second, that the results validate the horizontal orientation of the VSA axes; and third, that such results were in line with the geometry of the sea trial.

The experimental results on DOA estimation, previously discussed, were a pre-processing requirement for the estimation of seabed parameter based on experimental data. The estimation of the seabed parameters, using HF acoustic signals, will be presented in the next chapter.

Chapter 5

Seabed geoacoustic characterization

The process of estimating the seabed parameters from geoacoustic modelling based on measurements is known as geoacoustic inversion [76]. One of the classical references on geoacoustic inversion is from Hamilton [77], which provides the following definition of geoacoustic modelling:

"A geoacoustic model is defined as a model of the real seafloor with emphasis on measured, extrapolated, and predicted values of those properties important in underwater acoustics and those aspects of geophysics involving sound transmission".

In general, a geoacoustic model details the identification of sediment and rock types, the true thickness and the properties of sediment and sub-bottom layers in the seafloor. The geoacoustic information is important to geophysics to determine the characteristics of the seafloor, and to underwater acoustic studies to predict the effects of the seafloor on sound propagation. This is particularly true for shallow water, where the acoustic field has an increased interaction with the seafloor. The seabed properties can be best determined from *in situ* measurements by coring, can be predicted from archival information or can be estimated using remote sensing techniques like geoacoustic inversion.

The objective of this chapter is to define a geoacoustic model of the MakaiEx'05 area

based on particle velocity measurements. The characterization of the seabed will be obtained using HF acoustic signals with two different VSA-based inversion techniques. In the first one, the seabed parameters and layer structure will be estimated comparing the reflection loss of experimental data to the reflection loss modelled by the SAFARI model [57], thus taking advantage of the spatial filtering capabilities and directionality of the VSA. The reflection loss will be estimated using a method proposed by C. Harrison *et al.* [39], which will be adapted to the VSA processing. In the second one, the seabed parameters will be estimated using a MFI approach with the derived VSA-based Bartlett estimators, where the replica field is generated with the TRACEO model [56]. The knowledge of the source DOA estimation, principally the source azimuth angle determined in the previous chapter, will be used to define the horizontal particle velocity components for a given azimuthal direction.

5.1 Reflection loss estimation

C. Harrison *et al.* proposed in [39] a geoacoustic inversion technique, considering vertical array measurements of surface generated noise in the 200-1500 Hz frequency band, and extended the technique to the 1-4 kHz frequency band in [40], using traditional hydrophone arrays. The method uses the ratio between downward looking energy (energy reaching the array from the surface) to upward looking energy (energy reaching the array from the seabed); this ratio produces an approximation of the bottom reflection loss, which can be inverted for seabed properties. This technique, which was originally proposed with a long hydrophone array, could be adapted for vertical measurements of a few elements VSA, bearing in mind the spatial filtering capabilities of the VSA and that different components can estimate different types of environmental parameters (discussed in chapter 3).

In the following, the method proposed by C. Harrison *et al.* will be used to compare the beam response obtained with p-only measurements with that of particle velocity measurements. In order to invert the seabed parameters, the bottom reflection loss deduced from experimental VSA data will be compared to the bottom reflection loss modelled by the SAFARI model. The best agreement between both bottom reflection losses gives an estimation of bottom layering structure, together with its most relevant geoacoustic parameters.

5.1.1 The method

This section recalls the method proposed by C. Harrison *et al.* in [39, 40] for the estimation of the bottom reflection coefficient. Let us consider an emitted signal S in a range independent environment, as shown in Fig. 5.1. The acoustic field propagates through the water column and reaches the receiver R through multiple ray paths. The ray paths can be surface and bottom reflected and impinge the receiver with different elevation angles ϕ_0, as shown in Fig. 5.1. Taking into account the plane-wave beamforming described in section 2.1, the array beam pattern $B(\phi)$ is computed in order to obtain the vertical beam response $A(\phi_0)$ for each elevation angle ϕ_0. The acoustic field travelling from downward, i.e., rays reaching the receiver from surface reflections at elevation angle $(-\phi_0)$ can be separated from those travelling from upward, i.e., rays reaching the receiver from bottom reflections at elevation

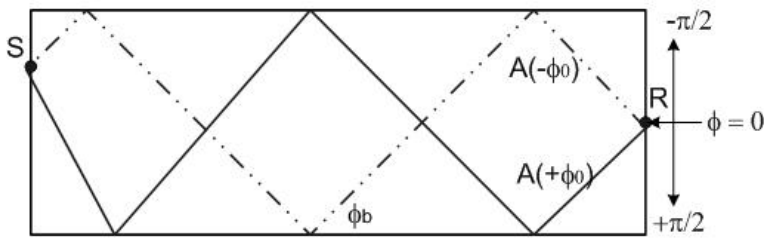

Figure 5.1: Sketch of the ray approached geometry of a plane wave emitted by an acoustic source (S) and received by a receiver (R) at the elevation angle ϕ_0.

angle ($+\phi_0$). According to [39], the ratio between the downward and upward beam response is an approximation to the bottom reflection coefficient R_b as:

$$\frac{A(-\phi_0)}{A(+\phi_0)} = R_b(\phi_b(\phi_0)), \tag{5.1}$$

where the angle ϕ_0, measured by beamforming at the receiver, is corrected to the angle at the seabed ϕ_b, according to the Snell's law:

$$\phi_b = \arccos\left[\frac{c_b}{c_r}\cos(\phi_0)\right], \tag{5.2}$$

where c_b is the sound speed at the water-bottom interface and c_r is the sound speed at the receiver.

5.1.2 VSA beam response

The method previously described will be adapted for vertical measurements of a VSA, considering the azimuth angle θ of an acoustic source. Then, the array beam pattern $B(\theta, \phi)$ for the source look direction will be estimated taking into account the plane-wave beamforming described in section 2.1, of which the results were discussed in chapter 4.

The following results were obtained for the VSA data acquired on September 25th, near the VSA location (approximately at range of 500 m to 200 m) as shown in Fig. 5.2. The goal of these ranges is that, from the TL analysis in Fig. 3.7, the acoustic field propagates through the sediment below 0.5 km for large grazing angles. Therefore, such ranges potentially provide sufficient information to characterize the sediment regarding the most relevant parameters. The source-ranges of 500 m and 200 m correspond to the period of data acquisition time between the minute 38 and the minute 48 consequently, this period of time was used for data processing. On September 25th, the VSA was deployed with the deepest element at

39.9 m depth and the signals were emitted by the acoustic source Lubell 916C, which was towed by the RHIB at 10 m depth (as described in section 4.3.3). The 2 s of LFM's in the 8-14 kHz band were used for data processing (see Fig. 4.23).

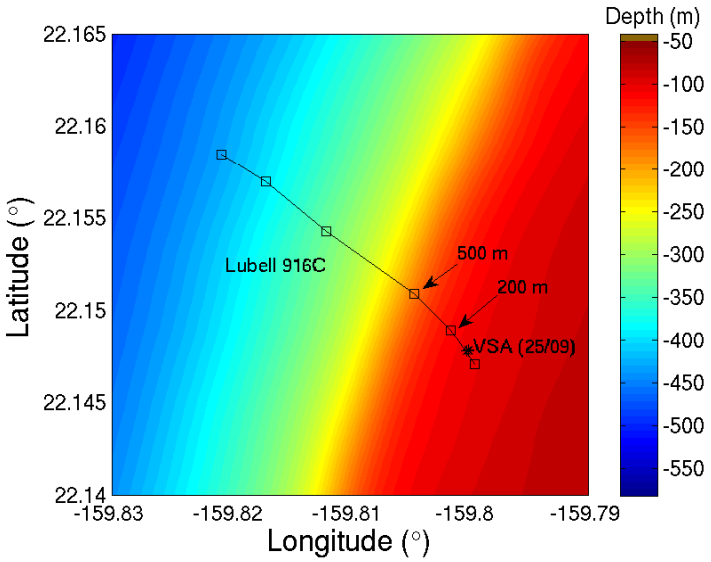

Figure 5.2: The location of VSA and the RHIB track during part of September 25th (deployment 3), where the source position is shown at approximately 200 m and 500 m range.

The vertical beam response for each frequency extracted, considering the four p-only sensors of the VSA, is shown in Fig. 5.3. Four instants of time were processed: the vertical beam response for minute 38 is shown in Fig. 5.3 (a), while (b), (c) and (d) show the vertical beam response for minutes 41, 44 and 48, respectively. This figure shows that the p-only beam response is nearly symmetric for the negative (downward or surface reflections) and positive (upward or bottom reflections) elevation angles. This issue results in a poor information about the bottom attenuation, which is similar for the four instants of time considered.

The vertical beam response for each frequency extracted for the source azimuthal direction of interest, considering the four-element VSA, is shown in Fig. 5.4. The same instants

of time were considered and the results are shown in Fig. 5.4 (a), (b), (c) and (d) for minute 38, 41, 44 and 48, respectively. The figure reveals, generically for all instants of time, that the upward energy (reaching from $+\phi_0$) is more attenuated after bottom reflections than the downward energy (reaching from $-\phi_0$). This is clearly a unique capability resulting from the processing gain provided by the vector sensors. The comparison between Fig. 5.3 and Fig. 5.4 shows that the VSA differentiates the energy reaching the array from multiple directions better than the p-only sensors, due to different particle velocity components. This issue will be further illustrated when the vertical beam response is obtained using the individual particle velocity components.

The vertical beam response obtained with the individual particle velocity components is shown in Fig. 5.5 for minute 38 (left) and for minute 48 (right), corresponding at the source-range of 500 m and of 200 m, respectively (see Fig. 5.2). The results for the v_x-only component are shown in Fig. 5.5 (a) and (b), while (c) and (d) present the results for the v_y-only component, and (e) and (f) present the results for the v_z-only component. From the analysis of the Fig. 5.5 the following conclusions can be drawn:

1. The figure reveals that the beam response for minute 48 has higher energy power than that for minute 38, because the data was acquired near the VSA location (approximately 200 m range). This feature can be seen comparing the left and the right side of Fig. 5.5;

2. The beam response of the v_x-only and v_y-only components exhibit similar results, since these components are mostly affected by the direct and refracted ray paths. The energy is more concentrated at elevation angles around 0°, related to the contribution of the

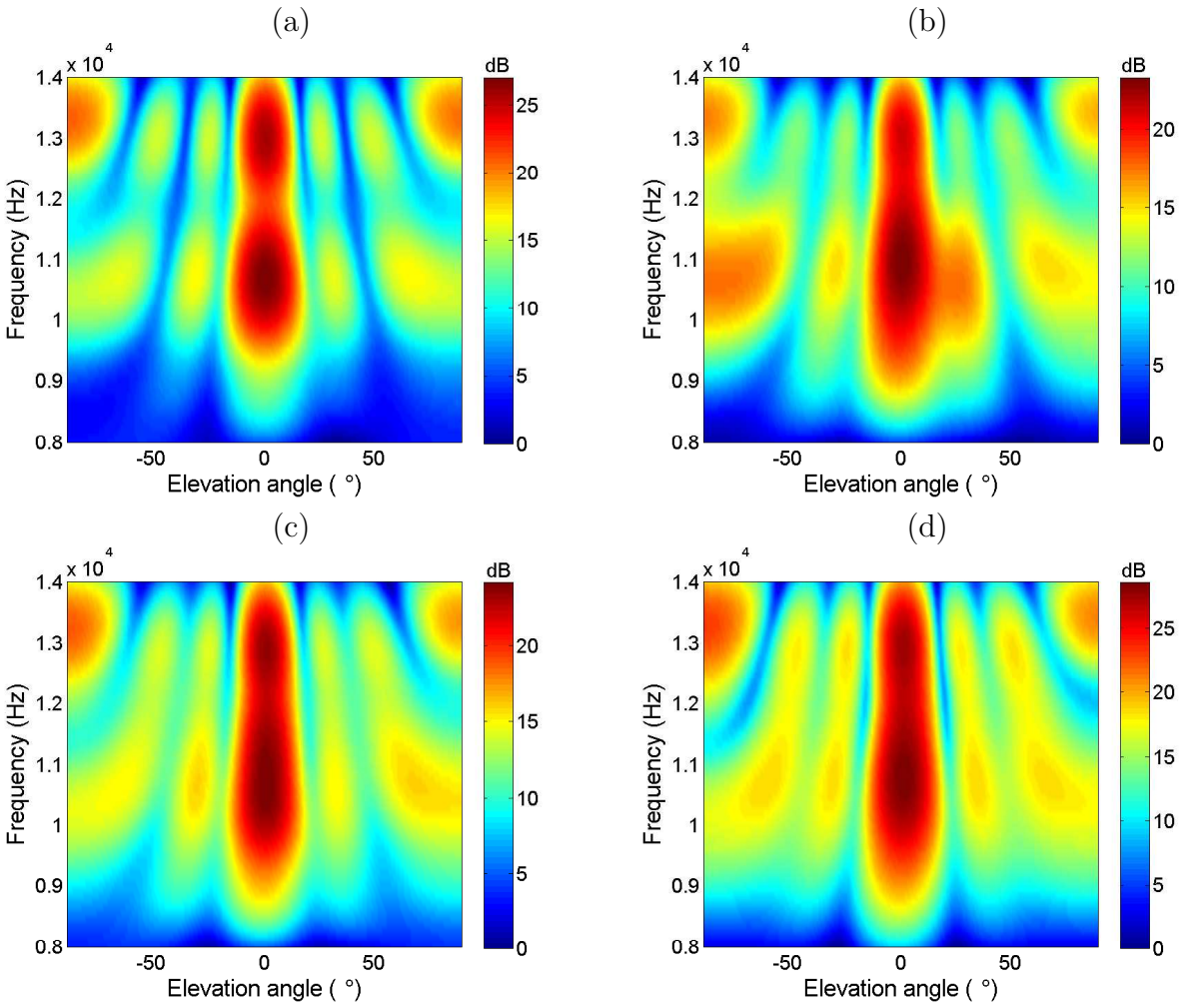

Figure 5.3: The vertical beam response at the source azimuth angle obtained using the four p-only sensors of the VSA for minute 38 (a), 41 (b), 44 (c) and 48 (d).

direct ray paths; for high elevation angles, the attenuated energy may be due to the refracted ray paths that are also bottom reflected;

3. The v_z-only component shows, as expected, no energy along the horizontal direction. In fact, the vertical component is influenced by the rays with strong interactions with the bottom and surface according to their grazing angles. The bottom reflected rays energy ($0 < \phi_0 < +90°$) suffer higher attenuation than the surface reflected rays energy ($-90° < \phi_0 < 0$), as shown in Fig. 5.5 (e) and (f);

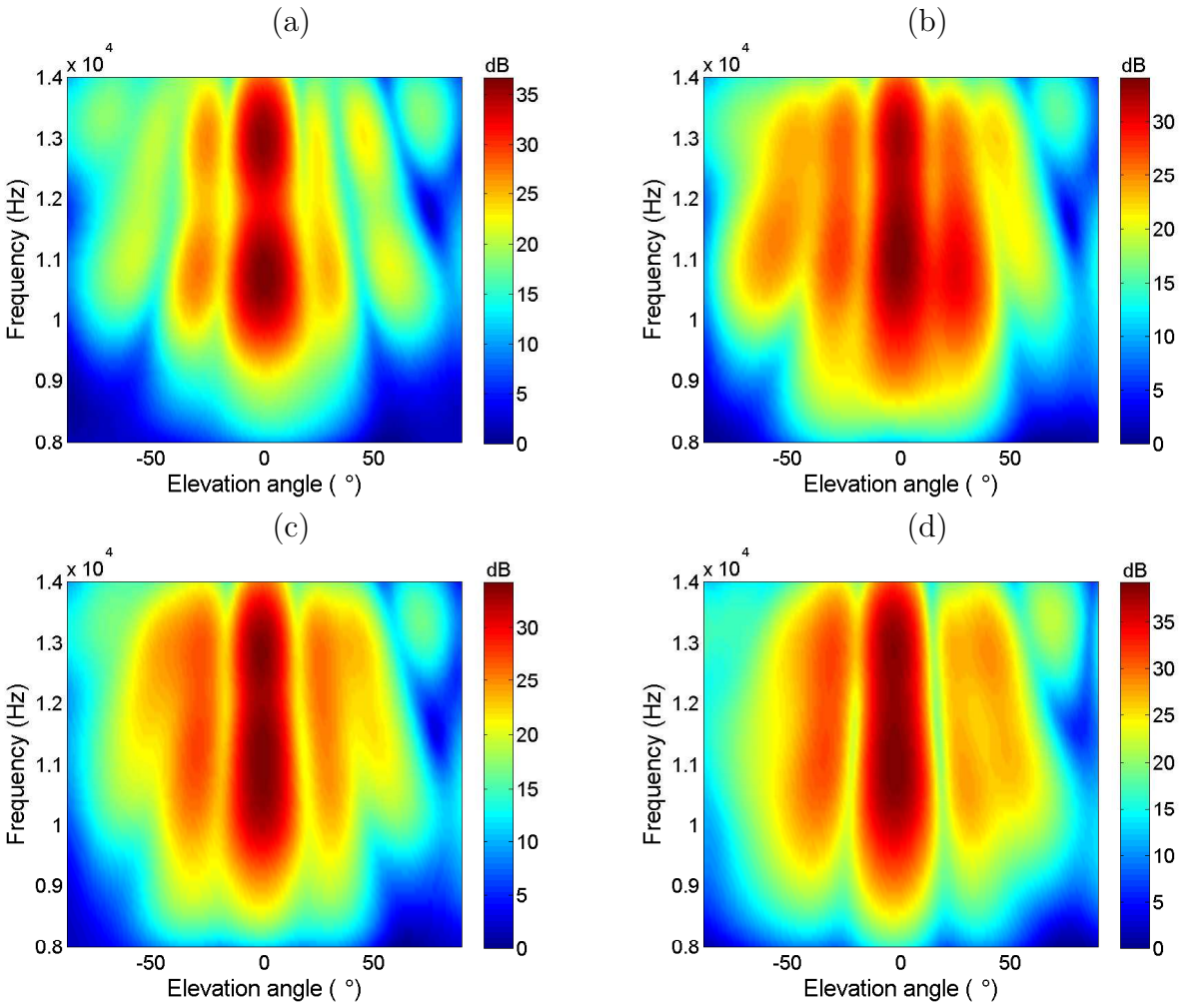

Figure 5.4: The vertical beam response at the source azimuth angle obtained using the four-elements VSA for minute 38 (a), 41 (b), 44 (c) and 48 (d).

4. The contribution of the acoustic field to the different particle velocity components is important for bottom characterization;

5. A VSA with few elements is able to significantly increase the estimation resolution of the reflection loss over p-only sensors.

5.1.3 Ocean bottom characterization

The VSA beam response results discussed in the previous section will be used to determine the bottom reflection coefficient using the method proposed by C. Harrison *et al.*, adapted for

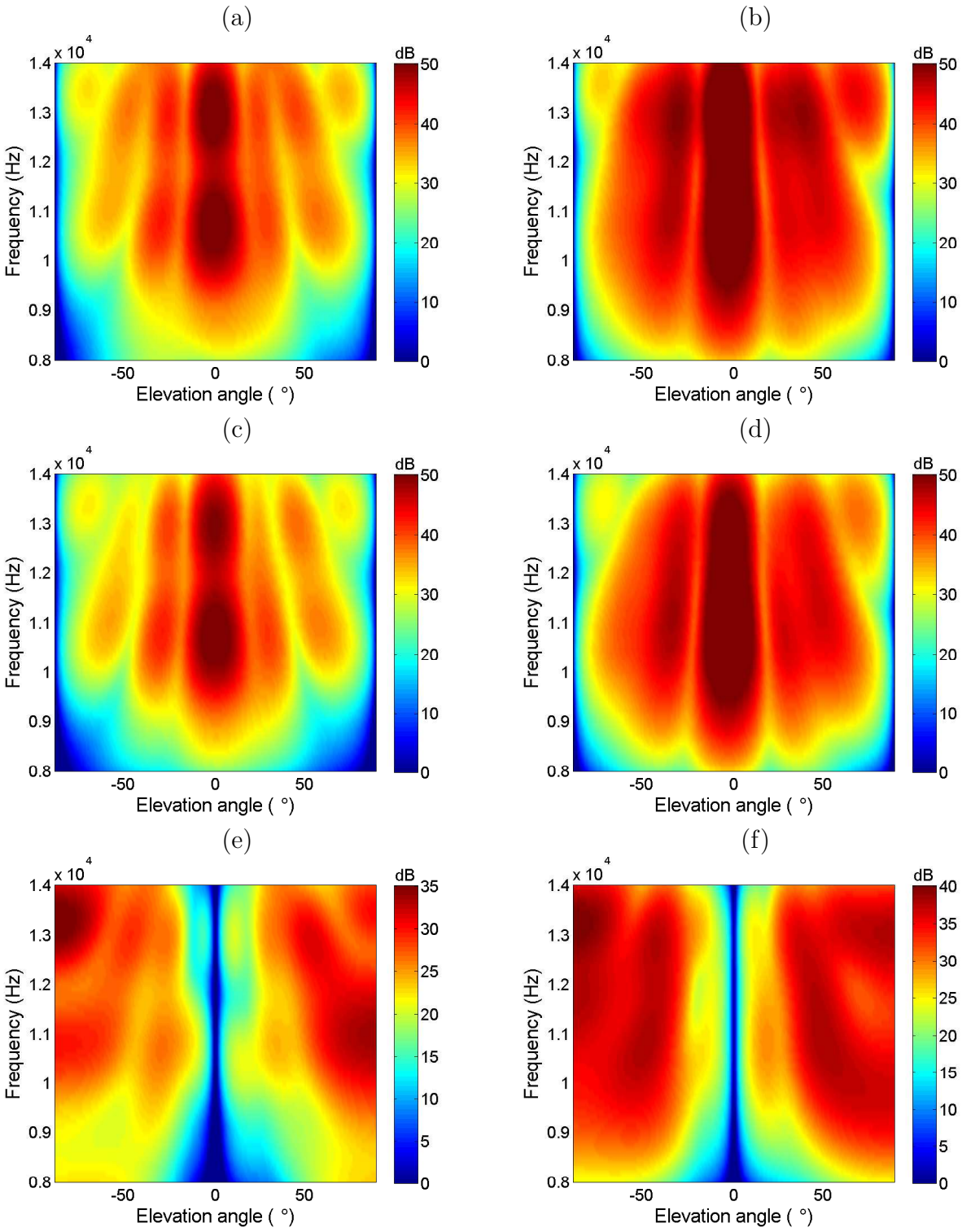

Figure 5.5: The vertical beam response at the source azimuth angle obtained using the four individual particle velocity components of the VSA: v_x-component (a) and (b), v_y-component (c) and (d), and v_z-component (e) and (f). The results where obtained for minute 38 on the left side and for minute 48 on the right side, source-range 500 m and 200 m respectively

VSA data. The bottom reflection coefficient is determined through Eq. (5.1) with the vertical measurements of the VSA. The ocean bottom characterization is achieved by comparing, using a trial and error approach, the frequency versus bottom angle reflection loss curves, given by the experimental data with those modelled by the SAFARI model [57]. Such comparison provides the following set of sediment and/or bottom parameters: compressional speed c_p, shear speed c_S, compressional attenuation α_p, shear attenuation α_S and density ρ. Initial values of the parameters were found in the literature based on the available qualitative description of the area [2]. Then, manual adjustments were made to estimate a reflection loss figure similar to the one obtained with experimental data. It was found that the most relevant parameters are the layer thickness (which is important for fringe separation agreement), and the sound speed on the various layers and in the half-space, which influences the critical angles of the form:

$$\phi_{c_i} = \arccos(\frac{c_W}{c_{s_i}}), \tag{5.3}$$

where c_W is the water sound speed near the water sediment interface, and c_{s_i} is the ith sediment layer or sub-bottom sound speed.

The bottom reflection loss at 8-14 kHz frequency band, deduced from the down-up ratio of the experimental VSA data at minute 48, is shown in Fig. 5.6 (a). The figure reveals three critical angles, namely $\phi_{c_1} \simeq 13°$, $\phi_{c_2} \simeq 26°$ and $\phi_{c_3} \simeq 49°$. According to Eq. (5.3) and knowing that the water sound speed near the water sediment interface is $c_W = 1530\,\mathrm{m/s}$, the sediment and sub-bottom sound speeds can be calculated. The results of such sound speeds are $c_{s_1} = 1570\,\mathrm{m/s}$, $c_{s_2} = 1700\,\mathrm{m/s}$ and $c_{s_3} = 2330\,\mathrm{m/s}$, respectively for each critical angle. Therefore, the reflection loss modelled by SAFARI, with the same features as those found with the experimental data, is shown in Fig. 5.6 (b). This structure suggests that

the experimental area, near the VSA location, can be modelled as a four-layer environment (three boundaries) namely the water column, two sediments and the bottom half-space.

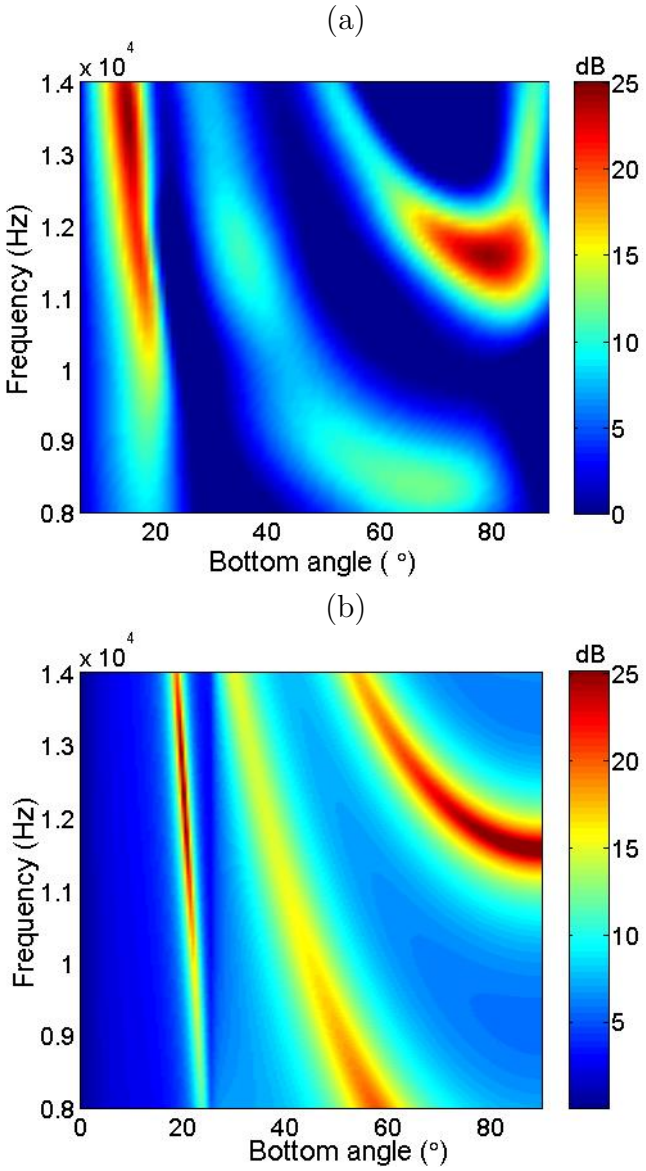

Figure 5.6: The bottom reflection loss at 8-14 kHz frequency band, deduced from the down-up ratio of the experimental data on September 25th at minute 48 and 200 m source-range (a) and as modelled by the SAFARI model (b).

The results of the estimated bottom structure with its most relevant parameters are presented in Table 5.1. Such results were obtained taking into account the bottom reflection loss deduced from the experimental VSA data, and manual adjustments on the SAFARI

model. The estimated results suggest a four-layer environment, where a first layer with 0.175 m of thickness is found. However, regarding the ground truth described in section 4.1.1, the MakaiEx'05 area suggested from [74] is covered with coral sands over a basalt hard bottom, where the sound velocity in coral sands is approximately 1700 m/s. Although the first sediment sound speed is different from 1700 m/s, this value is achieved for the second sediment layer. Furthermore, the sediment sound speed of $c_s = 1570$ m/s is in line with the results that will be obtained by MFI, in the following section. At this point, one can conclude that:

1. The three-layer environment suggested in [74] could be in fact a four-layer environment (water column, soft sediment, sand and basalt) with a soft sediment over the sand;

2. Due to the small value of the thickness of this first sediment, it was not considered in the description made for the MakaiEx'05 area, before the acoustic experiment took place. Based on the generic geological characteristics of the area and incorporating information from previous experiments, the geological description may have overlooked this first thin sediment layer due either to imprecise core data or low frequency resolution on acoustic techniques;

3. This first thin sediment may not be present at all locations of the MakaiEx'05 area.

The previous conclusions were achieved from the analysis of the bottom reflection loss deduced from the experimental VSA data at minute 48 and near the VSA location. However, analyzing the bottom reflection loss for ranges above 200 m, the presence of the first sediment may or may not hold. To illustrate such statement, the bottom reflection loss deduced from the experimental VSA data at minute 38 and at minute 44 are shown in Fig. 5.7 (a) and (b),

Sediment	First layer	Second layer	Sub-bottom
Thickness (m)	0.175	20	–
ρ (g/cm^3)	1.6	2.1	2.1
c_p (m/s)	1570	1700	2330
c_S (m/s)	67	700	1000
α_p (dB/λ)	0.6	0.1	0.1
α_S (dB/λ)	1.0	0.2	0.2

Table 5.1: The estimated bottom parameters taking into account the measured VSA data on September 25th and manual adjustments on SAFARI model, considering a four-layer structure.

respectively. This figure reveals that the critical angles $\phi_{c_2} \simeq 26°$ and $\phi_{c_3} \simeq 49°$ appear for the two instants of time considered. Moreover, the first critical angle $\phi_{c_1} \simeq 13°$ only starts to appear at minute 44; such critical angle is clearly found at the minute 48 (see Fig. 5.6 (a)). One can conclude that the first sediment only exists near VSA location and for depths around 100 m.

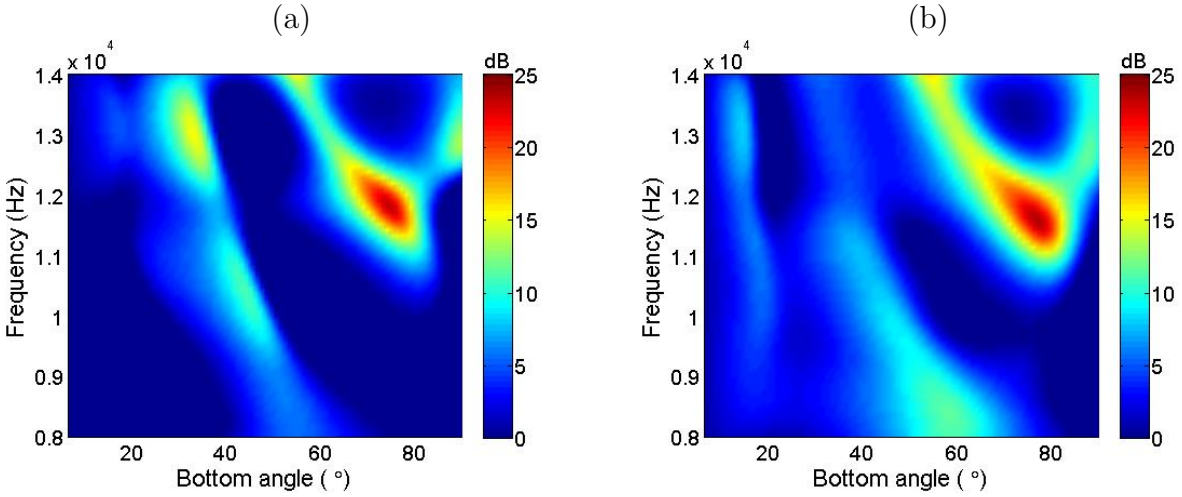

Figure 5.7: The bottom reflection loss at 8-14 kHz frequency band, deduced from the down-up ratio of the experimental data on September 25th at minute 38 (a) and at minute 44 (b).

The method was also applied for the signals acquired on September 20th, where the VSA and the source TB2 were fixed at 1830 m range. The results of the bottom reflection loss deduced from the data acquired on September 20th, at initial data acquisition period, is shown in Fig. 5.8. The figure reveals that the first and the third critical angle appear,

approximately, at the same position than the bottom reflection loss found on September 25th. Similars features, in particular the first critical angle, are observed for both days despite the fact that in September 25th the source-range was 200 m. One can conclude that the same bottom structure appears in different locations of the MakaiEx'05 experimental area. The bathymetry map of the MakaiEx'05 area for both days is shown in Fig. 5.9, where the locations of the acoustic source TB2 and Lubell 916C trajectory are also represented. The figure reveals that the VSA for both days is located over the same isobathymetric line; therefore, the bottom parameters presented in Table 5.1 are plausible for the two VSA locations. Moreover, the first sediment layer is perhaps only found above this isobathymetric line.

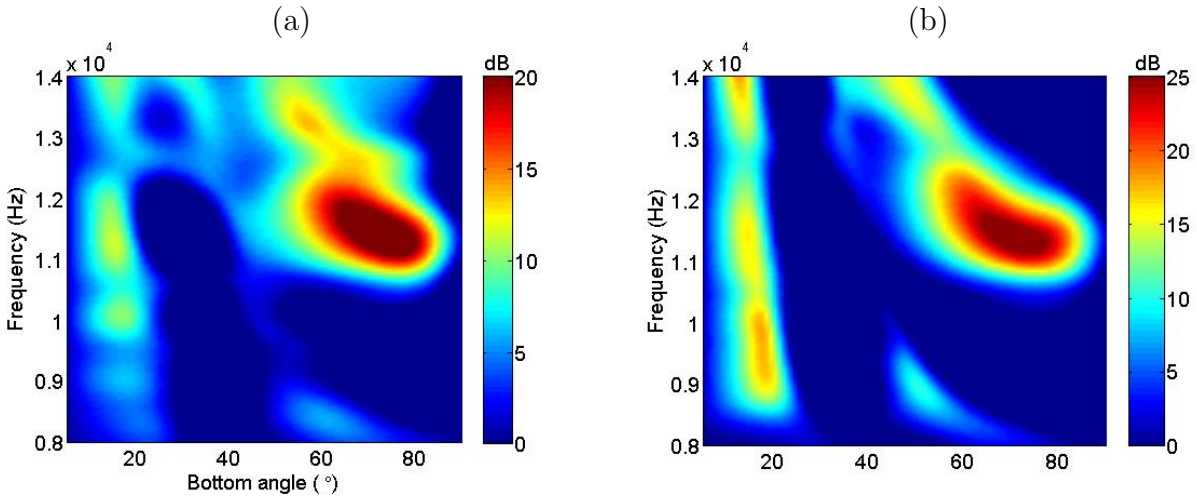

Figure 5.8: The bottom reflection loss in the 8-14 kHz frequency band, deduced from the down-up ratio of the experimental data on September 20th (deployment 1) at minute 19 (a) and at minute 27 (b).

5.2 MFI results based on particle velocity information

The previous section defined the geoacoustic model of the MakaiEx'05 area based on the inversion of bottom reflection loss. In this section, the seabed parameters for the first sediment

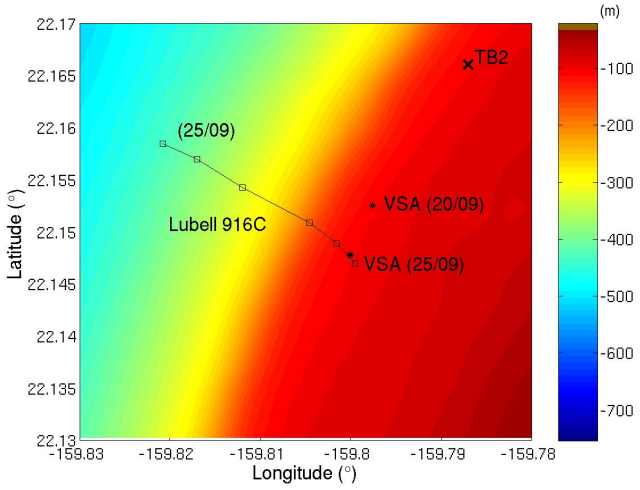

Figure 5.9: The bathymetry map of the MakaiEx'05 area, the location of the VSA on September 20th (deployment 1) and September 25th (deployment 3), the location of the acoustic source TB2 and the Lubell 916C trajectory.

layer will be estimated with experimental results based on the MFI technique.Therefore, the vector sensor based MFI technique discussed in sections 3.3 and 3.5 will be tested on the experimental data acquired by the VSA on September 20th. In this day, the signals were emitted by acoustic sources TB1 and TB2, as described in section 4.3.1, but only the signals emitted by the TB2 were used to process the data due to the more favorable range independent bathymetry of approximately 104 m. As already explained in section 3.5, the MakaiEx'05 sea trial area was known to a degree of accuracy that allows one to consider only seabed parameters in the inversion problem. Therefore, it will be considered that the geometrical and water column parameters are known, and the seabed parameters that will be considered for the inversion are the sediment compressional speed c_p, the density ρ and the compressional attenuation α_p.

5.2.1 Experimental setup

The bathymetry map of the MakaiEx'05 sea trial on September 20th with the VSA and the acoustic source TB2 locations is depicted in Fig. 5.10 (a), while (b) shows the experimental baseline environment with the mean sound speed profile considered for this day. The VSA and source TB2 were in a fixed-fixed configuration over a range independent bathymetry with a water depth of approximately 104 m. The four-element 10 cm spacing vertical VSA was deployed with the deepest element at 79.9 m depth and the source TB2 was bottom moored at 98 m depth and 1830 m range, as shown in Fig. 5.10 (b). On September 20th, the source TB2 transmitted a sequence of LFM's, multitones, an M-sequence and a communication signal sequence, as shown in Fig 4.16 (b) and discussed on section 4.3.1; the tone transmitted at 13078 Hz was used for the processing.

5.2.2 Experimental results of seabed parameter estimation

MFI was discussed in section 3.5 with simulated data and in this section it will be applied to experimental data. In general, the estimator in the parameter space will correspond to a hypercube. Within such hypercube there is a possibility of finding concurrent lobes. Therefore, in order to process the experimental data, the following strategy will be applied:

- At each time instant, the hypercube is calculated;
- The hypercube will be sliced along the sediment compressional speed dimension and the position of the maximum will be calculated;
- The obtained curves will be aligned along time and such alignment will reveal the position of concurrent lobes.

(a)

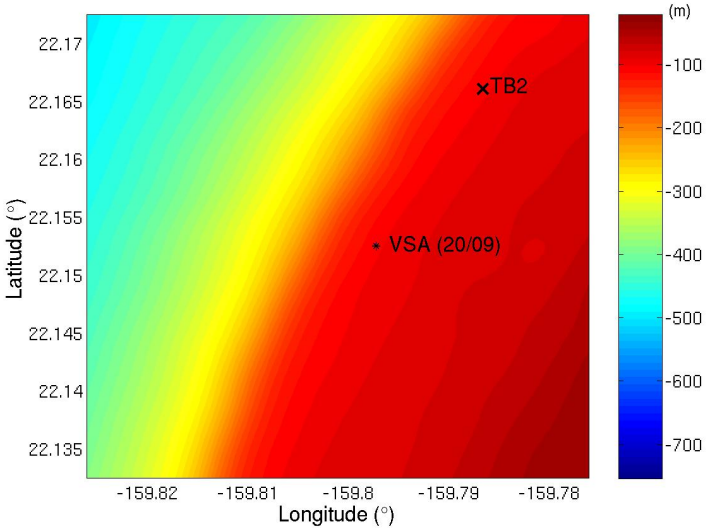

(b)

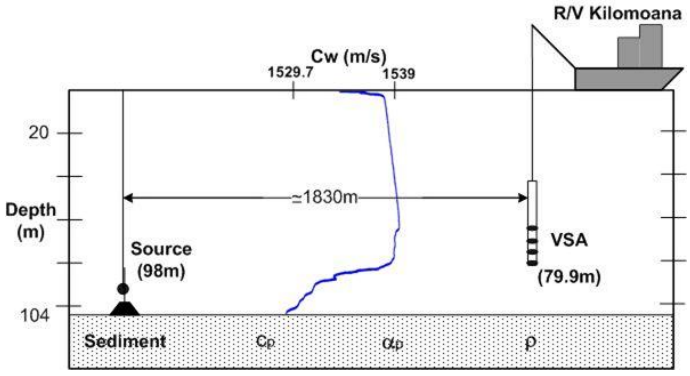

Figure 5.10: The bathymetry map of the MakaiEx'05 area with the locations of the VSA and the acoustic source TB2 (a) and baseline environment with the mean sound speed profile (b) on September 20th (deployment 1). The VSA was deployed with the deepest element at 79.9 m and the TB2 was bottom moored at 98 m.

The results based on such strategy were calculated at a frequency of 13078 Hz and for several instants of data acquisition period of almost two hours on September 20th. Such results considering the VSA (p+v) and the v_z-only Bartlett estimators are shown in Fig. 5.11 (a) and (b), respectively. This figure reveals the following: first, the results are relatively stable in time; second, the v_z-only estimator provides better estimation resolution for the sediment compressional speed than the VSA (p+v) estimator (compare Fig. 5.11 (a) and (b)); and third, the sediment compressional speed points to values of approximately 1580 m/s,

although in some instants of time (see Fig. 5.11 (b)), the results exhibit two lobes, being one of them below 1550 m (at the sound speed of the water-bottom interface).

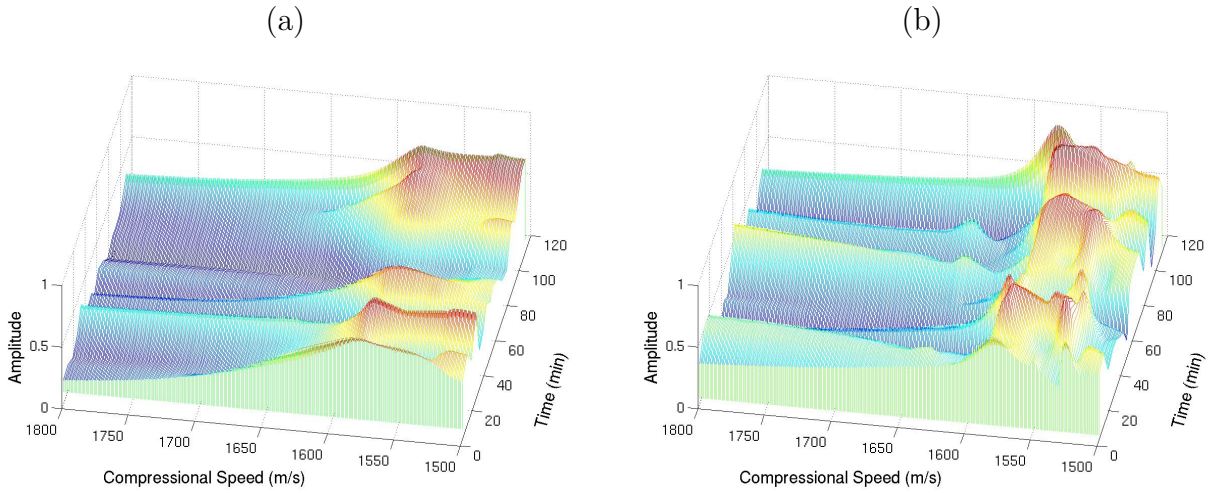

Figure 5.11: Maxima of hypercube slices along time for the sediment compressional speed at frequency 13078 Hz, considering the VSA ($p + v$) Bartlett estimator (a) and the v_z-only Bartlett estimator (b).

After the previous discussion of the sediment compressional speed estimation, the density and the compressional attenuation will be estimated taking into account the estimated value of 1580 m/s for the sediment compressional speed. Since MFI is less sensitive to such parameters, the following results are obtained considering the geometric mean [1] of the ambiguity surfaces over time, to enhance the best estimation results for both parameters.

The ambiguity surfaces for compressional attenuation and density are shown in Fig. 5.12. The ambiguity surface for p-only (Eq. (3.27)), VSA (p+v) (Eq. (3.36)) and v_z-only (Eq. (3.32)) Bartlett estimators are shown in Fig. 5.12 (a), (b) and (c), respectively. This figure reveals that:

[1] For a sequence of n positive numbers x_1, x_2 ... the geometric mean is defined as:

$$\bar{x} = \sqrt[n]{x_1 x_2 \dots} .$$

1. The p-only Bartlett estimator presents a wide main lobe, consequently a reasonable estimation of the compressional attenuation and density is difficult (see Fig. 5.12 (a));

2. The VSA $(p + v)$ Bartlett estimator presents a narrower main lobe when compared with the p-only Bartlett estimator.

3. The v_z-only Bartlett estimator confirms the result found with the VSA $(p+v)$ Bartlett estimator, but with an even narrower main lobe. The v_z-only Bartlett estimator achieves the best estimation resolution of seabed parameters, as shown in Fig. 5.12 (c), confirming with experimental data that the vertical particle velocity component is the most important component for bottom characterization;

4. Although the lobes of density and compressional attenuation are larger than the lobe of sediment compressional speed one can conclude from Fig. 5.12 (c), with a high degree of certainty, that the estimate values of density and compressional attenuation correspond to $1.35\,\mathrm{g/cm^3}$ and $0.5\,\mathrm{dB}/\lambda$, respectively.

In order to further validate the estimate of sediment compressional speed, an additional set of ambiguity surfaces was calculated repeating the initial strategy of slicing the hypercube. At this time, however, the slices were performed along the density and compressional attenuation parameters one at the time. The result of such procedure provides two ambiguity surfaces: the first for sediment compressional speed versus density, and the second for sediment compressional speed versus compressional attenuation.

The results using the VSA $(p + v)$ and the v_z-only Bartlett estimators are shown in Fig. 5.13, for the first and second pair of parameters in cases (a) & (b) and (c) & (d), respectively. This figure reveals the following: first, that both estimators show a main lobe

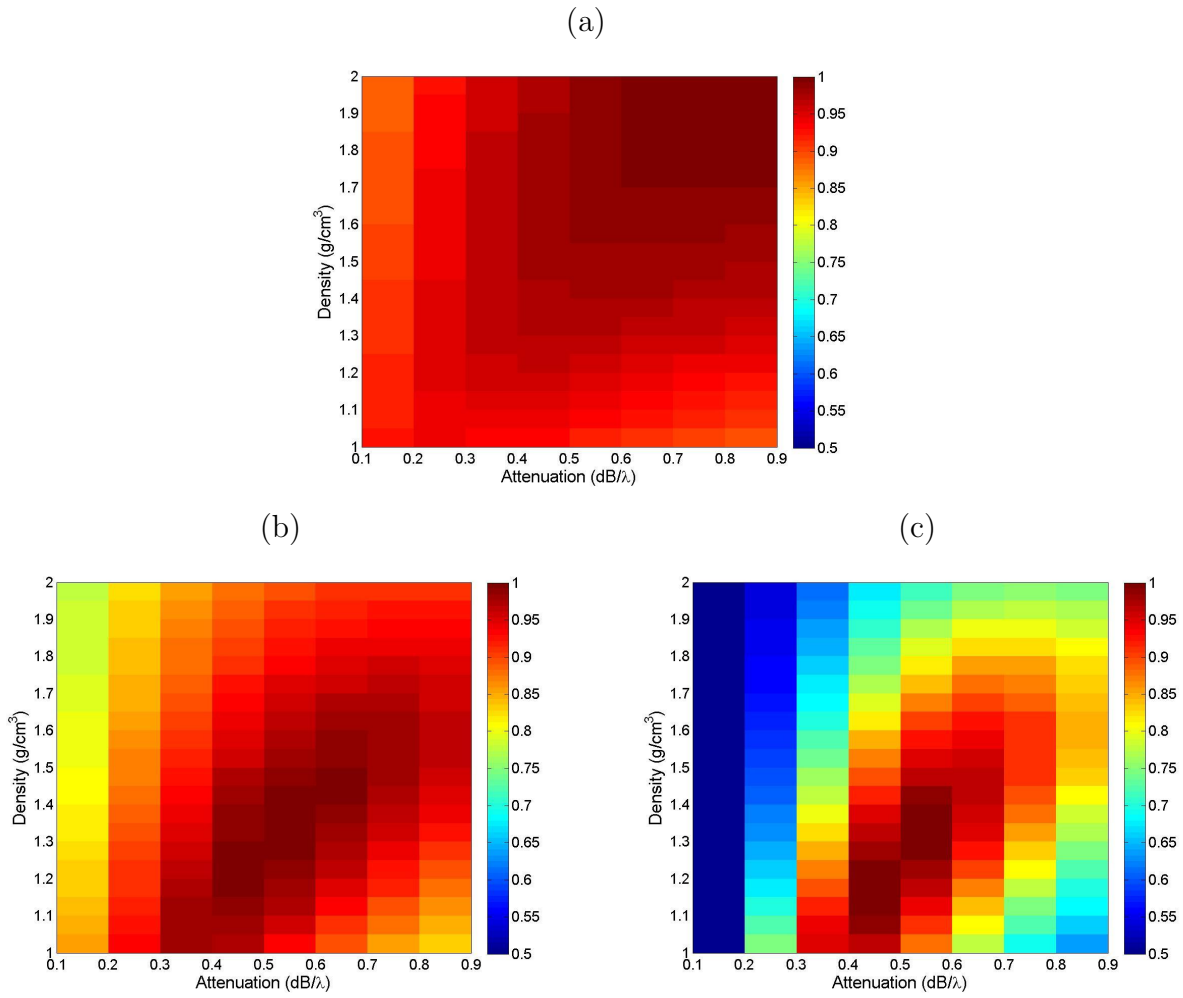

Figure 5.12: The experimental data normalized ambiguity surfaces for compressional attenuation and density, taking into account the sediment compressional speed value of 1580 m/s, using the p-only Bartlett estimator (a), the VSA $(p + v)$ Bartlett estimator (b) and the v_z-only Bartlett estimator (c).

well defined and at the same position for all parameters, but the v_z-only Bartlett estimator presents a narrower main lobe than the VSA $(p + v)$ Bartlett estimator; second, that the sediment compressional speed is found with higher estimation resolution than the density and the compressional attenuation, although these parameters are found with a good estimation resolution, specially with the v_z-only Bartlett estimator (see Fig. 5.13 (c) and (d)). Such results closely resemble those found in simulations, confirming the conclusions discussed in section 3.5. Moreover, these results are in agreement with those obtained from the inversion

technique based in the bottom reflection loss estimation, already discussed in section 5.1.3.

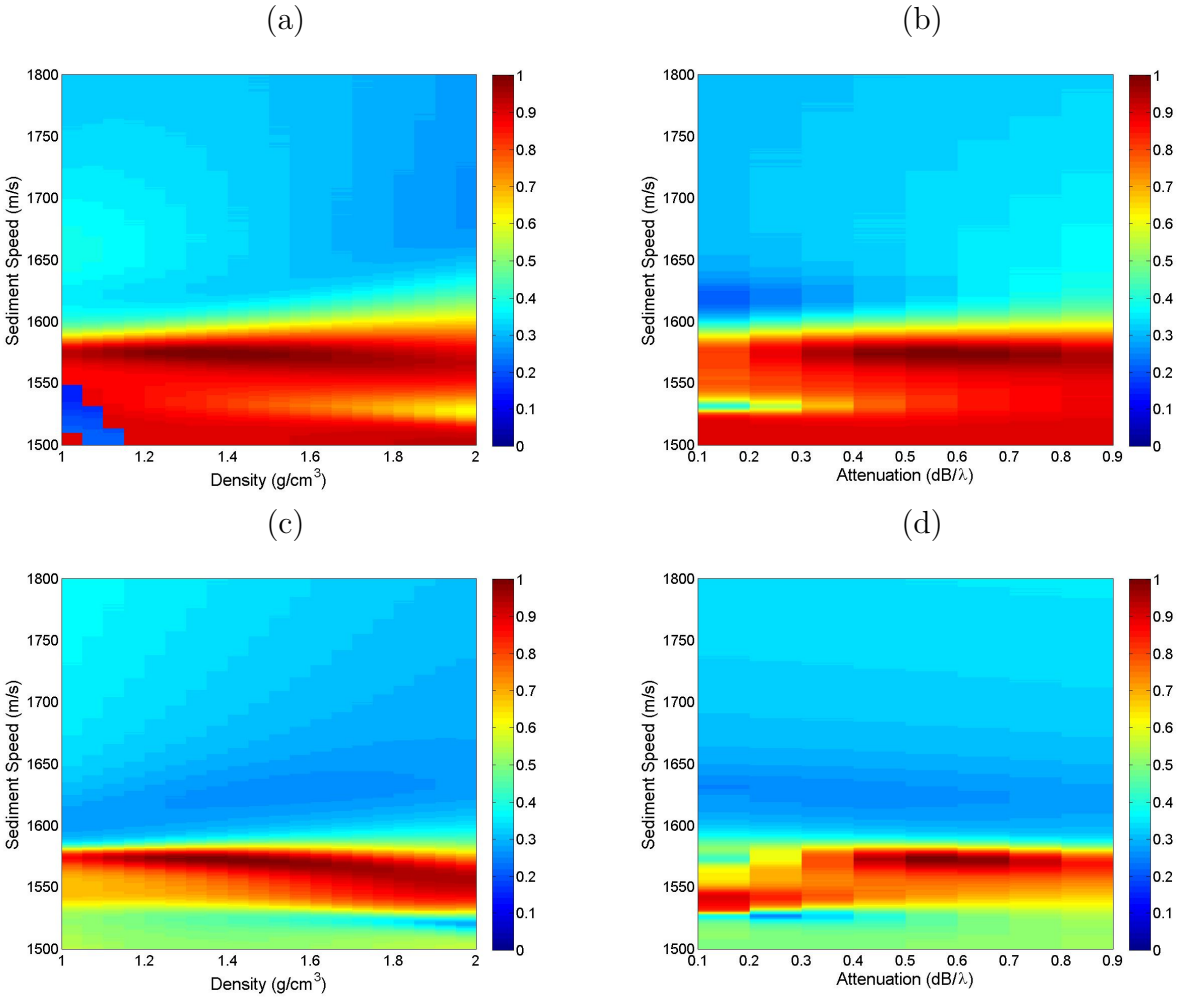

Figure 5.13: The experimental data normalized ambiguity surfaces using the geometric mean of estimates over time (two hours), considering: the VSA $(p + v)$ Bartlett estimator for sediment compressional speed versus density (a) and sediment compressional speed versus attenuation (b) and the v_z-only Bartlett estimator for sediment compressional speed versus density (c) and sediment compressional speed versus attenuation (d).

On the basis of the previous analysis, the estimates of density and compressional attenuation are going to be used to validate the estimates of sediment compressional speed along acquisition time. The corresponding ambiguity surfaces for sediment compressional speed, considering the p-only, the VSA $(p + v)$ and v_z-only Bartlett estimators, throughout almost two hours, are shown in Fig. 5.14 (a), (b) and (c), respectively. This figure reveals that the

sediment compressional speed parameter has an increasing order of estimation resolution from the p-only to the v_z-only Bartlett estimator, and confirms that the estimation of this parameter corresponds approximately to 1580 m/s. This figure also reveals the stability of the results during the data acquisition period, which is consistent with the previous analysis of the Fig. 5.11. One can notice also that the p-only estimator, in Fig. 5.14 (a), exhibits two lobes, during most of the acquistion time; one of them appears at the expected value of 1580 m/s, while the other appears around 1520 m/s [2]. The obtained value of 1580 m/s is consistent with the estimate found from the VSA $(p + v)$ and v_z-only Bartlett estimators. The previous results from the v_z-only Bartlett estimator are consistent with the results obtained with simulations and the results obtained from the bottom reflection loss technique; the v_z-only Bartlett estimator, shown in Fig. 5.14 (c), in fact has a narrower main lobe due to the higher sensitivity of the vertical particle velocity component to bottom structure.

Summary

In this chapter a geoacoustic model based on particle velocity measurements of the MakaiEx'05 area was defined.The characterization of the seabed was obtained using HF signals and with two different VSA-based techniques, which can be described as follows:

- In the first technique, the bottom reflection loss obtained from the VSA experimental data was compared with the bottom reflection loss modelled by the SAFARI model, considering a method proposed by C. Harrison *et al.*, which was adapted for the VSA experimental data. The best agreement between such comparisons provided the number of layers and the layer structure, with their most characteristic physical parameters.

[2] This is the value of sound speed at the sediment interface.

It was confirmed from the VSA beam response that different types of raypaths contribute to different types of particle velocity components, which is important for bottom characterization. Similar results were achieved from experimental data acquired on September 20th and on September 25th, consistent with a four-layer environment;

- In the second technique, sediment compressional speed, density and compressional attenuation were obtained using the VSA-based Bartlett estimators derived in section 3.3. The results revealed that the VSA-based Bartlett estimator has not only an increased estimation resolution, verified for all seabed parameters when compared with that of hydrophone arrays, but also that the high estimation resolution can be attained using only the vertical particle velocity component.

The estimation results from the VSA-based techniques are consistent with the historical data of the area.

(a)

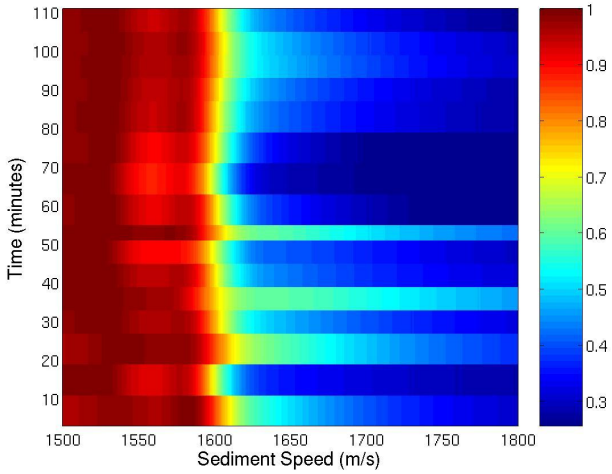

(b)

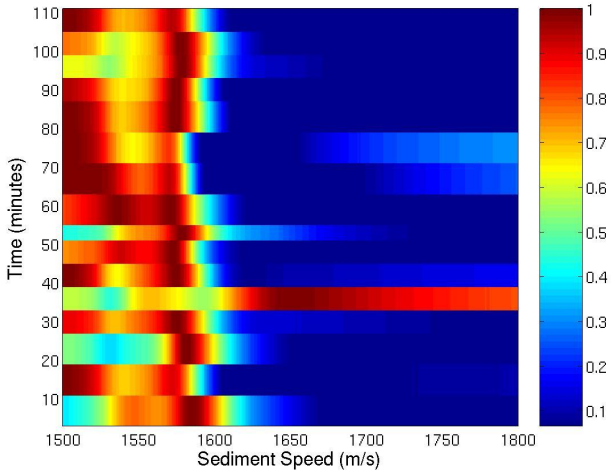

(c)

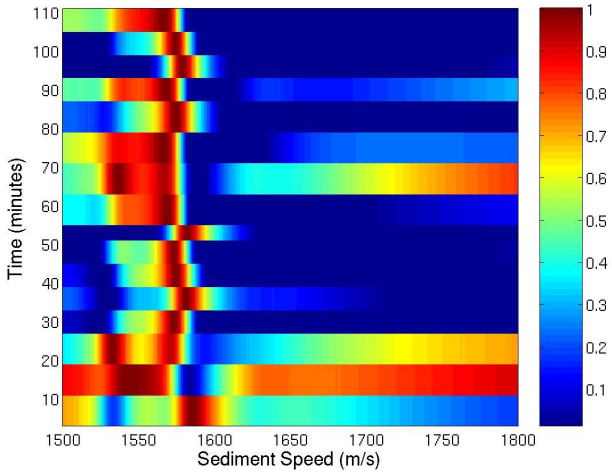

Figure 5.14: The experimental data normalized ambiguity surfaces for sediment compressional speed during data acquisition period (two hours), using : the p-only Bartlett estimator (a), the VSA $(p + v)$ Bartlett estimator (b) and v_z-only Bartlett estimator (c).

Chapter 6

Conclusion

The propagation of sound in the ocean is fundamental for communications, for target detection, for measuring water depth, or even for predicting environmental parameters. The estimation of ocean bottom parameters with sufficient resolution is crucial in underwater acoustic applications, to define a geoacoustic model of the real seabed. To such end, low frequency signals and traditional omni-directional hydrophone arrays, with large aperture, have been used to provide high estimation resolution of such parameters. Those systems are complex and may cause operational difficulties in array deployment and its recovery. Therefore, in order to create less complex, compact and easy-to-deploy systems, new ways can be investigated. In particular: the use of high-frequency signals to reduce the dimensions of both emitters and receivers, and the use of a new generation of sensors - vector sensors - to improve the directivity of the receiver system with simple configurations.

The present work discusses the usage of vector sensors in underwater high-frequency acoustic applications for ocean parameter estimation. Vector sensors have the ability to provide directional information since they measure the components of the particle motion along each spatial direction. Most of the research involving vector sensors was related to the capabilities of such sensors for DOA estimation, where a higher performance was exhibited

over pressure-only sensors. But the high directivity of the vector sensors and the advantages verified for DOA estimation could be used in the estimation of other parameters. Understand the common and differentiating features of the particle velocity field when compared to the pressure field, understand how the vector sensor influences the parameter estimation, identify whether various particle velocity components may contribute to the estimation of different ocean parameters, and extend the potential gain of the VSA for geoacoustic inversion, were the motivations of this work.

Based on the discussion of those subjects, standard estimation techniques were extended in order to include the particle velocity information. As a result of such extension, the following contributions were achieved:

- A VSA data model for generic parameter estimation was derived, which includes the particle velocity components and the acoustic pressure. The VSA data model is based on a ray physical description, using the Gaussian beam approximation of the ray pressure, and taking into account the relationship of the particle velocity with the acoustic pressure from the linear acoustic equation (Euler's equation);

- The conventional Bartlett processor was extended to include particle velocity outputs and two VSA-based estimators were proposed, namely the v-only and the VSA ($p + v$) Bartlett estimators. The performance of the VSA-based Bartlett estimators over pressure-only estimator was analytically deduced. It was shown that the v-only and VSA ($p + v$) Bartlett estimators are proportional to the p-only Bartlett estimator, where the inner product between the replica vector and the data vector are the terms of proportionality, called directivity factors. The two directivity factors provide an

improved sidelobe reduction (for v-only) or sidelobe suppression (for VSA (p+v)), when compared with the p-only Bartlett response. Such factors contribute to an improvement of the estimation resolution of the ocean parameters, and are the crucial advantage of the usage of particle velocity information.

The proposed VSA-based Bartlett estimators were tested, with simulated and experimental high-frequency data (in the 8-14 kHz band) acquired during the MakaiEx'05 experiment, for DOA estimation, and in the estimation of the seabed parameters, which is a relevant and to our knowledge an original contribution for underwater acoustic applications.

The features of vector sensors that influence DOA estimation were reviewed in Chapter 2 using the plane-wave beamforming technique. The performance of the VSA was compared, through simulations, with different spatial configurations of hydrophone arrays. The discussion allowed one to conclude that the VSA is a viable alternative to traditional omnidirectional hydrophone arrays because of the following:

- the VSA resolves both elevation and azimuth angles in a linear configuration;
- the VSA eliminates the well known left/right ambiguity;
- a VSA with a few elements provides better estimation resolution than equivalent hydrophone arrays;
- the VSA can be very compact providing a good alternative to be embarked on reduced dimension autonomous vehicles.

Such conclusions were also confirmed with the proposed VSA-based Bartlett estimators. The higher DOA estimation resolution of the VSA over p-only arrays was tested with ex-

perimental VSA data in Chapter 4. The fixed and towed acoustic sources DOA in the HF band were estimated for the three VSA deployments. Such results were validated with the expected bearings found from GPS information. After the discussion of experimental results on DOA estimation, which was a pre-processing requirement for the analysis of the seabed characterization, the VSA was used for geoacoustic inversion.

Before the application of the VSA for geoacoustic inversion, a brief study of the transmission loss with HF signals for acoustic pressure, horizontal and vertical particle velocity components was presented, allowing to differentiate the types of field contributions (which can be obtained when a vector sensor is used). Such study was performed using two different models, the TRACEO Gaussian beam model and the Monterey-Miami Parabolic Equation (MMPE) model, which are capable of particle velocity calculations. The acoustic pressure, horizontal and vertical particle velocity fields presented the same behaviour for both models. The results revealed that:

- the propagation field (at the considered HF band) reaches the receivers, with a sufficient amount of energy, after bottom reflections for the considered setup;

- the horizontal component is mostly affected by the direct and refracted ray paths, while the vertical component is mostly affected by surface and bottom reflected ray paths;

- the features of the acoustic field, principally the vertical particle velocity component, were shown to have a potential for geoacoustic inversion. The field contribution to the vertical particle velocity is important for seabed characterization and this was confirmed with simulations and experimental results.

The applicability of a few elements VSA using experimental HF signals for geoacoustic inversion was tested with two different VSA-based techniques, where the performance of the VSA was compared with that of equivalent hydrophone arrays (which was discussed in Chapter 5). In the first technique, the characterization of the seabed with its most relevant parameters was determined using a method proposed by C. Harrison *et al.*, which was adapted for the VSA experimental data. The method consists on the determination of the ratio between the downward and upward beam response, providing an approximation of the bottom reflection loss. The best agreement between the bottom reflection loss, obtained from the VSA experimental data and that predicted by the SAFARI model, provided the number of layers and the layer structure, with their most characteristic physical parameters. From the analysis of the VSA beam response and of the corresponding bottom reflection loss, the following conclusions were achieved, confirming with experimental data, the conclusions found with the TL study:

- different ray paths contribute to different particle velocity components;
- the contribution of the acoustic field to the different particle velocity components is important for seabed characterization;
- a VSA with few elements is able to increase significantly the estimation resolution of the reflection loss over p-only arrays.

In the second technique, the derived VSA-based Bartlett estimators were proposed for MFI, where the seabed parameters, such as the sediment compressional speed, density and compressional attenuation, were estimated. From the analysis of MFI results one can conclude that:

- the density and the compressional attenuation are difficult to obtain with hydrophone arrays, even with large aperture arrays;

- the VSA-based Bartlett estimator has an increased estimation resolution, verified for all seabed parameters when compared with that of hydrophone arrays;

- the highest estimation resolution were obtained using only the vertical particle velocity component. It should be remarked that this component is fundamental for seabed characterization.

The geoacoustic inversion results found from the VSA-based MFI technique are consistent with those obtained from the bottom reflection loss and with the historical data of the area.

In general, the work developed in this thesis revealed that the particle velocity information is of great importance for underwater acoustic applications, mainly for DOA and for seabed parameters estimation. The results discussed during the different chapters showed that a few elements VSA provide a higher estimation resolution of parameters, in particular seabed parameters, than hydrophone arrays. The band of the probe signal used is well above the band traditionally used in geoacoustic inversion; however, it was found that in this HF band, a significant amount of energy reaches the receivers after bottom reflections, which allows the propagated field to provide sufficient information for geoacoustic inversion. Therefore, a system based on a few elements VSA operating in such HF band represents a compact and easy-to-deploy system to install in a light mobile platform like AUV or in various underwater acoustical applications, becoming a viable alternative to existing bottom profilers.

Future work

Following the work developed in this thesis several aspects, regarding the use of vector sensors in underwater acoustic applications, can be explored in the future.

- Derive other types of estimators taking advantage of the particle velocity information, comparing the performance between the VSA-based Bartlett estimator with other processors, even with the considered high-resolution processors.

- Since the improved resolution of ocean bottom parameters estimation could be obtained using only the vertical particle velocity component, other methods should be investigated in order to develop simple and fast techniques to be applied in real time processing.

- To apply methods used in tensor analysis, such as the quaternion model (which is a four dimensional hyper complex number system), to ocean bottom parameter estimation. Such technique has already been applied for localization problems.

- The knowledge acquired with the development of this work can be used for applications within the context of the SENSOCEAN project, which aims at the development of an acoustic vector sensor array for an underwater mobile platform, with applications in acoustic exploration of the marine environment.

Bibliography

[1] H. Medwin. *Sounds in the sea, from ocean acoustics to acoustical oceanography.* Cambridge, University Press, New York, USA, 2005.

[2] F. B. Jensen, W. A. Kuperman, M. B. Porter, and H. Schmidt. *Computational Ocean Acoustics.* 2nd Edition. Series in Modern Acoustics and Signal Processing, Springer, NY, 2011.

[3] C. Soares. *Broadband Matched-field tomography using simplified acoustic systems.* PhD thesis, Universidade do Algarve, Faro, Portugal, 2007.

[4] W. Munk and C. Wunsch. Ocean acoustic tomography: A scheme for large scale monitoring. *Deep Sea Research*, 26(A):123–161, 1979.

[5] W. Munk, P. Worcester, and C. Wunsch. *Ocean acoustic tomography.* Cambridge Monographs on Mechanics, University Press, Cambridge, 1995.

[6] E. De Marinis, O. Gasparini, P. Picco, S. M. Jesus, A. Crise, and S. Salon. Passive ocean acoustic tomography: theory and experiment. In *Proceedings of ECUA'02 Conference*, pages 497–502, Gdansk, Poland, June 2002.

[7] S. M. Jesus, E. F. Coelho, J. Onofre, P. Picco, C. Soares, and C. Lopes. The INTIFANTE'00 sea trial: Preliminar source localization and ocean tomography data

analysis. In *Proceedings of MTS/IEEE Oceans 2001 Conference*, pages 40–45, Hawai, USA, November 2001.

[8] W. A. Kuperman and J. F. Lynch. Shallow water acoustics. *Physics Today*, pages 55–61, October 2004.

[9] J. Lewis, J. Rudzinsky, S. Rajan, P. Stein, and A. Vandiver. Model-oriented ocean tomography using higher frequency, bottom-mounted hydrophones. *J. Acoust. Soc. Am.*, 117(6):3539–3554, June 2005.

[10] J. C. Shipps and B. M. Abraham. The use of vector sensors for underwater port and waterway security. In *Proceedings of Sensors for Industry conference*, pages 41–44, New Orleans, Louisiana, USA, January 27–29 2004.

[11] A. Nehorai and E. Paldi. Acoustic vector-sensor array processing. *IEEE Trans. Signal Processing*, 42(9):2481–2491, September 1994.

[12] B. A. Cray and A. H. Nuttall. Directivity factors for linear arrays of velocity sensors. *J. Acoust. Soc. Am.*, 110(1):324–331, July 2001.

[13] C. Wan, A. Kong, and C. Liu. A comparative study of DOA estimation using vector/gradient sensors. In *Proceedings of Oceans06*, pages 1–4, Asia, Pacific, May 16–19 2007.

[14] M. Hawkes and A. Nehorai. Acoustic vector-sensor beamforming and capon direction estimation. *IEEE Trans. Signal Processing*, 46(9):2291–2304, September 1998.

[15] H. Krim and M. Viberg. Two decades of array signal processing research. *IEEE Signal processing magazine*, pages 67–94, July 1996.

[16] B. D. Van Veen and K. M. Buckley. Beamforming: A versatile approach to spatial filtering. *IEEE ASSP magazine*, 5(2):4–24, April 1988.

[17] M. J. Hinich. Maximum-likelihood signal processing for a vertical array. *J. Acoust. Soc. Am.*, 54:499–503, 1973.

[18] H. P. Bucker. Use of calculated sound fields and matched-detection to locate sound source in shallow water. *J. Acoust. Soc. Am.*, 59:368–373, 1976.

[19] T. C. Yang. A method of range and depth estimation by modal decomposition. *J. Acoust. Soc. Am.*, 82(5):1736–1745, November 1987.

[20] M. D. Collins and W. A. Kuperman. Focalization: environmental focusing and source localization. *J. Acoust. Soc. Am.*, 90(3):1410–1422, September 1991.

[21] A. Tolstoy. *Matched Field Processing for Underwater Acoustics*. World Scientific, Singapore, 1993.

[22] A. Tolstoy. Matched field estimation of environmental parameters. In *21st Annual Congress of Canadian Meteorological and Oceanographic Soc.*, June 1987.

[23] A. Tolstoy, O. Diachok, and L. N. Frazer. Acoustic tomography via matched field processing. *J. Acoust. Soc. Am.*, 89:1119–1127, 1991.

[24] A. Tolstoy. Matched field tomographic inversion to determine environmental properties. *Current Topics in Acoustic Research*, 1:53–61, 1994.

[25] L. J. Hamilton. Acoustical seabed classification systems. Technical Report DSTO–TN–0401, DSTO Aeronautical and Maritime Research Laboratory, Australia, November 2001.

[26] S. E. Dosso, M. L. Yeremy, J. M. Ozard, and N. R. Chapman. Estimating of ocean bottom properties by matched-field inversion of acoustic field data. *IEEE Journal of Oceanic Engeneering*, 18(3):232–239, July 1993.

[27] P. Gerstoft. Inversion of seismoacoustic data using genetic algorithms and a posteriori probability distributions. *J. Acoust. Soc. Am.*, 95(2):770–782, February 1994.

[28] J. P. Hermand and P. Gerstoft. Inversion of broad-band multitone acoustic data from the YELLOW SHARK summer experiments. *IEEE Journal of Oceanic Engeneering*, 21(4):324–346, October 1996.

[29] C. E. Lindsay and N. R. Chapman. Matched-field inversion for geoacoustic model parameters using adaptive simulated annealing. *IEEE Journal of Oceanic Engeneering*, 18(3):224–231, July 1993.

[30] N. R. Chapman and C. E. Lindsay. Matched-field inversion for geoacoustic model parameters in shallow water. *IEEE Journal of Oceanic Engeneering*, 21(4):347–354, October 1996.

[31] S. E. Dosso. Quantifying uncertainty in geoacoustic inversion. I - A fast Gibbs sampler approach. *J. Acoust. Soc. Am.*, 111(1):129–142, January 2002.

[32] S. M. Jesus and A. Caiti. Estimating geoacoustic bottom properties from towed array data. *J. Acoust. Soc. Am.*, 4(3):273–290, 1996.

[33] C. F. Mecklenbräuker, J. F. Böhme, and A. Gershman. Broadband ML-approach to environmental parameter estimation in shallow ocean at low SNR. *Signal processing, Elsevier*, 81:389–401, 2001.

[34] R. M. S. Barlee, M. J. Wilmut, and N. R. Chapman. Geoacoustic model parameter estimation using a bottom moored hydrophone array. *IEEE Journal of Oceanic Engeneering*, 30(4):773–783, 2005.

[35] J.P. Hermand. Broad-band geoacoustic inversion in shallow water from waveguide impulse response measurements on a single hydrophone: theory and experimental results. *IEEE Journal of Oceanic Engeneering*, 24(1):41–66, January 1999.

[36] A. Caiti, J. P. Hermand, S. M. Jesus, and M. B. Porter. *Experimental acoustic inversion methods for exploration of the shallow water environment*. Klumer Academic Publishers, Dordrecht, The Netherlands, 2000.

[37] N. P. Chotiros. Geophysical parameters in a poro-elastic sediment. In A. Caiti *et al.* (eds.), editor, *Experimental acoustic inversion methods for exploration on the shallow water environment*, pages 211–218, Dordrecht, The Netherlands, 2000. Klumer Academic Publisher.

[38] N. R. Chapman. Estimation of the elastic properties of sea floor sediments. In *Proceedings of IEEE Oceans 89 Conference*, pages 1071–1075, September 18–21 1989.

[39] C. H. Harrison and D. G. Simons. Geoacoustic inversion of ambient noise: A simple method. *J. Acoust. Soc. Am.*, 112(4):1377–1387, October 2002.

[40] C. H. Harrison and M. Siderius. High-frequency geoacoustic inversion of ambient noise data using short arrays. In *Proceedings of High-frequency Ocean Acoustics Conference*, volume 728, pages 22–31, La Jolla, California, March 1–5 2004.

[41] W. W. L. Au and K. Andrews. Feasibility of using acoustic DIFAR technology to localize and estimate Hawai´ian humpback whale population. Technical report, U.S. Department of Commerce and Department of Land and Natural Resources, State of Hawaii, June 2001.

[42] J. C. Nickles, G. L. Edmonds, R. A. Harriss, F. H. Fisher, W.S. Hodgkiss, J. Giles, and G.L. D'Spain. A vertical array of directional acoustic sensors. In *Proceedings MTS/IEEE Oceans 92 Conference*, pages 340–345, Newport, RI (USA), October 1992.

[43] G.L. D'Spain, W.S. Hodgkiss, G. L. Edmonds, J. C. Nickles, F. H. Fisher, and R. A. Harriss. Initial analysis of the data from the vertical DIFAR array. In *Proceedings MTS/IEEE Oceans 92 Conference*, pages 346–351, Newport, RI (USA), October 1992.

[44] J. Tabrikian, R. Shavit, and D. Rahamim. An efficient vector sensor configuration for source localization. *IEEE Signal Processing Letters*, 11(8):690–693, August 2004.

[45] A. Nehorai and E. Paldi. Vector-sensor array processing for electromagnetic source localization. *IEEE Trans. Signal Processing*, 42(2):376–398, February 1994.

[46] S. Miron, N. Le Bihan, and J. I. Mars. Quaternion-MUSIC for vector-sensor array processing. *IEEE Trans. Signal Processing*, 54(4):1218–1229, April 2006.

[47] S. Miron, N. Le Bihan, and J. I. Mars. High-resolution vector sensor array processing based on biquaternions. In *IEEE International Conference on Acoustic, Speech and Signal Processing*, pages 1077–1080, Toulouse, France, May 2006.

[48] Y. H. Wang, J. Q. Zhang, B. Hu, and J. He. Hypercomplex model of acoustic vector sensor array with its application for the high resolution two dimensional direction of ar-

rival estimation. In *Proceedings I²MTC 2008, IEEE International Instrumentation and Measurement Technology Conference*, pages 1–5, Victoria, Vancouver, Canada, 2008.

[49] D. Lindwall. Marine seismic surveys with vector acoustic sensors. In *Proceedings of Soc. Exploration Geophysicists annual meeting*, pages 1208–1212, New Orleans, USA, 2006.

[50] A. Abdi, H. Guo, and P. Sutthiwan. A new vector sensor receiver for underwater acoustic communication. In *Proceedings MTS/IEEE Oceans*, pages 1–10, Vancouver, BC, Canada, 2007.

[51] A. Song, M. Badiey, P. Hursky, and A. Abdi. Time reversal receivers for underwater acoustic communication using vector sensors. In *IEEE*, pages 1–10, Quebec, Canada, September 2008.

[52] H. Peng and F. Li. Geoacoustic inversion based on a vector hydrophone array. *Chin. Phys. Lett.*, 24(7):1997–1980, 2007.

[53] M. B. Porter, M. Siderius, and W. A. Kuperman. *High-Frequency Ocean Acoustics*. AIP Conference Proceedings, Volume 728, Melville, New York, 2004.

[54] F. B. Jensen, P. L. Nielson, M. Zampolli, M. D. Collins, and W. L. Siegmann. Benchmarling range-dependent seismo-acoustic propagation problems. In S. M. Jesus and O. C. Rodríguez, editors, *Proceedings of 8th ECUA,Carvoeiro,Portugal*, volume 1, pages 45–508, 2006.

[55] M. Porter, B. Abraham, M. Badiey, M. Buckingham, T. Folegot, P. Hursky, S. Jesus, K. Kim, B. Kraft, V. McDonald, C. deMoustier, J. Preisig, S. Roy, M. Siderius, H. Song, and W. Yang. The Makai Experiment: High-frequency acoustics. In S. M. Jesus and

O. C. Rodríguez, editors, *Proceedings of 8th ECUA,Carvoeiro,Portugal*, volume 1, pages 9–18, 2006.

[56] O. C. Rodríguez. *The TRACE and TRACEO ray tracing programs.* http://www.siplab.fct.ualg.pt/models.shtml, date last viewed 6/7/10.

[57] H. Schmidt. SAFARI - Seismo-Acoustic Fast field Algorithm for Range-Independent environments, user's guide. Technical Report SR–113, SACLANTCEN Undersea Research Centre Report, La Spezia, Italy, September 1988.

[58] P. Santos, P. Felisberto, and P. Hursky. Source localization with vector sensor array during Makai experiment. In *Proceedings of 2nd International Conference and Exhibition on Underwater Acoustic Measurements: Technologies and Results*, pages 985–990, Heraklion,Greece, June 25–29 2007.

[59] P. Santos, P. Felisberto, and S. M. Jesus. Estimating bottom properties with a vector sensor array during MakaiEx 2005. In *Proceedings of 2nd International workshop on Marine Techonology, Martech07*, page 77, Vilanova i la Geltrú,Spain, November 15–16 2007.

[60] P. Santos, O. C. Rodríguez, P. Felisberto, and S. M. Jesus. Geoacoustic matched-field inversion using a vertical vector sensor array. In *Proceedings of 3rd International Conference and Exhibition on Underwater Acoustic Measurements: Technologies and Results*, pages 29–34, Nafplion,Greece, June 21–26 2009.

[61] P. Santos, O. C. Rodríguez, P. Felisberto, and S. M. Jesus. Seabed geoacoustic characterization with a vector sensor array. *J. Acoust. Soc. Am.*, 128(5):2652–2663, November,2010.

[62] P. Santos, P. Felisberto, and S. M. Jesus. Vector sensor array in underwater acoustic applications. In L. Camarinha-Matos, P. Pereira, and L. Ribeiro, editors, *Proceedings of DoCEIS 10, Doctoral Conference on Computing, Electrical and Industrial Systems*, volume 314, pages 316–323, Caparica, Lisbon, Portugal, February 22–24 2010. Springer Boston.

[63] P. Santos, J. João, P. Felisberto, and S. M. Jesus. Experimental results of geometric and geoacoustic parameter estimation using a vector sensor array. In *Proceedings of IX ETAS, IX Encontro de Tecnologia em Acústica Submarina*, Arraial do Cabo, RJ, Brasil, November 9–11 2010.

[64] P. Santos, J. João, O. C. Rodríguez, P. Felisberto, and S. M. Jesus. Geometric and seabed parameter estimation using a vector sensor array - Experimental results from Makai experiment 2005. In *Proceedings of Oceans 11 IEEE/OES Santander Conference*, Santander, Spain, June 6–9 2011.

[65] C. H. Sherman and J. L. Butler. *Transducers and Arrays for Underwater Sound*. The Underwater Acoustic series. Springer, 2007.

[66] J. P. Feuillet, W. S. Allensworth, and B. K. Newhall. Nonambiguous beamforming for a high resolution twin-line array. *J. Acoust. Soc. Am.*, 97(5):3292–3292, May 1995.

[67] R. M. Zeskind, J. P. Feuillet, and W. S. Allensworth. Acoustic performance of a multiline system towed in several ocean environments. In *Proceedings of Oceans 98 Conference*, pages 124–128, Nice, 28 September to 1 October 1998.

[68] A. B. Baggeroer, W. A. Kuperman, and P. N. Mikhalevsky. An overview of matched field methods in ocean acoustics. *IEEE Journal of Oceanic Engeneering*, 18(4):401–424, October 1993.

[69] C. Soares and S. M. Jesus. Broadband matched-field processing: Coherent and incoherent approaches. *J. Acoust. Soc. Am.*, 113(5):2587–2598, 2003.

[70] M. Hawkes and A. Nehorai. Effects of sensor placement on acoustic vector-sensor array performance. *IEEE J. Oceanic Eng.*, 24(1):33–40, January 1999.

[71] M. Hawkes and A. Nehorai. Acoustic vector-sensor processing in the presence of a reflecting boundary. *IEEE Trans. Signal Processing*, 48(11):2981–2993, November 2000.

[72] M. Hawkes and A. Nehorai. Acoustic vector-sensor correlations in ambient noise. *IEEE J. Oceanic Eng.*, 26(3):337–347, July 2001.

[73] K. B. Smith. *Monterey-Miami Parabolic Equation model.* http://oalib.hlsresearch.com/PE/index.html, date last viewed 25/11/10.

[74] S. M. Jesus, A. Silva, and F. Zabel. *Acoustic Oceanographic Buoy Data Report: MakaiEx 2005.* Internal Rep 04/05 – SiPLAB/CINTAL, Universidade do Algarve, Faro, Portugal, November 2005.

[75] J. A. Clark and G. Tarasek. Localization of radiating sources along the hull of a submarine using a vector sensor array. In *Proceedings of Oceans'06 MTS/IEEE - Boston*

conference and Exhibition, pages 1–3, Boston, Massachusetts, USA, September 18–21 2006.

[76] M. A. Larsen and J. M. Hovem. Geoacoustic inversion. In P. Blondel and A. Caiti, editors, *Buried Waste in the seabed - Acoustic imaging and Bio-toxicity, Results from the European SITAR project*, pages 105–111. Springer, 2007.

[77] E. L. Hamilton. Geoacoustic modeling of the sea floor. *J. Acoust. Soc. Am.*, 68(5):1313–1340, November 1980.

Appendix A

Derivation of the Bartlett estimator for particle velocity

For the derivation of the Bartlett estimator taking into account the particle velocity components, the following properties of the Kronecker product are considered:

1. $\mathbf{A} \otimes (a\mathbf{B}) = (a\mathbf{A}) \otimes \mathbf{B} = a(\mathbf{A} \otimes \mathbf{B})$ where a is a scalar,

2. $(\mathbf{A} \otimes \mathbf{B})^H = \mathbf{A}^H \otimes \mathbf{B}^H$,

3. $(\mathbf{A} \otimes \mathbf{B})(\mathbf{C} \otimes \mathbf{D}) = \mathbf{AC} \otimes \mathbf{BD}$

4. if $\mathbf{A}_1, \mathbf{A}_2, \cdots, \mathbf{A}_p$ are $M \times M$ and $\mathbf{B}_1, \mathbf{B}_2, \cdots, \mathbf{B}_p$ are $N \times N$ then $(\mathbf{A}_1 \otimes \mathbf{B}_1)(\mathbf{A}_2 \otimes \mathbf{B}_2) \cdots (\mathbf{A}_p \otimes \mathbf{B}_p) = (\mathbf{A}_1\mathbf{A}_2 \cdots \mathbf{A}_p) \otimes (\mathbf{B}_1\mathbf{B}_2 \cdots \mathbf{B}_p)$.

In the following, $\mathbf{v}(\Theta_0, \Theta) = \mathbf{u}(\Theta_0, \Theta)$ when only particle velocity components are considered in the data model - v-only; or $\mathbf{v}(\Theta_0, \Theta) = \begin{bmatrix} 1 & \mathbf{u}(\Theta_0, \Theta) \end{bmatrix}^T$ when both pressure and particle velocity components are considered - VSA $(p + v)$. For simplicity, the following notation $\mathbf{v}(\Theta_0) \rightarrow \mathbf{v_0}$ and $\mathbf{v}(\Theta) \rightarrow \mathbf{v}$ is used.

The correlation matrix $\mathbf{R_0}$ depending on the particle velocity data model, with or without pressure, can be written as:

$$\mathbf{R_0} = \left[\mathbf{v_0} \otimes \mathbf{h_{0}}_p\right] \left[\mathbf{v_0} \otimes \mathbf{h_{0}}_p\right]^H \sigma_s^2 + \sigma_n^2 \mathbf{I}, \tag{A.1}$$

where the additive noise is zero mean, white both in time and space, with variance σ_n^2 and uncorrelated with the signal s, itself with zero mean and variance σ_s^2, $\mathbf{h_{0}}_p$ is the channel frequency response at the L pressure sensors and $\mathbf{v_0}$ is the data vector.

A possible estimator $\hat{\mathbf{e}}$ of $\mathbf{e}$ is obtained as:

$$\hat{\mathbf{e}} = \arg\max_{\mathbf{e}} \left\{\mathbf{e}^H \mathbf{R_0} \mathbf{e}\right\}, \tag{A.2}$$

subject to $\mathbf{e}^H\mathbf{e} = 1$.

Using the eigen decomposition of the correlation matrix associated with the signal and noise subspaces according to structure (A.1) and for this case in particular, it can be shown that $\mathbf{v_0} \otimes \mathbf{h_{0}}_p$ is one of the eigenvectors of $\mathbf{R_0}$, since post-multiplying (A.1) by this eigenvector and using the properties of the Kronecker product 2 and 3, gives:

$$\begin{aligned}
\mathbf{R_0}\left[\mathbf{v_0} \otimes \mathbf{h_{0}}_p\right] &= \left\{\left[\mathbf{v_0} \otimes \mathbf{h_{0}}_p\right] \left[\mathbf{v_0}^H \otimes \mathbf{h_{0}}_p^H\right] \sigma_s^2 + \sigma_n^2 \mathbf{I}\right\} \left[\mathbf{v_0} \otimes \mathbf{h_{0}}_p\right] \\
&= \left[\mathbf{v_0} \otimes \mathbf{h_{0}}_p\right] \left[\mathbf{v_0}^H \mathbf{v_0} \otimes \mathbf{h_{0}}_p^H \mathbf{h_{0}}_p\right] \sigma_s^2 + \sigma_n^2 \left[\mathbf{v_0} \otimes \mathbf{h_{0}}_p\right] \\
&= \left[\mathbf{v_0} \otimes \mathbf{h_{0}}_p\right] \left\{\mathbf{v_0}^2 \mathbf{h_{0}}_p^2 \sigma_s^2 + \sigma_n^2\right\},
\end{aligned} \tag{A.3}$$

where the quantity in brackets {} is simply the eigenvalue associated with this eigenvector. Then a maximization with respect to $\mathbf{e}$ is the eigenvector associated with the largest eigenvalue as given by:

$$\hat{\mathbf{e}} = \frac{\mathbf{v} \otimes \mathbf{h}_p}{\sqrt{\left[\mathbf{v} \otimes \mathbf{h}_p\right]^H \left[\mathbf{v} \otimes \mathbf{h}_p\right]}}$$

$$
\begin{aligned}
&= \frac{\mathbf{v} \otimes \mathbf{h}_p}{\sqrt{\mathbf{v}^H\mathbf{v} \otimes \mathbf{h}_p^H\mathbf{h}_p}} \\
&= \frac{\mathbf{v}}{\sqrt{\mathbf{v}^H\mathbf{v}}} \otimes \hat{\mathbf{e}}_p, \qquad \text{(A.4)}
\end{aligned}
$$

where $\hat{\mathbf{e}}_p$ is the replica vector estimator for the pressure defined in section 3.3 and where properties 2 and 3 were used.

Replacing (A.4) and (A.1) in the generic Bartlett estimator (3.21), using the properties of the Kronecker product 2, 3 and 4 with subject to $\mathbf{e}_p^H\mathbf{e}_p = 1$, the Bartlett estimator for the particle velocity model is given by:

$$
\begin{aligned}
P_B &= \frac{\mathbf{v}^H}{\sqrt{\mathbf{v}^H\mathbf{v}}} \otimes \hat{\mathbf{e}}_p^H \left\{ \left[\mathbf{v_0} \otimes \mathbf{h_0}_p\right] \left[\mathbf{v_0}^H \otimes \mathbf{h_0}_p^H\right] \sigma_s^2 + \sigma_n^2\mathbf{I} \right\} \frac{\mathbf{v}}{\sqrt{\mathbf{v}^H\mathbf{v}}} \otimes \hat{\mathbf{e}}_p \\
&= \frac{\left(\mathbf{v}^H\mathbf{v_0}\mathbf{v_0}^H\mathbf{v}\right) \otimes \left(\hat{\mathbf{e}}_p^H\mathbf{h_0}_p\mathbf{h_0}_p^H\hat{\mathbf{e}}_p\right)\sigma_s^2 + \mathbf{v}^H\mathbf{v}\hat{\mathbf{e}}_p^H\hat{\mathbf{e}}_p\sigma_n^2}{\mathbf{v}^H\mathbf{v}} \\
&= \frac{\left[\mathbf{v}^H\mathbf{v_0}\right]^2}{\mathbf{v}^H\mathbf{v}} B_p\sigma_s^2 + \sigma_n^2. \qquad \text{(A.5)}
\end{aligned}
$$

where B_p is the noise-free beam pattern for acoustic pressure only. Taking into account (3.27), one can conclude that the vector sensor estimator (with or without pressure) is proportional to the noise-free acoustic pressure response, where the inner product $\mathbf{v}^H\mathbf{v_0}$ is the constant of proportionality herein called directivity factor.

Appendix B

Publications

The relevant publications obtained with the work developed during the progress of this thesis are contained in the CD-ROM provided with this document and are referenced as [58, 59, 60, 61, 62, 63, 64].